NASA Technical Paper 1115

Effect of Propulsion System Characteristics on Ascent Performance of Dual-Fueled Single-Stage Earth-to-Orbit Transports

John J. Rehder

DECEMBER 1977

NASA

NASA Technical Paper 1115

Effect of Propulsion System Characteristics on Ascent Performance of Dual-Fueled Single-Stage Earth-to-Orbit Transports

John J. Rehder
Langley Research Center
Hampton, Virginia

National Aeronautics
and Space Administration

**Scientific and Technical
Information Office**

1977

SUMMARY

Vehicle systems design studies are being used by the National Aeronautics and Space Administration (NASA) to assess the effect of potential technology advancements on future aerospace programs. Dual-fueled single-stage Earth-to-orbit transports are among the vehicle concepts being investigated. An integral part of the design process is the rapid, accurate estimation of ascent performance. The data presented in this report provide this capability and can also be used as a guide for determining promising candidate configurations for more detailed study.

This report presents the results of a parametric study of the ascent performance of two dual-fueled single-stage-to-orbit concepts, obtained by using a mix of hydrocarbon and hydrogen fueled engines operating in either a series burn or parallel burn mode. The analysis was made by systematically varying a set of propulsion similarity parameters and calculating a trajectory for each combination of parameters. The parameters were initial thrust-weight ratio $(T/W)_o$, the proportion of the thrust due to dual-position nozzle engines R_e, expansion ratio of the hydrocarbon engines ϵ_{RP}, first expansion ratio of the hydrogen engines ϵ_{H1} (used for parallel burn concept only), second expansion ratio of the hydrogen engines ϵ_{H2}, and the proportion of hydrocarbon fuel used R_f.

The performance of both concepts was strongly influenced by $(T/W)_o$, R_e, and ϵ_{H2}, and in each case the performance improved as the parameter increased. The effects of changing ϵ_{RP} and ϵ_{H1} were small. The optimum fuel ratio R_f decreased with increasing $(T/W)_o$ and R_e and was nearly independent of expansion ratio. Varying R_f from the optimum had a large effect on the performance.

INTRODUCTION

Historically, major aerospace programs, like the Apollo and the Space Shuttle Programs, have required long lead times between the conceptual and operational phases, 15 years being a typical figure. It is important, therefore, to identify, early in the research process, technology areas which will offer significant benefits if applied to the particular concept being studied. Such an effort is currently underway within NASA with regard to future space transportation systems. The studies included in this effort, both in-house (refs. 1 and 2) and contractural (ref. 3), are aimed at identifying technology areas associated with future Earth-orbit transportation systems which are either critical to the development of such systems or which offer a significant cost and performance advantage as a result of their development.

The approach taken in these studies has been to choose a particular space transportation concept, a single-stage Earth-to-orbit (referred to herein as single-stage-to-orbit (SSTO)) vehicle, and use preliminary system design studies to assess the effects of applying various technology advancements. The SSTO

concept has generated considerable interest in recent years because of its potential for substantially reducing the operational costs of placing payloads in Earth orbit and because technology has reached a point where such vehicles appear to be feasible. (See refs. 3 to 6.) In particular, two projected advances in propulsion technology, dual-fuel propulsion and altitude-compensating nozzles, show potentially promising results. The dual-fuel concept, where both a high density hydrocarbon fuel and low density hydrogen are used in one stage with liquid oxygen (LOX), has been shown to have volume and mass advantages over a single-fuel system. (See refs. 4 to 7.) In these studies, optimum splits between the two fuels are determined; these splits take advantage of the lower volume of the hydrocarbon and higher performance of the hydrogen. The benefits of an altitude-compensating nozzle, in this case a two-position nozzle, have also been shown. (See ref. 2.) The performance of bell nozzles varies significantly with altitude. Nozzles with low expansion ratio perform better at low altitudes whereas high expansion ratio nozzles perform best at high altitudes. A dual-position nozzle allows the engine to deliver high performance at both low and high altitudes.

Concepts which use both of these advances are currently being studied by NASA through design studies. In these studies, an integral part of the design process is the accurate estimation of the ascent performance in terms of mass ratio for each vehicle configuration being studied. This usually requires a trajectory optimization program; however, such programs are too large and time consuming to be included in an automated design process. The current investigation provides the capability of estimating mass ratio by calculating trajectories for a large number of combinations of vehicle propulsion parameters and by presenting the results as families of curves. This is the same procedure used and described in greater detail in a previous parametric analysis of a hydrogen-fueled SSTO vehicle. (See ref. 1.) Ascent mass ratio data for virtually all parametric combinations of interest can be generated by various curve fit techniques for input to weight and sizing procedures such as those used in a nozzle optimization study for the all-hydrogen vertical take-off, horizontal landing (VTOHL) vehicle (ref. 2). In that study, the vehicle was designed for constant payload and for the appropriate ascent mass ratio for each combination of propulsion parameters.

SYMBOLS

In the case of the parameters I_{sp} and $(T/W)_o$, g is used to nondimensionalize the mixture of force and mass units that occurs when the International System of Units is used.

A^* engine nozzle throat area, m^2

A_e engine exit area, m^2

g acceleration of gravity at sea level, 9.80665 m/s^2

I_{sp} engine specific impulse, $\frac{T}{\dot{m}g}$, s

$\dot{m}$	total engine propellant mass flow rate, kg/s
m_o	initial vehicle mass, kg
m_f	burnout mass, kg
p_{sl}	sea-level atmospheric pressure, 101.325 kPa
R_e	engine thrust ratio, ratio of sea-level thrust of dual-position nozzle engines to total sea-level thrust
R_f	ratio of mass of hydrocarbon fuel and its associated liquid oxygen to total propellant mass
R_{OF}	ratio of oxidizer mass to fuel mass
R_m	ascent mass ratio, $\frac{m_o}{m_f}$
T	engine thrust, N
$(T/W)_o$	initial thrust-weight ratio, $\frac{T_{sl}}{m_o g}$
ε	engine nozzle expansion ratio, $\frac{A_e}{A^*}$

Subscripts:

H1	first position of hydrogen rocket nozzle
H2	second position of hydrogen rocket nozzle
RP	RP-1 fueled rocket nozzle
sl	sea-level conditions
vac	vacuum conditions
1	conditions at lift-off
2	conditions at nozzle transition

Abbreviations:

LH_2	liquid hydrogen
LOX	liquid oxygen
POST	program to optimize simulated trajectories
P/L	payload

RP-1 kerosene-like rocket fuel

SSME space shuttle main engine

SSTO single stage to orbit

VTOHL vertical take-off, horizontal landing

STUDY DESCRIPTION

The study consists of the results of trajectory calculations for a large number of combinations of propulsion system similarity parameters. The four basic parameters are initial nozzle expansion ratio, final nozzle expansion ratio, initial thrust-weight ratio, and the combination of single- and dual-position nozzles. There is an additional parameter for dual-fuel vehicles, the relative split between the amounts of the two fuels. The same set of parameters derived in an earlier parametric analysis (ref. 1) is used for the dual-fuel vehicles. Also, there are two dual-fuel vehicle types, series burn and parallel burn.

For the series burn, hydrocarbon fuel is burned initially with LOX at a low expansion ratio by all the engines, and, later in the trajectory, some or all the nozzles are moved to the higher expansion ratio and only hydrogen and LOX are burned. For the parallel burn, separate engines simultaneously burn hydrocarbon and hydrogen at lift-off at a low expansion ratio. Later, the nozzles of the hydrogen engines are moved to the higher expansion ratio position. In both cases, at the transition to the higher expansion ratio, the fixed-position hydrocarbon engines are shut down and the vehicle burns hydrogen exclusively.

In this paper, ascent mass ratio results are determined for various combinations of vehicle parameters for both concepts. To match trajectory results for different size vehicles of similar shape, the aerodynamic similarity parameters must also match. However, it was shown in the previous study that the results of varying the aerodynamic parameters were independent of those of the propulsion parameters (ref. 1). Thus, the variations in performance due to the aerodynamic parameters shown in the earlier study apply equally as well to the dual-fuel vehicles. Therefore, the aerodynamic parameter variations were not included in the current parametric analysis.

For this study, performance is measured by ascent mass ratio, defined as the ratio of initial mass to mass at burnout. For a given set of vehicle parameters, the configuration must be sized to the appropriate mass ratio to insure that the vehicle has the correct amount of fuel to perform the mission. This sizing process is described in more detail in the appendix.

VEHICLE DESCRIPTION

The vehicle concepts in this analysis are dual-fueled VTOHL-SSTO vehicles powered by a combination of advanced technology rockets with single- and dual-

position bell nozzles. The configurations for the concepts are similar and were derived during in-house studies at the Langley Research Center. A typical configuration is illustrated in figure 1. These studies were performed assuming that the vehicles are launched to the same initial orbit as space shuttle, 93 km by 185 km, and that, in two basic technology areas, structures and propulsion, 15-year advancements beyond the shuttle level have been made. These advancements include a 25-percent reduction in structural mass and the development of dual-position nozzles and dual-fuel engines.

For the current study, the initial mass m_o was assumed to be a constant 1 500 000 kg throughout the analysis. The engine characteristics in terms of I_{sp} were generated for use in contractural studies (ref. 3) and were varied parametrically in this study. The hydrocarbon fuel used was RP-1, a kerosene-like compound, with a mixture ratio of 2.9. The hydrogen engines used a mixture ratio of 6.0. The aerodynamic coefficients used were assumed to be those of an early shuttle orbiter design (ref. 8) and are presented in table 1. The reference area was assumed to be 850 m^2.

The individual characteristics of the two concepts, series burn and parallel burn, as they are used in this study, are now discussed as follows.

Series burn: The series burn concept uses a combination of dual-fuel engines with dual-position nozzles and single-fuel engines with single-position (fixed) bell nozzles. The rockets with fixed nozzles burn only RP-1 at a low expansion ratio. The dual-fuel engines burn RP-1 at the same expansion ratio as the fixed engines at lift-off. At some point in the trajectory, the fixed engines are shut down and the dual-fuel engine nozzles undergo transition to a higher expansion ratio and begin burning hydrogen. The expansion ratio at lift-off, the expansion ratio after transition, and the combination of the two types of engines are among the parameters varied during the current analysis.

Parallel burn: The parallel burn vehicle combines fixed-position nozzle RP-1 engines with dual-position nozzle hydrogen engines. At lift-off, the RP-1 engines burn in parallel with the hydrogen engines at low expansion ratios. At the transition point, the hydrocarbon engines are shut down, and the remaining engines continue to burn hydrogen at a higher expansion ratio. The parameters associated with this concept include the expansion ratio of the RP-1 engines, and the expansion ratios of the hydrogen engines at lift-off and after transition, and, as before, the relative thrust split between the two types of engines.

TRAJECTORY CALCULATION

The trajectories were calculated using the program to optimize simulated trajectories (designated POST) (ref. 9) by assuming a due east launch from the Kennedy Space Center. POST is a discrete parameter program having the capability to target and optimize point mass trajectories while satisfying a general user-selected set of equality and inequality constraints. In this case, the ascent propellant requirement was minimized subject to inflight inequality constraints and orbital insertion conditions. Continuous engine throttling was used to limit the total vehicle accleration to 3g. Dynamic pressure was constrained to be less than or equal to 48 kPa. The total normal force was also

limited by an upper bound of 4 MN. The altitude, velocity, and flight-path angle at trajectory termination were constrained to correspond to the perigee of a 93- by 185-km orbit. All the trajectories were divided into seven segments. The first segment was a 7-second vertical rise followed by a 13-second segment during which the vehicle pitched down at a constant rate. Within each of the remaining five segments, the vehicle was steered by a piecewise linear variation of angle of attack referenced to the inertial velocity vector of the vehicle. The lengths of the trajectory segments were determined optimally for one trajectory and were not changed during the study. At lift-off, the entire mixture of fixed- and dual-position engines was firing at low expansion ratios, the dual-position nozzles being retracted to their lower expansion ratio position. At some point in the trajectory, determined optimally by the program, when parametrically varying the basic similarity parameters, the fixed-position engines were shut down and the dual-position nozzles were extended to the high expansion ratio. The fuel split was varied by fixing the transition point at various values. The trajectory was iterated with POST by using the initial pitch rate, the values of the attitude angles at the end of each of the last five segments, and the point of nozzle transition (except when this point was used as a variable parameter) until the constraint values were within input tolerances and the optimality convergence criterion was satisfied. A typical trajectory is illustrated in figure 2.

PARAMETRIC STUDY MATRIX

The similarity parameters used in this analysis allow the results to be applied to various sizes of similar vehicle concepts and are selected by the same technique used in the previous study of a hydrogen fueled vehicle (ref. 1). Since trajectories are calculated by integrating acceleration with time, vehicles with similar acceleration profiles will have similar trajectories. The acceleration comes from three sources: gravity, vehicle aerodynamics, and the propulsion system. Since all vehicles experience the same acceleration due to gravity and, as discussed previously, aerodynamic variations were not considered in the study, only the acceleration provided by the propulsion system was used. Since the acceleration is equal to the ratio of force to mass, the desired ratio of thrust to mass must be initialized at lift-off and controlled throughout the trajectory to achieve similarity. The history of this ratio is determined by the thrust and mass flow rates of the engines which, in turn, are determined from the propulsion similarity parameters. These parameters differed somewhat between the two types of vehicles and are described.

Series Burn

The four basic similarity parameters for the series burn concept are the expansion ratio for all nozzles at lift-off ε_{RP}, the expansion ratio for all dual-position nozzles after nozzle transition ε_{H2}, initial thrust-weight ratio $(T/W)_o$, and engine thrust ratio R_e, defined as the thrust of dual-position, dual-fuel engines divided by the total thrust. Each of the similarity parameters took on three values: ε_{RP} of 20, 50, and 80; ε_{H2} of 100, 150, and 200; $(T/W)_o$ of 1.15, 1.30, and 1.45; and R_e of 0.4, 0.7, and 1.0. To include all these values, 81 trajectories were calculated. The point of nozzle transition

to the higher expansion ratio for these trajectories was determined by the trajectory program to give the maximum mass at burnout (minimum ascent mass ratio).

To define the curves further and to serve as a boundary for the data, a number of trajectories were calculated by using only hydrocarbon engines with single-position nozzles. This condition corresponds to $R_e = 0.0$ for both concepts.

Another parameter which affects the performance and mass of dual-fueled vehicles is the relative amounts of the two fuels. This parameter, the fuel ratio R_f, is defined for use in this study as the amount of RP-1 and its associated liquid oxygen (LOX) divided by the total of all consumed propellants. When varying the basic propulsion parameters, R_f was determined by the trajectory program to give minimum mass ratio. However, when this parameter was varied, it was done by using several different values for the nozzle transition point. The values used were chosen to give mostly later transition points, which gave values for R_f higher than that resulting from the minimum ascent mass ratio cases. This choice anticipates that using more of the denser hydrocarbon fuel will give a smaller, lighter vehicle. The computer resources required to vary R_f for all the 81 trajectories in the parametric study were prohibitive; therefore, certain cases were selected as being representative.

The first selected case used the midpoint values of three of the basic parameters as follows: $(T/W)_o$, 1.30; ε_{RP}, 50; and ε_{H2}, 150. Three other cases were selected in which $(T/W)_o$, ε_{RP}, and ε_{H2} were each varied in turn. Because of the strong coupling between engine combination and fuel ratio, the three values of R_e were used in these cases and the resulting 12 trajectories were selected for R_f variation. For each of these, four new values of R_f were chosen for a total of 48 additional trajectories.

Parallel Burn

Since the parallel burn concept uses hydrogen engines at a low expansion ratio in addition to hydrocarbon engines at lift-off, another variable parameter is required, namely, the initial expansion ratio of the hydrogen engines with dual-position nozzles. This parameter ε_{H1} also took on three values: 20, 50, and 80. Since the addition of a new parameter triples the number of trajectories to be calculated to 243, two actions were taken to reduce that number.

The results of the vehicle sizing in the all-hydrogen vehicle study (ref. 2) and preliminary calculations using the series burn performance data show that minimum vehicle dry mass occurs at or near a value of 1.30 for $(T/W)_o$. Therefore, the parallel burn trajectories were calculated by using only this value except for a small number of selected cases. This procedure eliminated $(T/W)_o$ as a variable parameter and reduced the required number of trajectories back to 81. Also, a value of 1.0 for R_e for the parallel burn concept means that only hydrogen engines with dual-position nozzles are used. Data for this case have been presented in the earlier parametric study (ref. 1) and are repeated herein. Eliminating one of the three values of R_e to be calculated further reduced the number of trajectory calculations to 54.

The fuel ratio R_f was varied in the same way as for the series burn vehicle and required 48 trajectories. The addition of the new parameter ϵ_{H1} requires 12 more trajectories which makes a total of 60 for this part of the study. Thus, a total of 114 trajectories were calculated for the parallel burn concept.

Trajectory Program Inputs

The values of the similarity parameters were translated into trajectory program inputs. The vacuum specific impulse was determined from the data in figure 3 which were generated for use in earlier studies (refs. 1 to 3). The equation for the vacuum thrust of each type of engine is derived as follows.

The sea-level thrust of the nozzle engines was calculated by

$$T_{sl} = \begin{cases} (1 - R_e)(T/W)_o(m_o g) & \text{(Single position)} \\ R_e(T/W)_o(m_o g) & \text{(Dual position)} \end{cases} \tag{1}$$

The vacuum thrust in terms of known values is determined from

$$T_{vac} = T_{sl} + p_{sl}A_e \tag{2}$$

and

$$T_{vac} = I_{sp,vac}\dot{m}g \tag{3}$$

where p_{sl} is sea-level atmospheric pressure and A_e is engine exit area. Substituting equation (3) into equation (2) and arranging terms gives

$$T_{vac} - \frac{T_{vac}p_{sl}A_e}{I_{sp,vac}\dot{m}g} = T_{sl}$$

or

$$T_{vac} = T_{sl}\left(1 - \frac{p_{sl}}{I_{sp,vac}}\frac{A_e}{\dot{m}g}\right)^{-1} \tag{4}$$

Substituting $A_e = A^*\epsilon$ into equation (4) gives

$$T_{vac} = T_{sl}\left(1 - p_{sl}\frac{\epsilon}{I_{sp,vac}}\frac{A^*}{\dot{m}g}\right)^{-1} \tag{5}$$

where $A^*/\dot{m}g$ is a constant for each fuel, 10.77 m^2s/MN when using hydrogen and 6.46 m^2s/MN when using RP-1. For dual-fuel engines, mass flow rate decreases after nozzle transition when the fuel is switched from RP-1 to hydrogen. Since the nozzle throat area A^* remains constant, the new flow rate is calculated as follows:

$$\dot{m}_2 = \dot{m}_1 \frac{A^*/\dot{m}_1 g}{A^*/\dot{m}_2 g} = \frac{6.46}{10.77} \dot{m}_1 = 0.60\dot{m}_1 \tag{6}$$

where

$$\dot{m}_1 = \frac{T_{vac,1}}{gI_{sp,vac,1}}$$

For the all-hydrogen dual-position nozzles, the flow rate did not change at transition. For either case, the vacuum thrust after transition is determined by

$$T_{vac,2} = \dot{m}_2 g I_{sp,vac,2} \tag{7}$$

For each nozzle, the exit area was calculated by using

$$A_e = T_{vac} \frac{\varepsilon}{I_{sp,vac}} \frac{A^*}{\dot{m}g} \tag{8}$$

RESULTS AND DISCUSSION

In all the trajectories the performance was measured by ascent mass ratio R_m defined as the ratio of initial mass to burnout mass. Performance is maximized when mass ratio is minimized. The results of the parametric study are shown by a series of curves in which R_m is plotted as a function of each of the similarity parameters. Since, for the most part, each parameter takes on only three values, the fairing of the curves is open to interpretation. However, the trends shown are established by the data and a different fairing should not have any gross effects in the application of the data.

Figure 4 shows the results for the all-hydrocarbon single-position nozzle case, which is equivalent to $R_e = 0.0$ for both the series and parallel burn vehicles. The mass ratio is strongly dependent on $(T/W)_o$ and ε_{RP}. The reduction in mass ratio for increasing $(T/W)_o$ is due to decreasing gravity losses, whereas the improvement for increasing ε_{RP} is due to an increase in specific impulse.

Series Burn

The variation of mass ratio with $(T/W)_o$ for the series burn vehicle is shown in figure 5. Again, there is the improvement in R_m with increasing $(T/W)_o$. All the curves in figure 5 are nearly parallel and indicate that the sensitivity of R_m with respect to $(T/W)_o$ is independent of ε_{RP}, ε_{H2}, and R_e. Although, the trend shown in these figures indicates that a high value for thrust-weight ratio is desirable, an integrated systems design may result in a heavier vehicle, since more or larger engines are required to achieve the higher $(T/W)_o$.

In figure 6, the strong dependence of mass ratio on the engine thrust ratio R_e is shown clearly. The decrease in R_m due to an increase in R_e is due to two factors. The bulk of the improvement comes from the higher specific impulse

due to the increased proportion of engines that switch to hydrogen fuel. Since more engines are shifted to the second position, there is a smaller drop in thrust at transition, and decreased gravity losses result. Inspection of figure 6 shows that the slopes of the curves decrease with increasing ε_{RP} since R_e has less influence when ε_{RP} and ε_{H2} are close together. Also, the curves become closer together with increasing $(T/W)_o$ since higher values of $(T/W)_o$ give changes in ε_{RP} and R_e less time to take effect. As in the case of $(T/W)_o$, the improvement in mass ratio due to increasing R_e may not lead to a lighter vehicle since dual-position nozzles weigh more than single-position nozzles.

Figure 7 shows a general decrease in R_m with respect to an increase in the initial expansion ratio ε_{RP} due to a corresponding increase in specific impulse. The curves are steeper for lower values of R_e because of the higher proportion of single-position nozzles. A comparison of figures 7(a) to 7(c) shows that mass ratio is less dependent on ε_{RP} for higher values of $(T/W)_o$, since a higher thrust-weight ratio results in an earlier nozzle transition and gives less time at the initial expansion ratio.

The decrease in mass ratio for increasing second expansion ratio ε_{H2} shown in figure 8 is due to increasing specific impulse. The curves for various values of ε_{RP} are closer together for higher values of R_e and indicate that the performance of the extended nozzles dominates as R_e approaches 1.0. For higher values of $(T/W)_o$, the curves become closer together and have less slope since a higher $(T/W)_o$ results in a shorter trajectory and gives less time for changes in expansion ratio to have an effect. An earlier observation concerning vehicle mass also applies to expansion ratio in that increasing either ε_{RP} or ε_{H2} improves mass ratio, but the associated increase in nozzle mass may tend to counteract the improvement.

The nozzle transition point was calculated by the trajectory optimization program to minimize mass ratio. The relative split between the mass of the hydrocarbon fuel and hydrogen used, represented by the fuel ratio R_f, is determined by the transition point. The relationship between R_f and the parameters $(T/W)_o$ and R_e is illustrated in figure 9. The curves of R_m as a function of R_e for various combinations of ε_{RP} and ε_{H2} would lie nearly on top of one another; thus, the slight spread due to expansion ratio is indicated by the bands on the figure. The value for R_f decreases for increasing $(T/W)_o$ and R_e since higher values for these parameters produce earlier transition times.

The insensitivity of R_f to expansion ratio is more clearly seen in figure 10, where the fuel ratio is plotted against ε_{RP}. Increasing ε_{RP} delays the transition point to take advantage of the higher specific impulse, which, in turn, causes less RP-1 to be used for the same performance level. These two processes tend to cancel one another and result in the insensitivity to ε_{RP}. The fuel ratio is only slightly more sensitive to ε_{H2}. Increased ε_{H2} advances the transition point and causes a slight reduction in R_f. The sensitivity is more pronounced at higher values of R_e because of the dominance of the higher performing extended nozzles.

By fixing the transition point at various values, the relationship between mass ratio and fuel ratio could be determined. The variation of R_m with R_f

for various combinations of the four propulsion parameters is shown in figure 11. The points connected by the dashed curve are the minimum mass ratio values plotted in the preceding figures and the remaining points are the result of varying the transition point. For any of the solid curves, where R_e is a constant, the portion to the left of the minimum is of little interest to a vehicle designer since not only is the mass ratio higher but also the lower value for R_f gives a higher proportion of hydrogen, whose low density leads to a higher volume, heavier vehicle. On the other hand, on the portion of the curve to the right of the minimum, the higher values of R_f mean a higher proportion of the dense hydrocarbon fuel, a mass advantage that may counteract the increase in mass ratio. Comparing figures 11(a) to 11(d) indicates that the relationship between R_m and R_f is not appreciably altered by changing the propulsion similarity parameters.

Parallel Burn

The relationships between mass ratio and the propulsion parameters for the parallel burn vehicle are similar to those for the series burn. The discussion of the parallel burn results will therefore concentrate on the differences shown for the two concepts and items that are unique to the parallel burn.

The variation of mass ratio with engine combination ratio for the parallel burn is shown in figure 12. The trends are the same as those shown for the series burn in figure 6(b), although the values for R_m are about 10 percent lower for the parallel burn.

The variation of mass ratio with respect to the expansion ratio of the RP-1 engines for the parallel burn vehicle is small as shown in figure 13, since the proportion of RP-1 engines is smaller than that for the series burn. The values of R_m for the case where $R_e = 1.0$ are shown as constants since there are no RP-1 engines when $R_e = 1.0$ and ε_{RP} has no meaning.

Figure 14 shows that the mass ratio is not strongly dependent on the first expansion ratio ε_{H1} of the dual-position hydrogen engines. Comparing all the curves in figure 14 indicates that the trends are not affected by changing any of the expansion ratios. The slopes of the curves are affected by R_e and become less steep with increasing R_e. When $R_e = 1.0$, the mass ratio actually increases with increasing ε_{H1}. The large nozzle exit area associated with large ε_{H1} causes a net decrease in thrust large enough to counteract the advantage of the higher specific impulse. The variation of mass ratio with final expansion ratio is shown in figure 15. The relationship is virtually the same as that shown in figure 8 for the series burn.

All the parallel burn results discussed so far have been for a thrust-weight ratio of 1.30. Since the results are insensitive to ε_{RP} and ε_{H1}, a number of trajectories were run with ε_{RP} and ε_{H1} fixed at 50 and with values of $(T/W)_o$ of 1.15, 1.30, and 1.45 for various combinations of R_e and ε_{H2}. The results are presented in figure 16 and are similar to the series burn results plotted in figure 5.

Figure 17 shows the variation of fuel ratio with R_e for the parallel burn vehicle. Curves for all combinations of the expansion ratios fall within the band shown and converge at $R_e = 1.0$ where $R_f = 0.0$ since, as discussed before, $R_e = 1.0$ means there are no RP-1 engines.

Figure 18 shows the same relationship between R_f and ε_{RP} that exists for the series burn case illustrated in figure 10. Comparing all the curves in figure 18 shows that R_f is virtually insensitive to ε_{RP}, ε_{H1}, and ε_{H2}. The fuel ratio is affected by $(T/W)_o$, as shown in figure 19. Higher values of thrust-weight ratio tend to cause an earlier transition point and thus a smaller amount of RP-1 fuel is used. The fuel ratio was varied in the same manner as for the series burn case and the results, shown in figure 20, are similar.

CONCLUDING REMARKS

A data base of ascent performance calculations has been developed for two vertically launched, dual-fueled, single-stage Earth-to-orbit vehicle concepts. These data were obtained by systematically varying a set of similarity parameters based on the vehicle propulsion characteristics and calculating a trajectory for each combination of parameters. The similarity parameters were initial thrust-weight ratio $(T/W)_o$; the proportion of the thrust due to engines with dual-position nozzles R_e; expansion ratio of the hydrocarbon engines ε_{RP}; first expansion ratio of the hydrogen engines ε_{H1} (used for parallel burn concept only); second expansion ratio of the hydrogen engines ε_{H2}; and fuel ratio R_f. The data base provides a means of rapidly estimating the performance of this type of vehicle in terms of ascent mass ratio and is intended for use as an integral part of a design process.

The ascent mass ratio for both types of vehicles was shown to be strongly dependent on $(T/W)_o$, R_e, and ε_{H2}, in all cases decreasing as the value of these parameters increase. For $(T/W)_o$, this trend comes from reduced gravity losses as $(T/W)_o$ increases. Larger values of R_e and ε_{H2} give greater specific impulse directly resulting in a lower mass ratio.

For small values of R_e, increasing ε_{RP} slightly reduced the mass ratio for both the series and parallel burn vehicles. This trend diminished with large values of R_e and, in the parallel burn case, disappeared entirely. The performance of the parallel burn concept was likewise insensitive to ε_{H1}.

The optimum fuel ratio decreased with increasing $(T/W)_o$ and R_e and was nearly independent of the expansion ratios. Varying R_f from the optimum had a large effect on mass ratio for both vehicles. A minimum weight vehicle may have a fuel ratio larger than that required for minimum mass ratio because of the favorable effect of higher fuel density.

Langley Research Center
National Aeronautics and Space Administration
Hampton, VA 23665
November 10, 1977

APPENDIX

USE OF ASCENT MASS RATIO IN VEHICLE SIZING

One technique for sizing single-stage-to-orbit vehicles is to assume a baseline geometric shape and photographically change the vehicle size until the volume is just sufficient to contain the correct amount of fuel to achieve the desired mission. The process is iterative, in that a number of estimates of the volume required are made before it converges to a solution.

For each succeeding estimate of fuel mass and volume, the vehicle mass must be calculated. First, the component masses, except for engine mass, are calculated from mass estimating relationships based on volume. An estimate is then made of the gross mass of the vehicle from the masses of the components, payload, and fuel. The thrust required to give the desired lift-off thrust-weight ratio is calculated; this thrust then determines the mass of the engines, which in turn is added to the gross mass calculation. The actual lift-off thrust-weight ratio is calculated and compared with the desired value. If the two values are not equal, the thrust and associated engine mass are adjusted iteratively until the desired thrust-weight ratio is achieved.

The ascent mass ratio R_m defined as the ratio of initial mass to mass at burnout (m_o/m_f) is used to calculate the amount of fuel required to perform the mission (Fuel mass = $m_o(1 - 1/R_m)$). If the fuel mass estimate is equal to the fuel mass required, then the vehicle is sized. If not, another estimate of fuel mass and volume is made and the process is repeated until it converges.

To assess the effect of various propulsion system parameters on the vehicle mass, various combinations of the parameters can be used. The appropriate mass ratio for each combination is determined from the trajectory parametric study. The entire sizing logic may be automated by a computer program according to the following flow chart:

APPENDIX

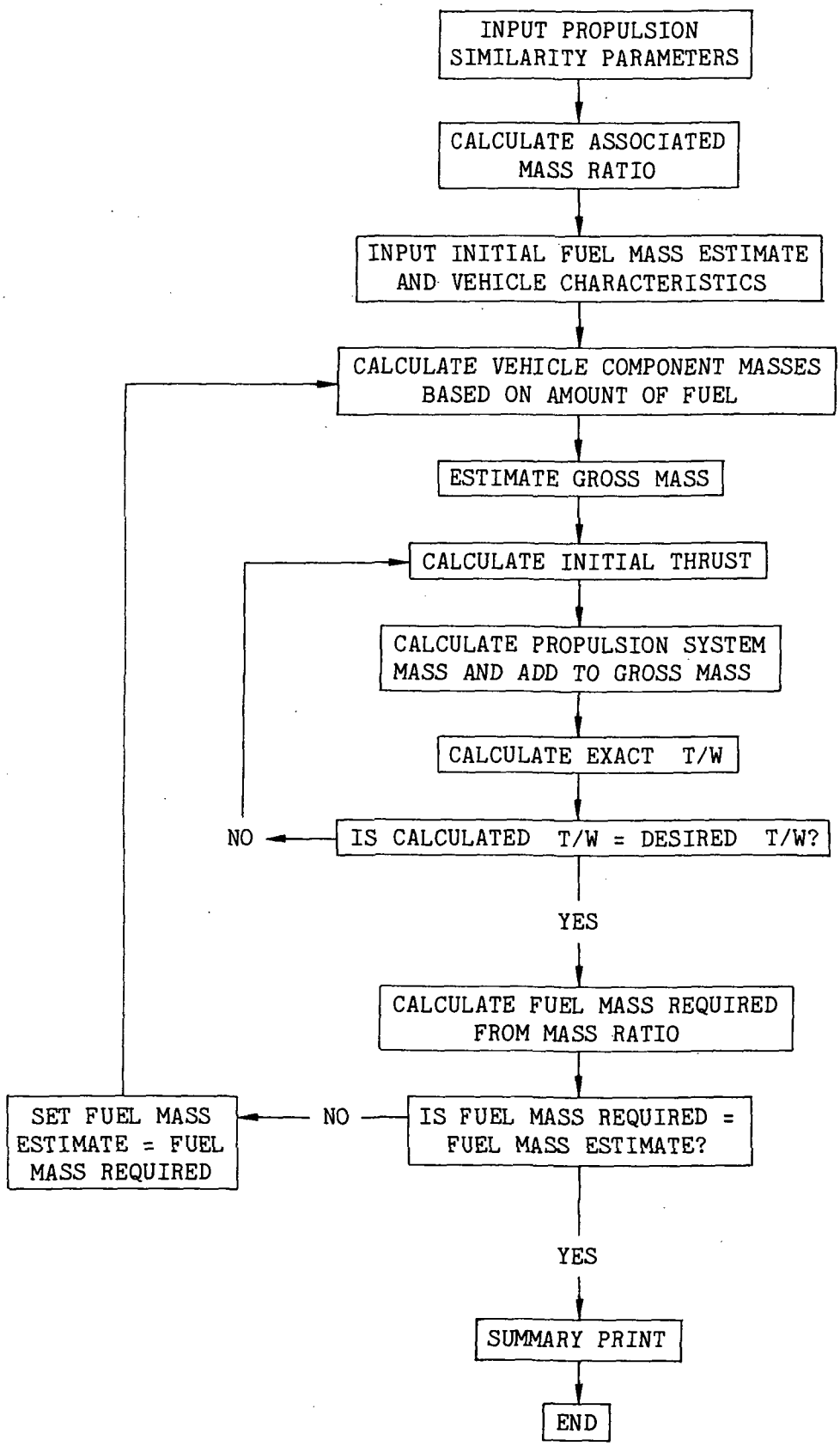
INPUT PROPULSION SIMILARITY PARAMETERS
CALCULATE ASSOCIATED MASS RATIO
INPUT INITIAL FUEL MASS ESTIMATE AND VEHICLE CHARACTERISTICS
CALCULATE VEHICLE COMPONENT MASSES BASED ON AMOUNT OF FUEL
ESTIMATE GROSS MASS
CALCULATE INITIAL THRUST
CALCULATE PROPULSION SYSTEM MASS AND ADD TO GROSS MASS
CALCULATE EXACT T/W
IS CALCULATED T/W = DESIRED T/W?
NO
YES
CALCULATE FUEL MASS REQUIRED FROM MASS RATIO
IS FUEL MASS REQUIRED = FUEL MASS ESTIMATE?
NO
SET FUEL MASS ESTIMATE = FUEL MASS REQUIRED
YES
SUMMARY PRINT
END

REFERENCES

1. Rehder, John J.: Parametric Study of Ascent Performance of a Vertically Launched Hydrogen-Fueled Single-Stage Reusable Transport. NASA TP-1045, 1977.

2. Eldred, Charles H.; Rehder, John J.; and Wilhite, Alan W.: Nozzle Selection for Optimized Single-Stage Shuttles. [Preprint] IAF-76-162, Oct. 1976.

3. Haefeli, Rudolph C.; Littler, Ernest G.; Hurley, John B.; and Winter, Martin G.: Technology Requirements for Advanced Earth-Orbital Transportation Systems. Final Report. NASA CR-2866, 1977.

4. Salkeld, Robert: Mixed-Mode Propulsion for the Space Shuttle. Astronaut. & Aeronaut., vol. 9, no. 8, Aug. 1971, pp. 52-58.

5. Salkeld, Robert; and Beichel, Rudi: Reusable One-Stage-to-Orbit Shuttles: Brightening Prospects. Astronaut. & Aeronaut., vol. 11, no. 6, June 1973, pp. 48-58.

6. Henry, Beverly Z.; and Decker, John P.: Future Earth Orbit Transportation Systems/Technology Implications. Astronaut. & Aeronaut., vol. 14, no. 9, Sept. 1976, pp. 18-28.

7. Martin, James A.: Optimal Dual-Fuel Propulsion for Minimum Inert Weight or Minimum Fuel Cost. AIAA Paper 73-1246, Nov. 1973.

8. Rainey, Robert W.; Ware, George M.; Powell, Richard W.; Brown, Lawrence W.; and Stone, David R.: Grumman H-33 Space Shuttle Orbiter Aerodynamic and Handling-Qualities Study. NASA TN D-6948, 1972.

9. Brauer, G. L.; Cornick, D. E.; and Stevenson, R.: Capabilities and Applications of the Program To Optimize Simulated Trajectories (POST). NASA CR-2770, 1977.

TABLE 1.- VEHICLE AERODYNAMIC COEFFICIENTS

Mach number	Lift coefficient at an angle of attack, deg, of -						
	-2	0	2	6	10	15	20
0.25	-0.070	0	0.070	0.215	0.370	0.555	0.715
.60	-.070	0	.070	.215	.370	.530	.660
.80	-.070	0	.070	.215	.375	.490	.560
.90	-.085	0	.085	.240	.400	.520	.600
.95	-.085	0	.085	.240	.400	.570	.695
1.20	-.085	0	.085	.220	.350	.495	.640
1.60	-.060	.010	.070	.165	.270	.420	.560
1.90	-.070	-.020	.040	.140	.240	.375	.520
2.16	-.070	-.030	.020	.120	.225	.350	.490
2.86	-.085	-.040	.005	.100	.195	.310	.425
3.95	-.100	-.055	-.010	.075	.160	.270	.380
4.63	-.105	-.065	-.020	.065	.150	.255	.360
5.96	-.090	-.070	-.045	.020	.110	.220	.330
10.20	-.070	-.060	-.045	.005	.090	.205	.315
20.30	-.070	-.060	-.045	.005	.090	.200	.300

Mach number	Drag coefficient at an angle of attack, deg, of -						
	-2	0	2	6	10	15	20
0.25	0.020	0.019	0.020	0.028	0.043	0.085	0.170
.60	.025	.024	.025	.039	.058	.123	.250
.80	.026	.025	.026	.039	.074	.146	.235
.90	.034	.033	.034	.057	.107	.186	.286
.95	.071	.070	.071	.081	.133	.248	.397
1.20	.106	.105	.106	.120	.170	.268	.400
1.60	.100	.095	.100	.114	.159	.240	.370
1.90	.100	.100	.095	.102	.133	.188	.283
2.16	.095	.095	.090	.100	.120	.170	.258
2.86	.085	.080	.085	.090	.105	.151	.220
3.95	.083	.079	.078	.081	.090	.132	.197
4.65	.081	.081	.076	.080	.088	.124	.186
5.96	.078	.077	.076	.075	.080	.107	.169
10.20	.074	.069	.075	.073	.075	.105	.168
20.30	.070	.067	.073	.072	.072	.100	.154

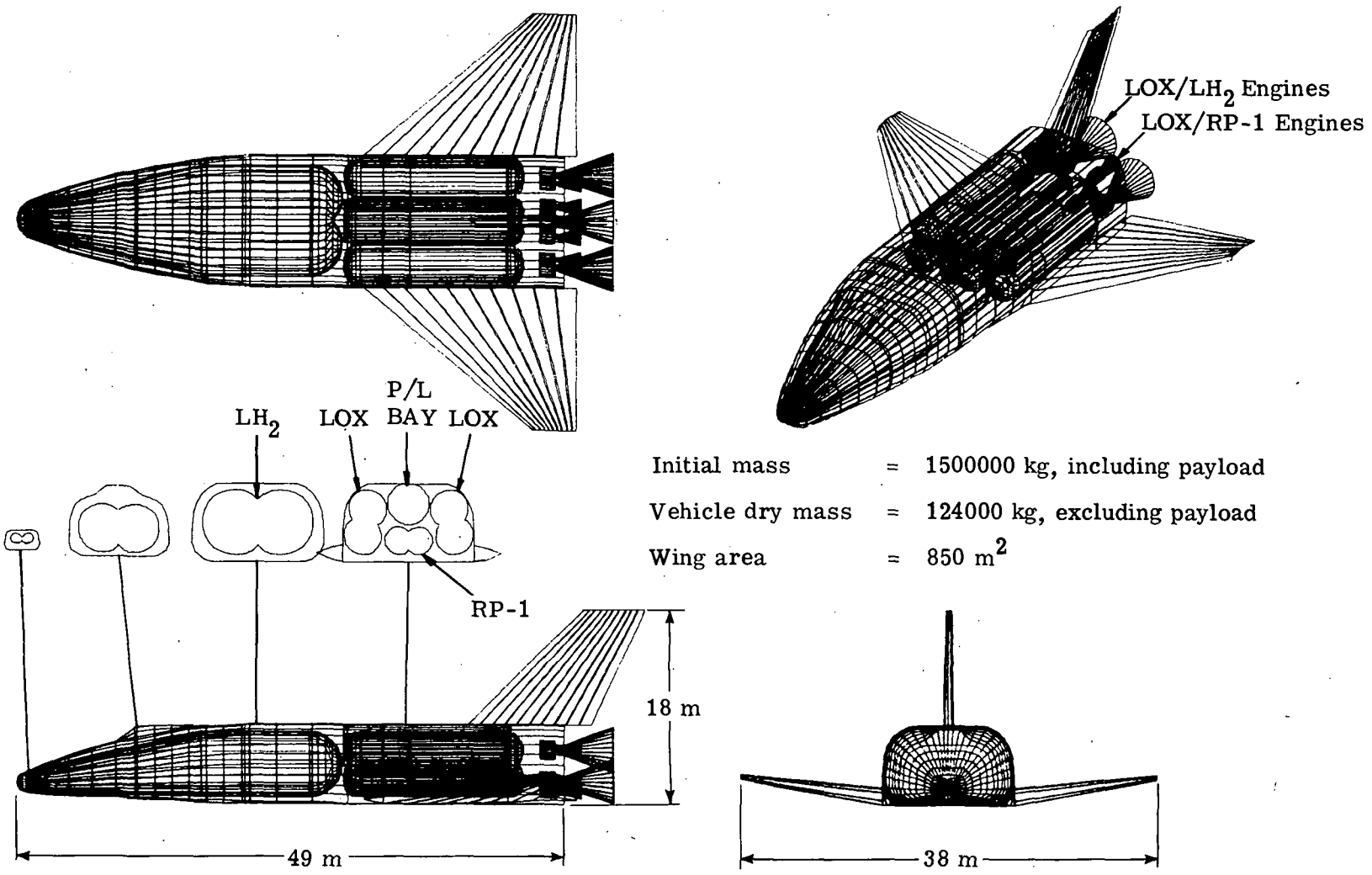

Figure 1.- VTOHL-SSTO configuration. Dual fuel.

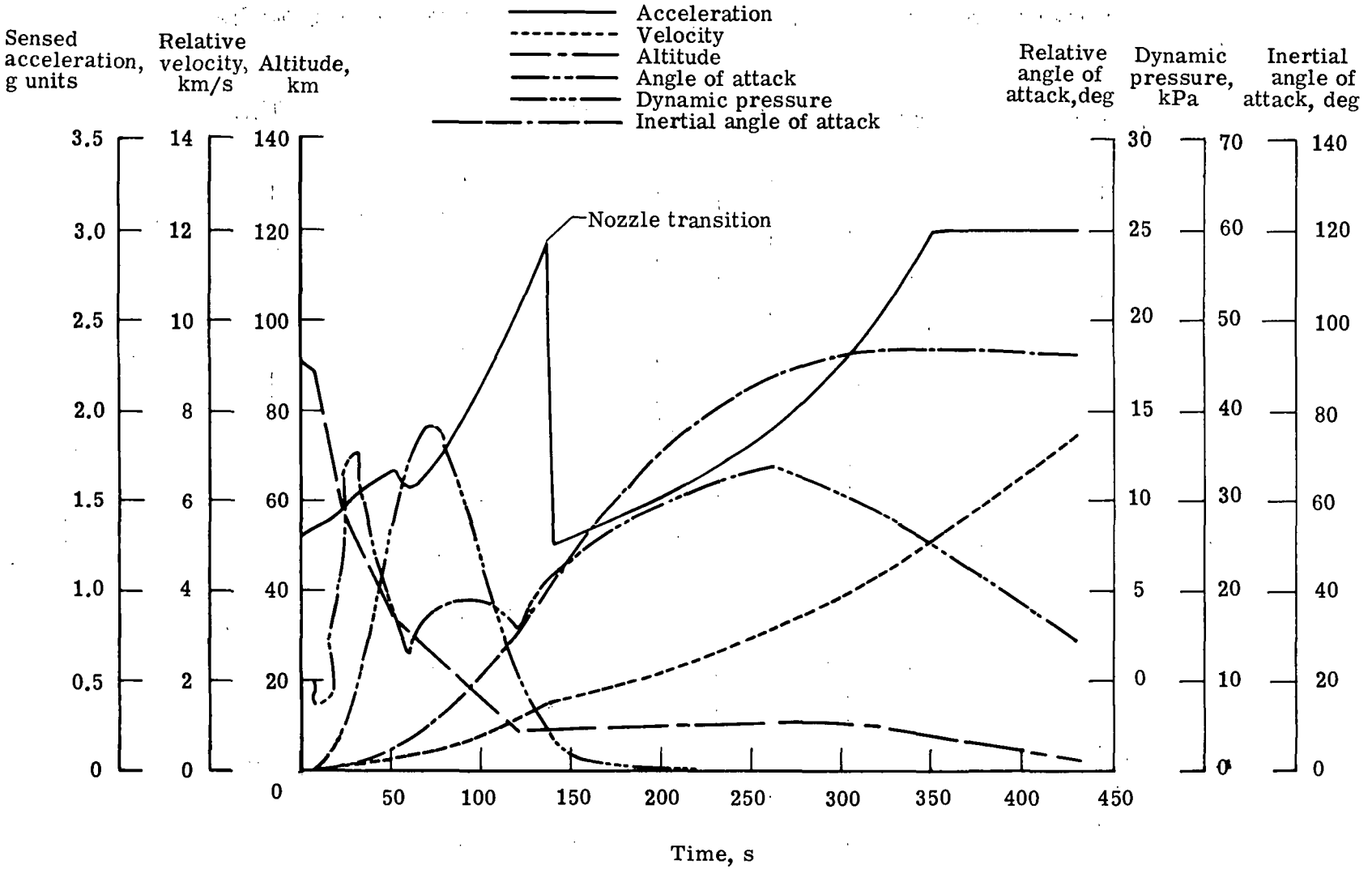

Figure 2.- Ascent trajectory parameters. Parallel burn; $\epsilon_{RP} = 50$; $\epsilon_{H1} = 50$; $\epsilon_{H2} = 150$; $(T/W)_o = 1.30$; $R_e = 0.4$.

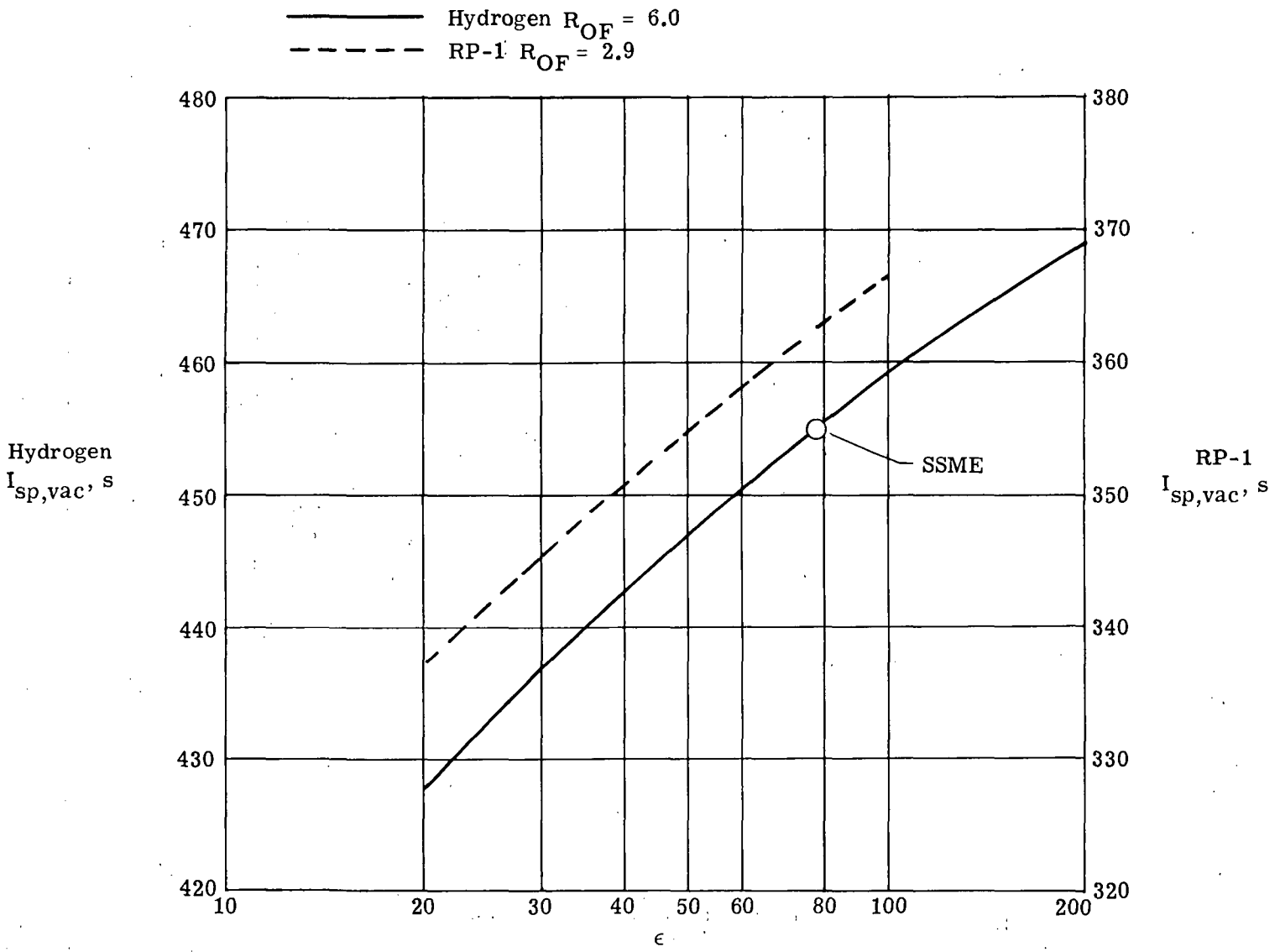

Figure 3.- Variation of vacuum specific impulse with expansion ratio.

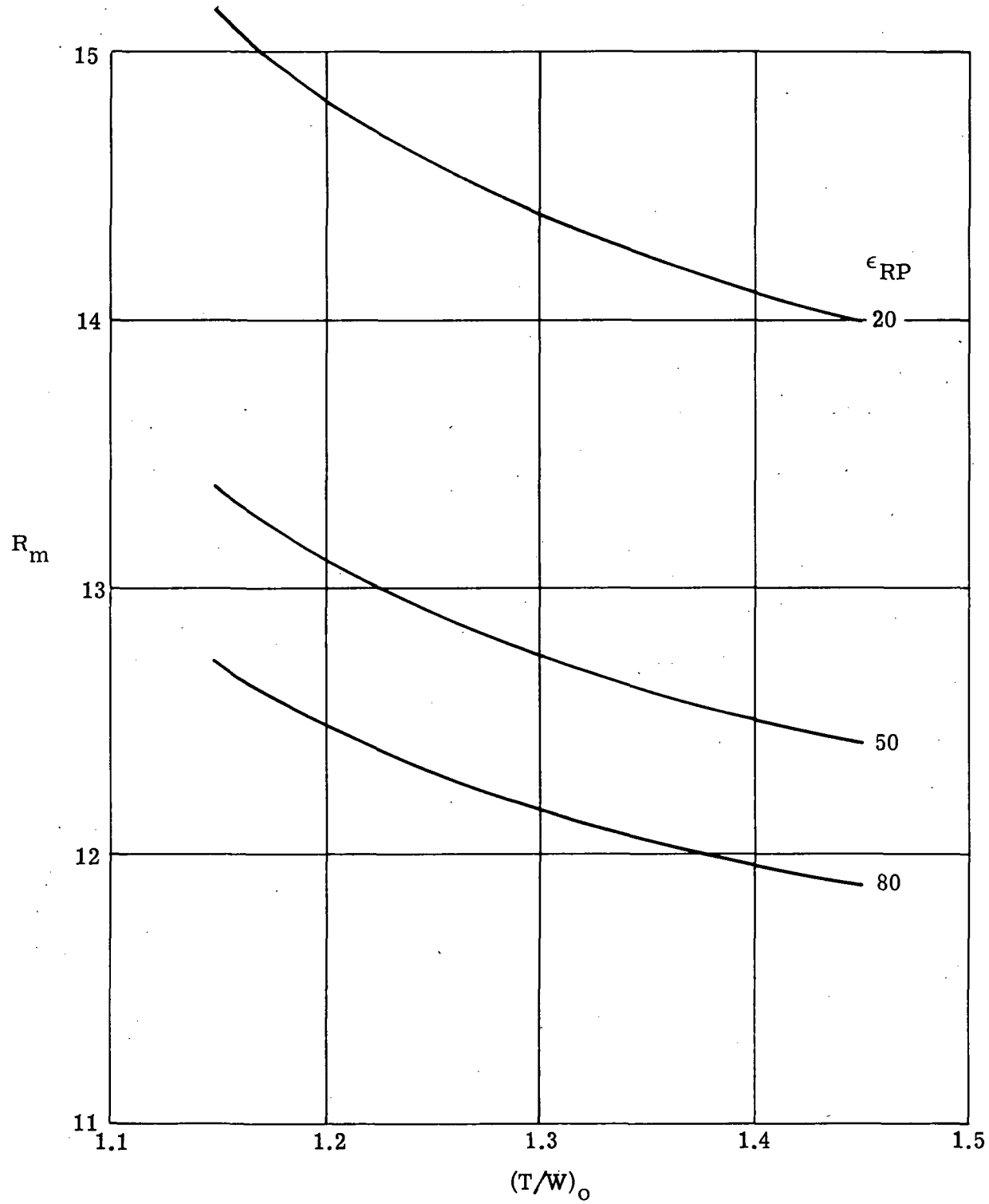

Figure 4.- Variation of mass ratio with initial thrust-weight ratio for all single position RP-1 engines. R_e = 0.

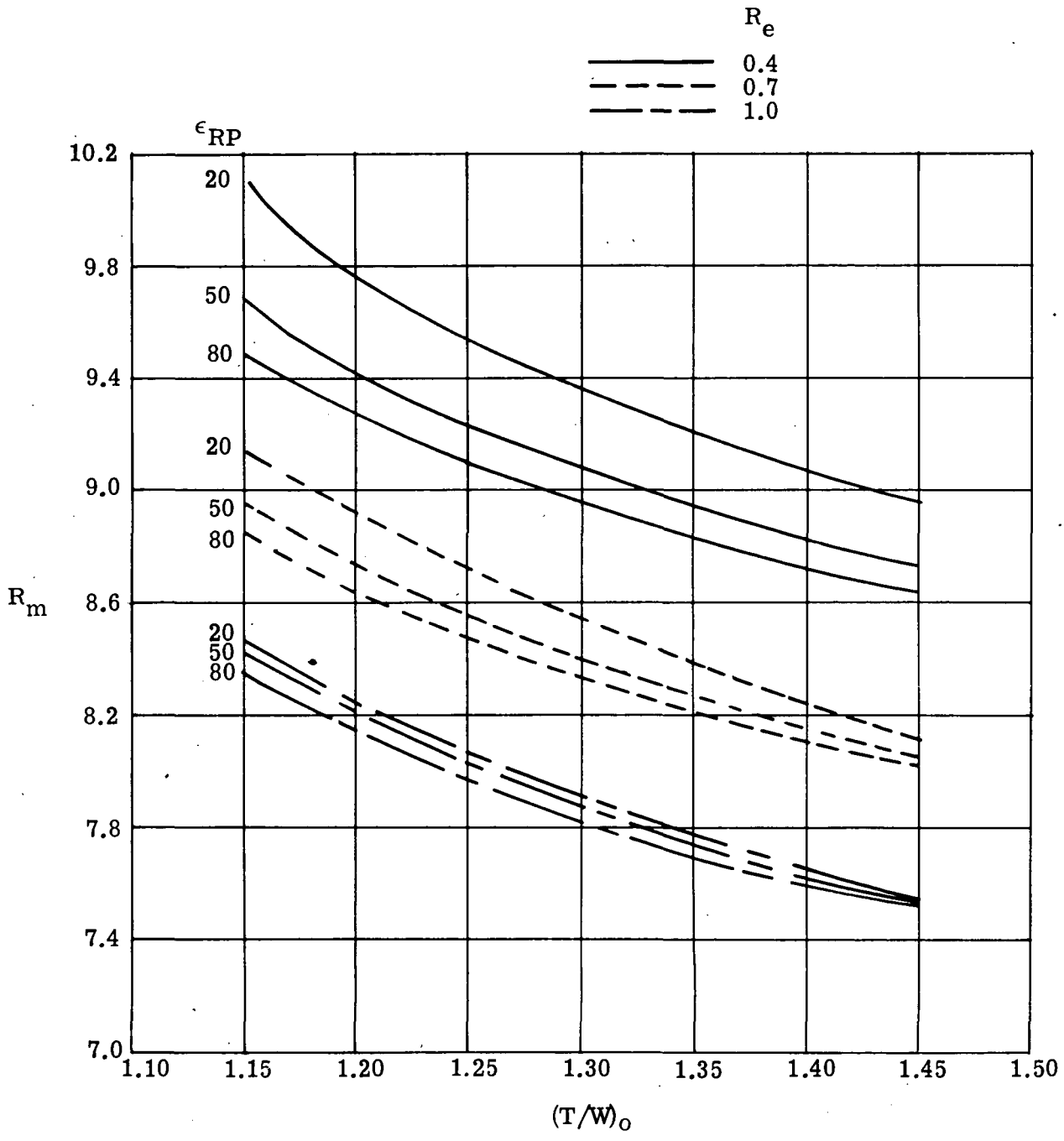

(a) $\epsilon_{H2} = 100.$

Figure 5.- Variation of mass ratio with initial thrust-weight ratio. Series burn.

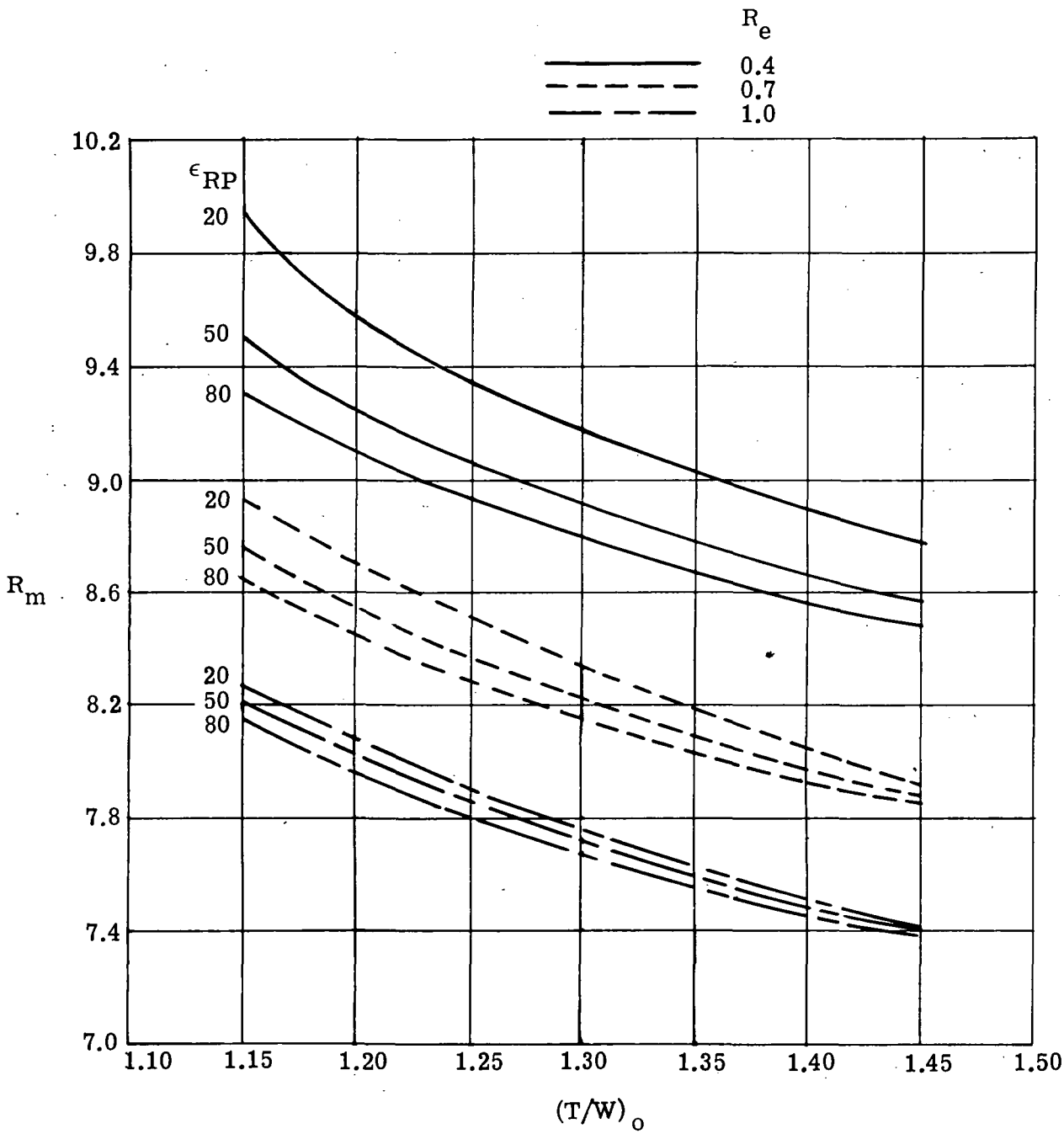

(b) $\epsilon_{H2} = 150.$

Figure 5.- Continued.

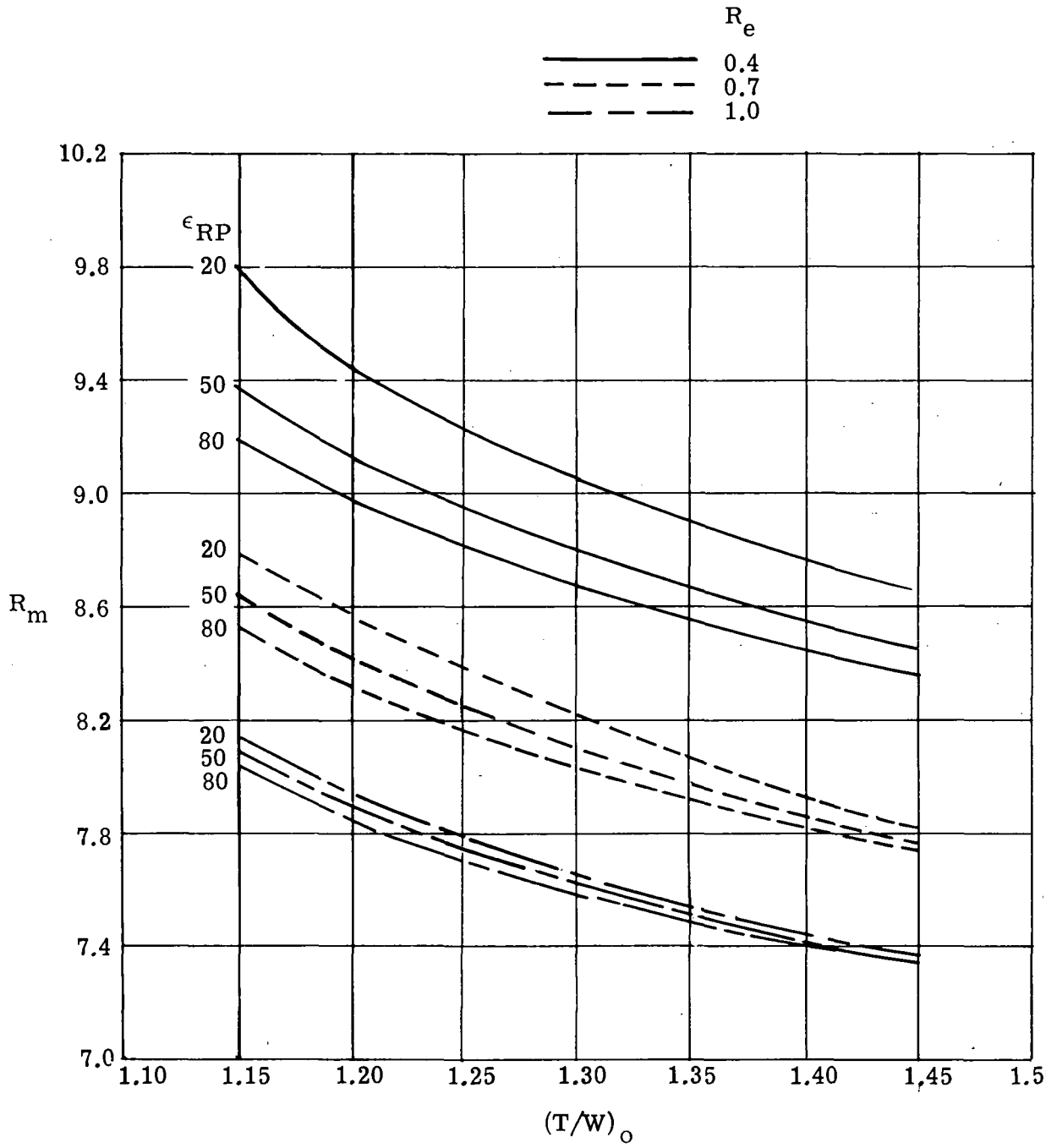

(c) $\varepsilon_{H2} = 200.$

Figure 5.- Concluded.

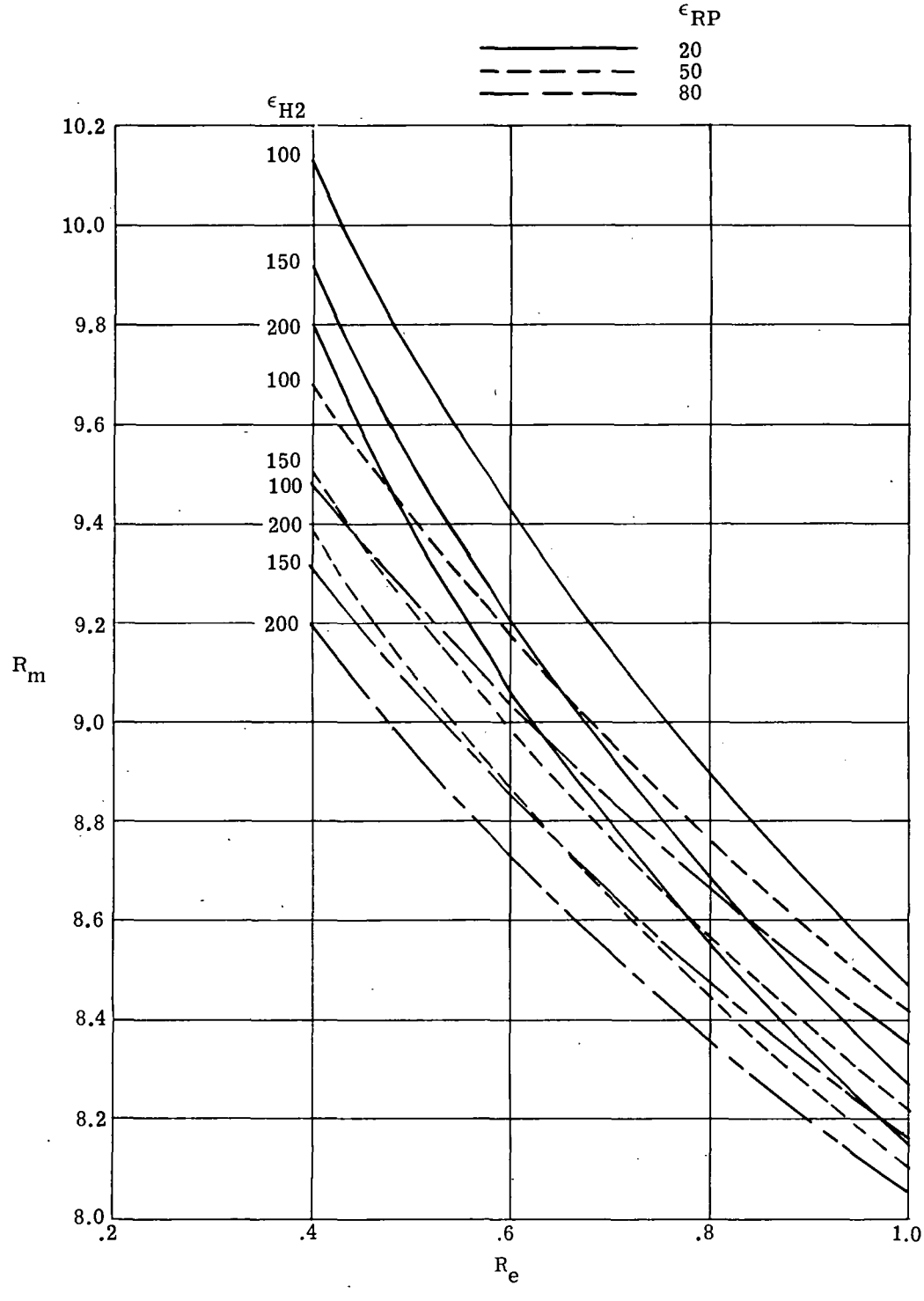

(a) $(T/W)_o = 1.15$.

Figure 6.- Variation of mass ratio with engine thrust ratio. Series burn.

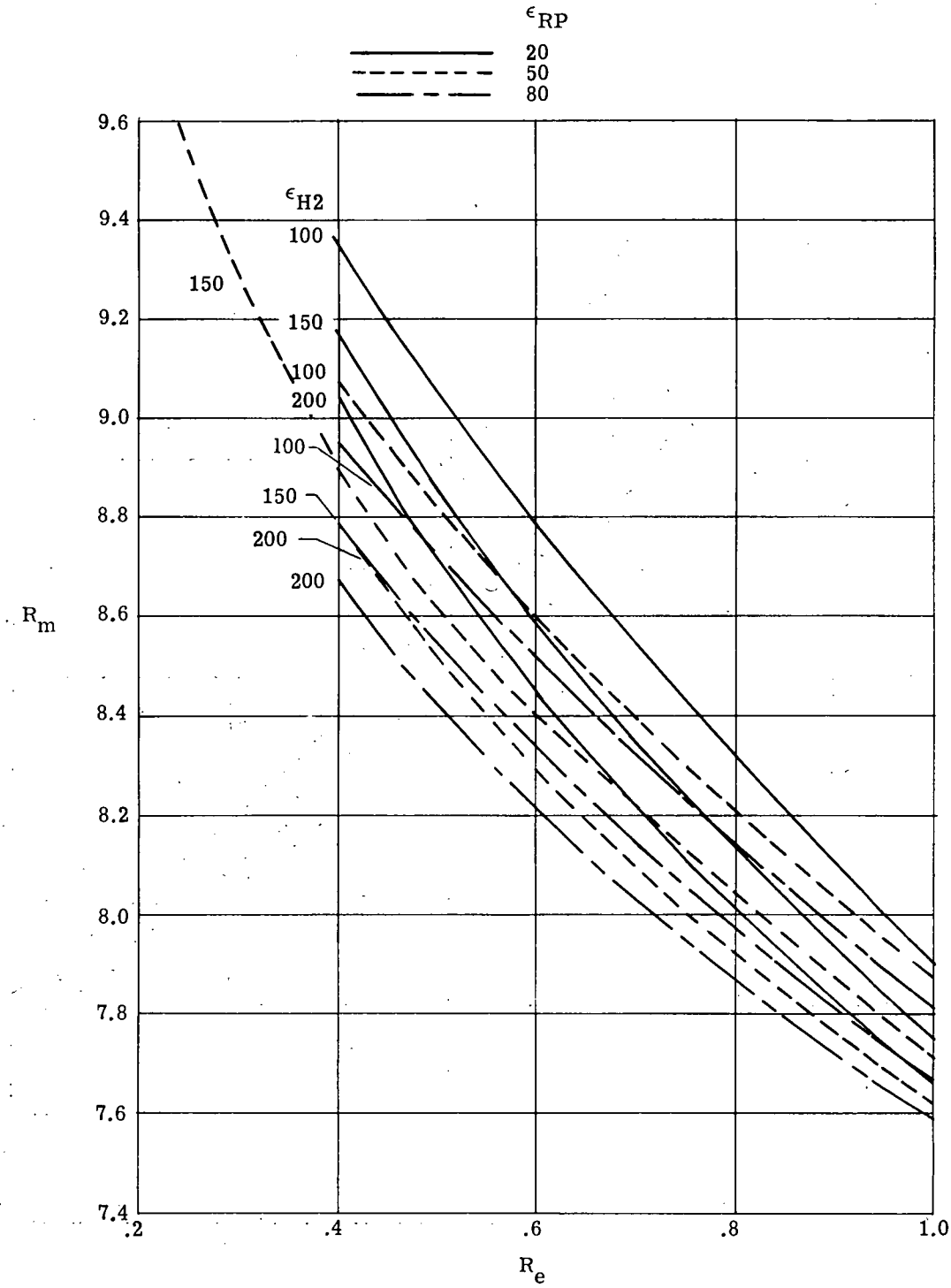

(b) $(T/W)_o = 1.30$.

Figure 6.- Continued.

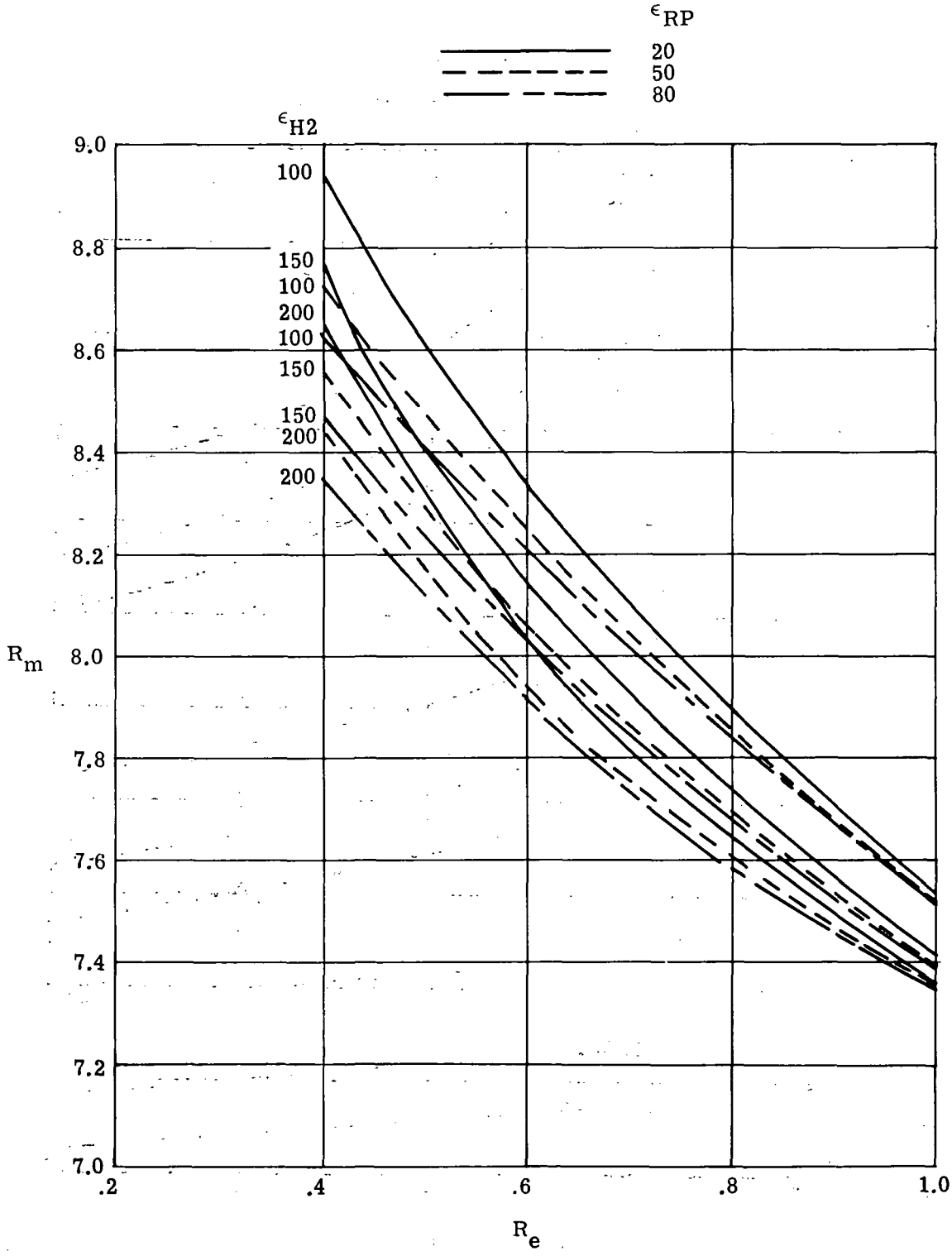

(c) $(T/W)_o = 1.45$.

Figure 6.- Concluded.

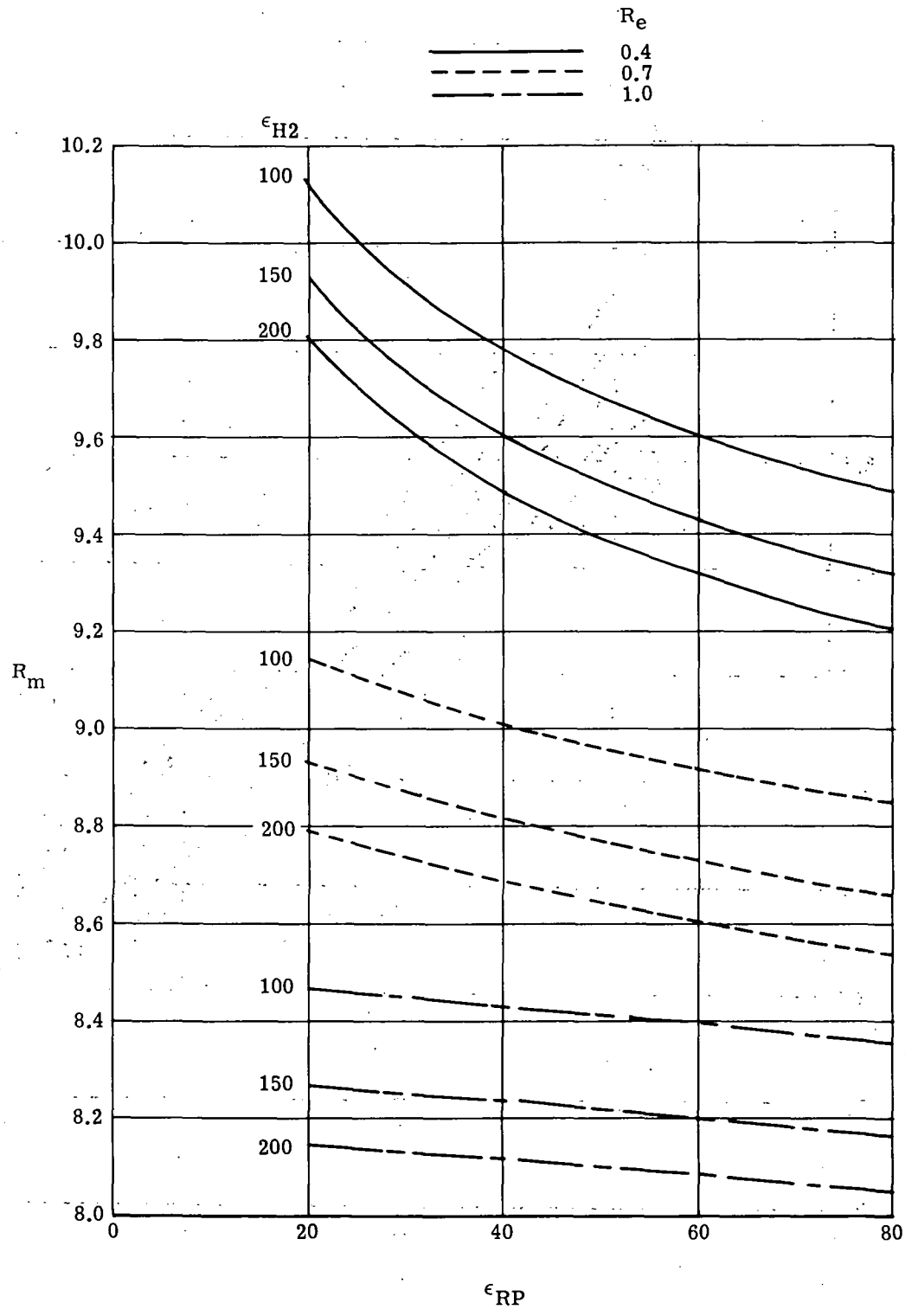

(a) $(T/W)_o = 1.15$.

Figure 7.- Variation of mass ratio with initial expansion ratio. Series burn.

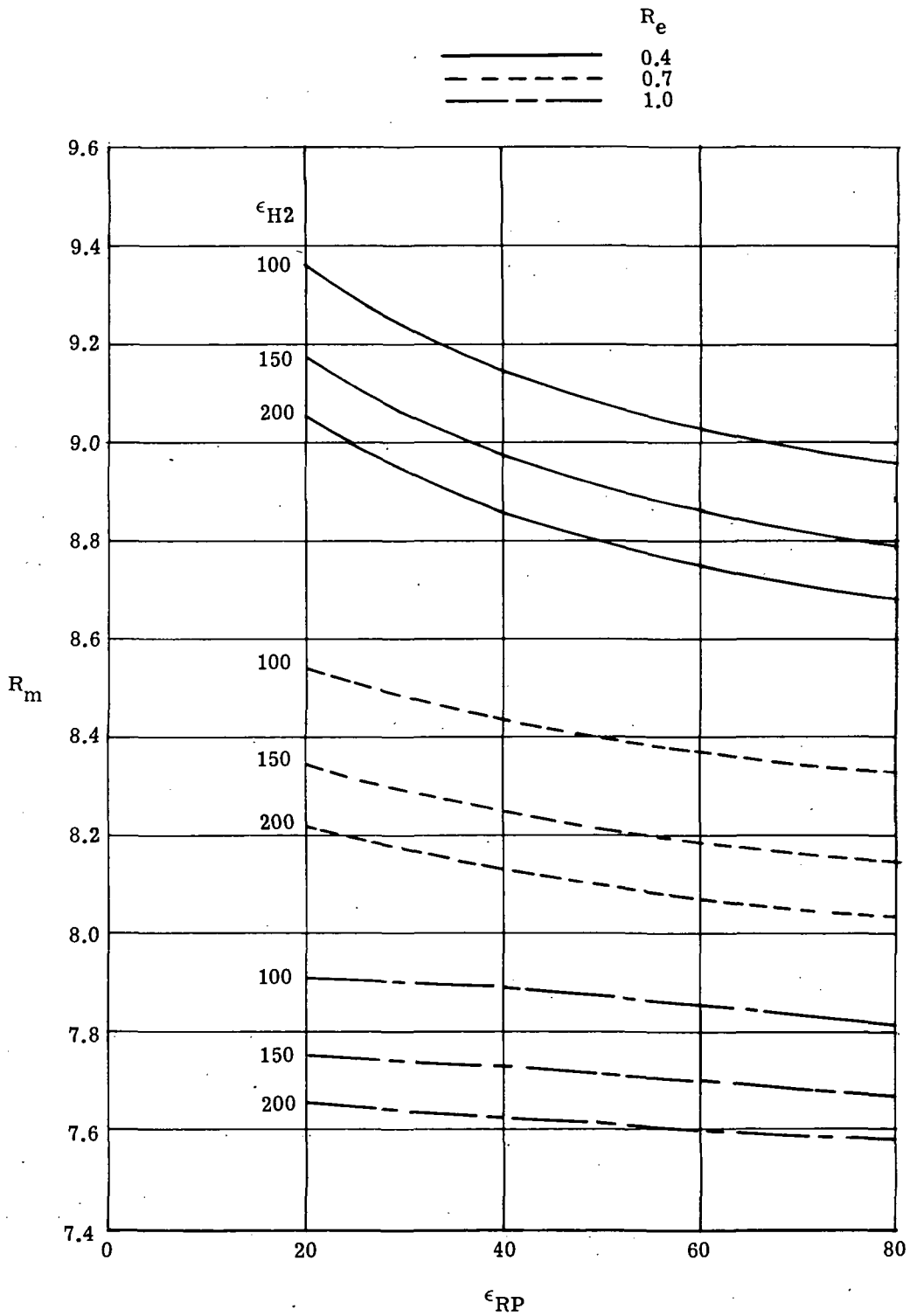

(b) $(T/W)_o$ = 1.30.

Figure 7.- Continued.

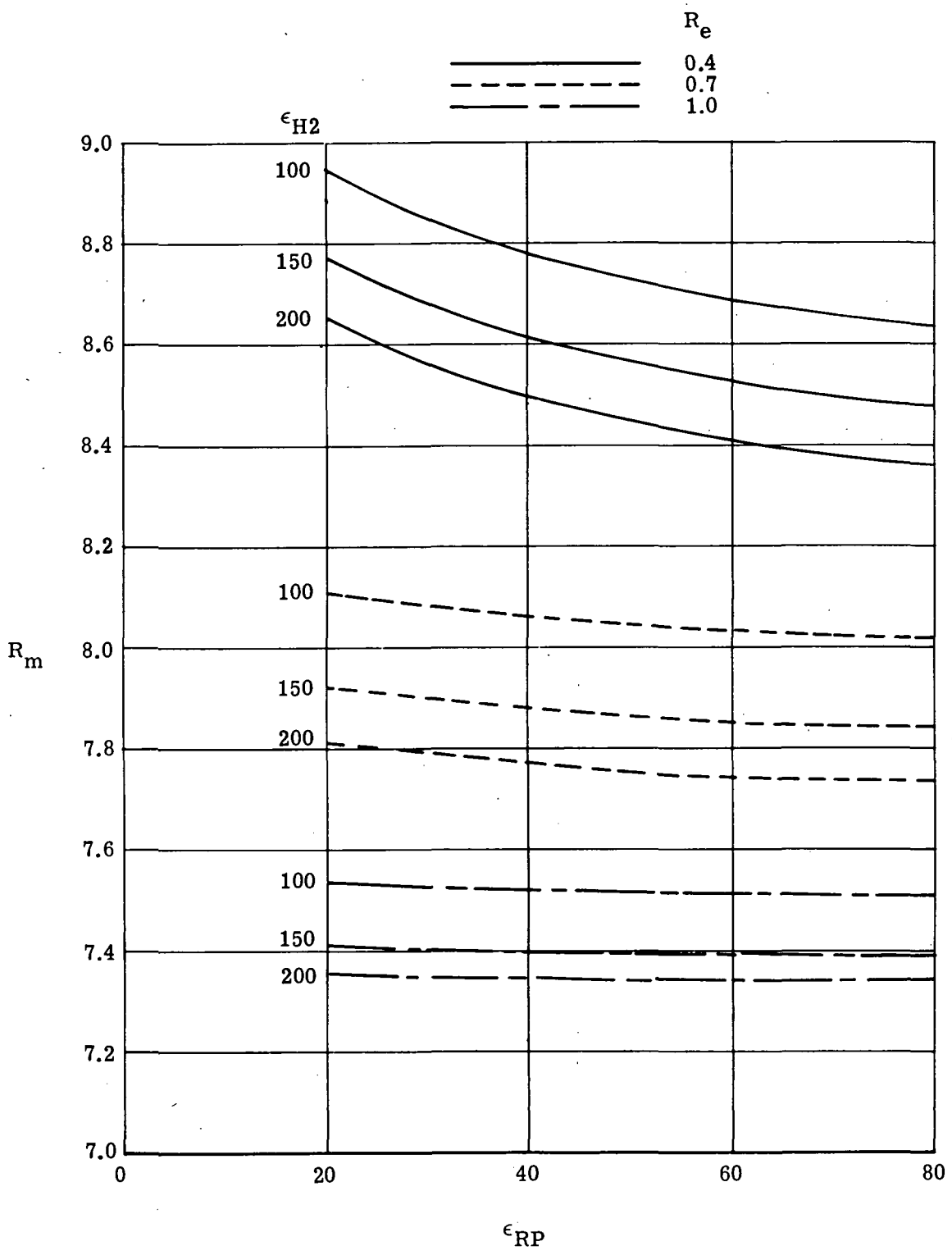

(c) $(T/W)_o = 1.45$.

Figure 7.- Concluded.

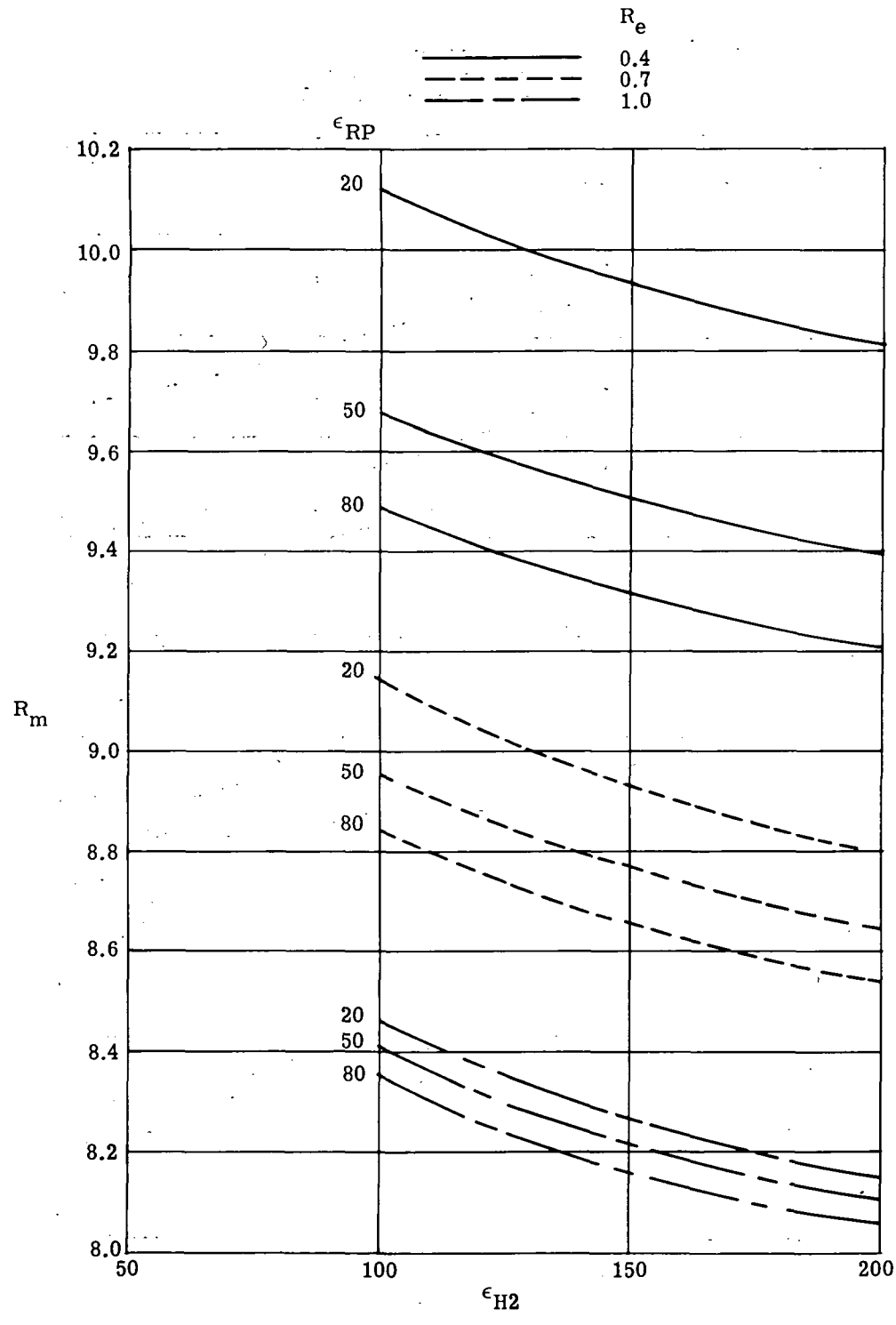

(a) $(T/W)_o = 1.15$.

Figure 8.- Variation of mass ratio with second expansion ratio. Series burn.

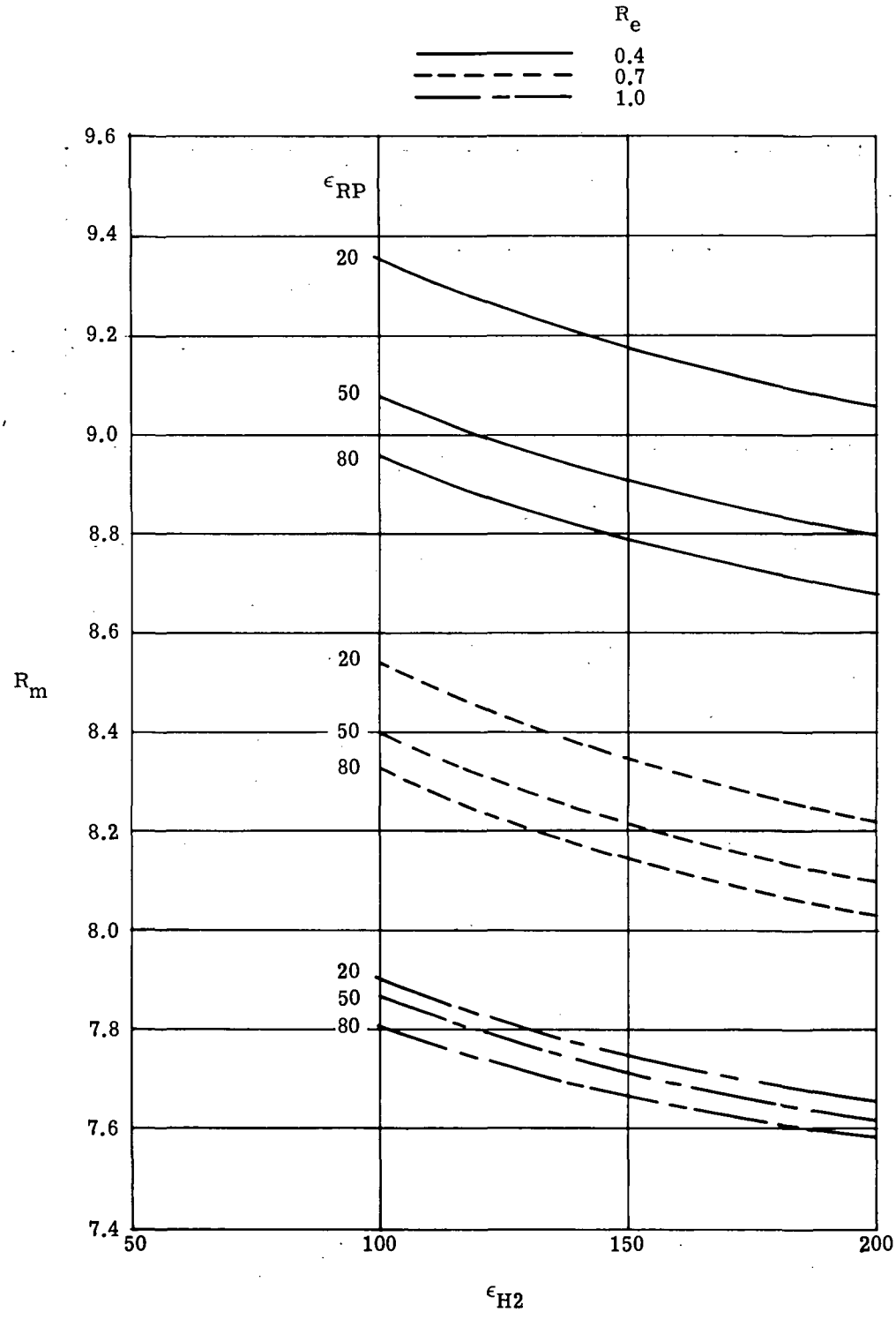

(b) $(T/W)_o = 1.30$.

Figure 8.- Continued.

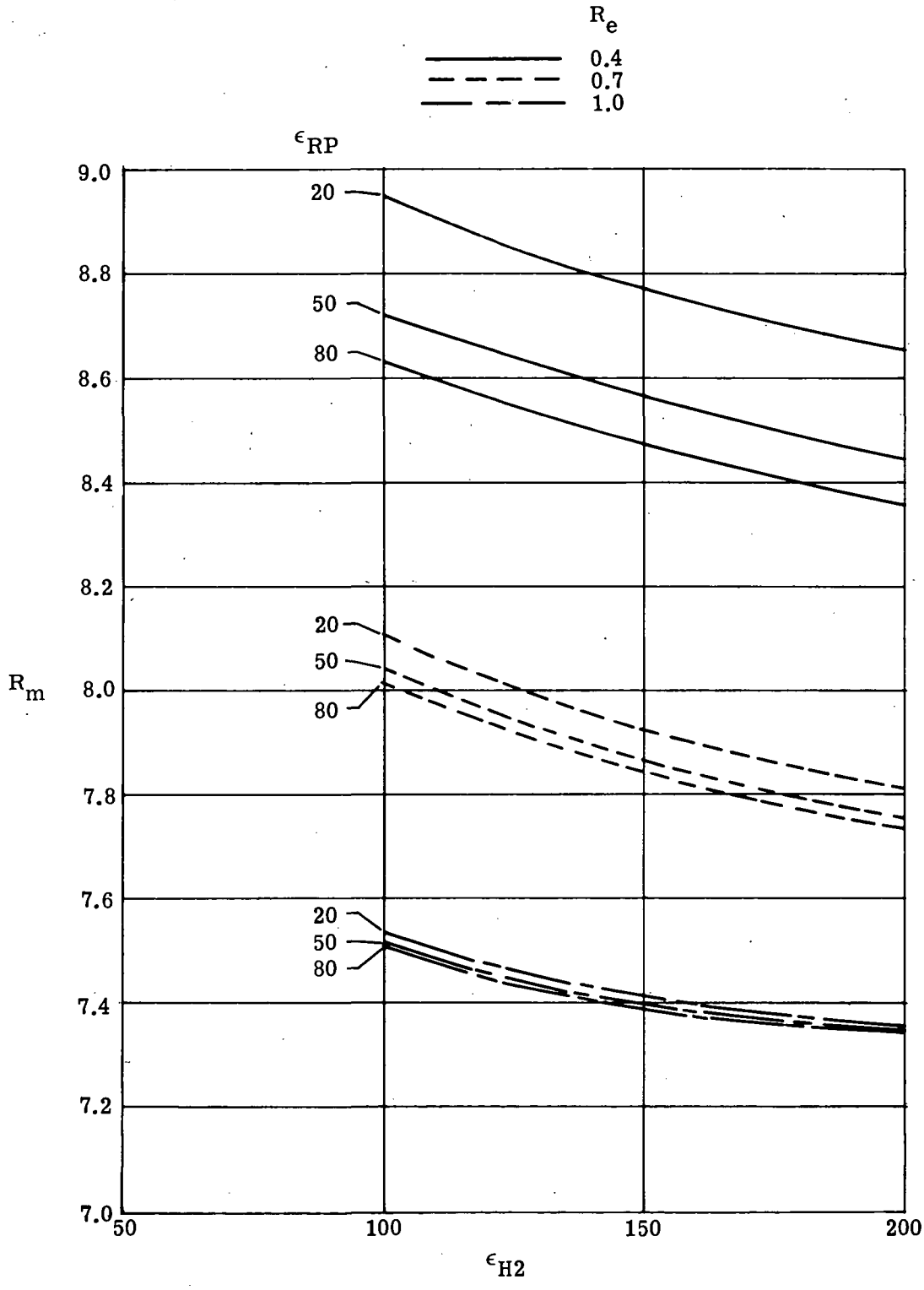

(c) $(T/W)_o = 1.45$.

Figure 8.- Concluded.

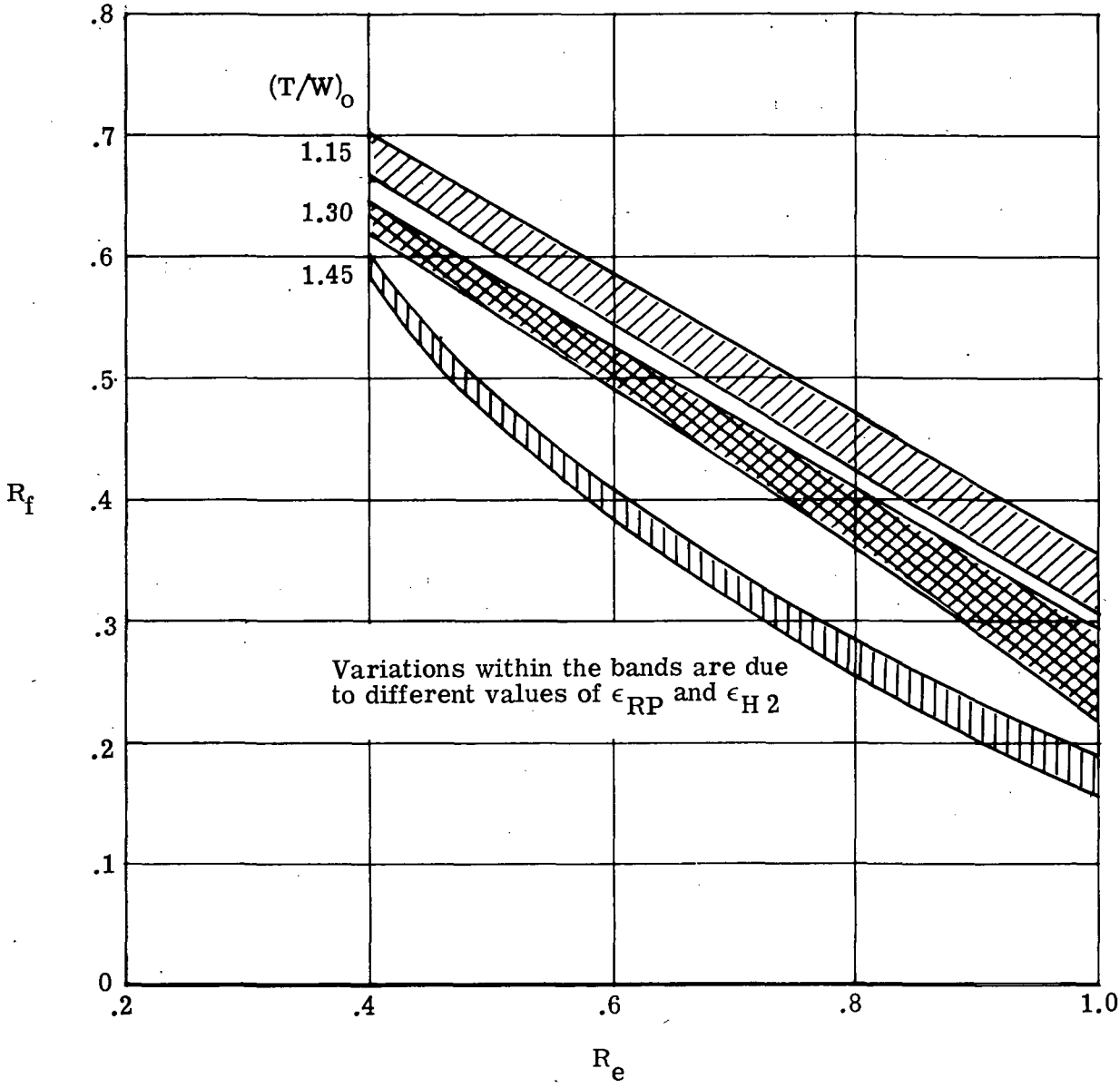

Figure 9.- Variation of fuel ratio with engine thrust ratio. Series burn.

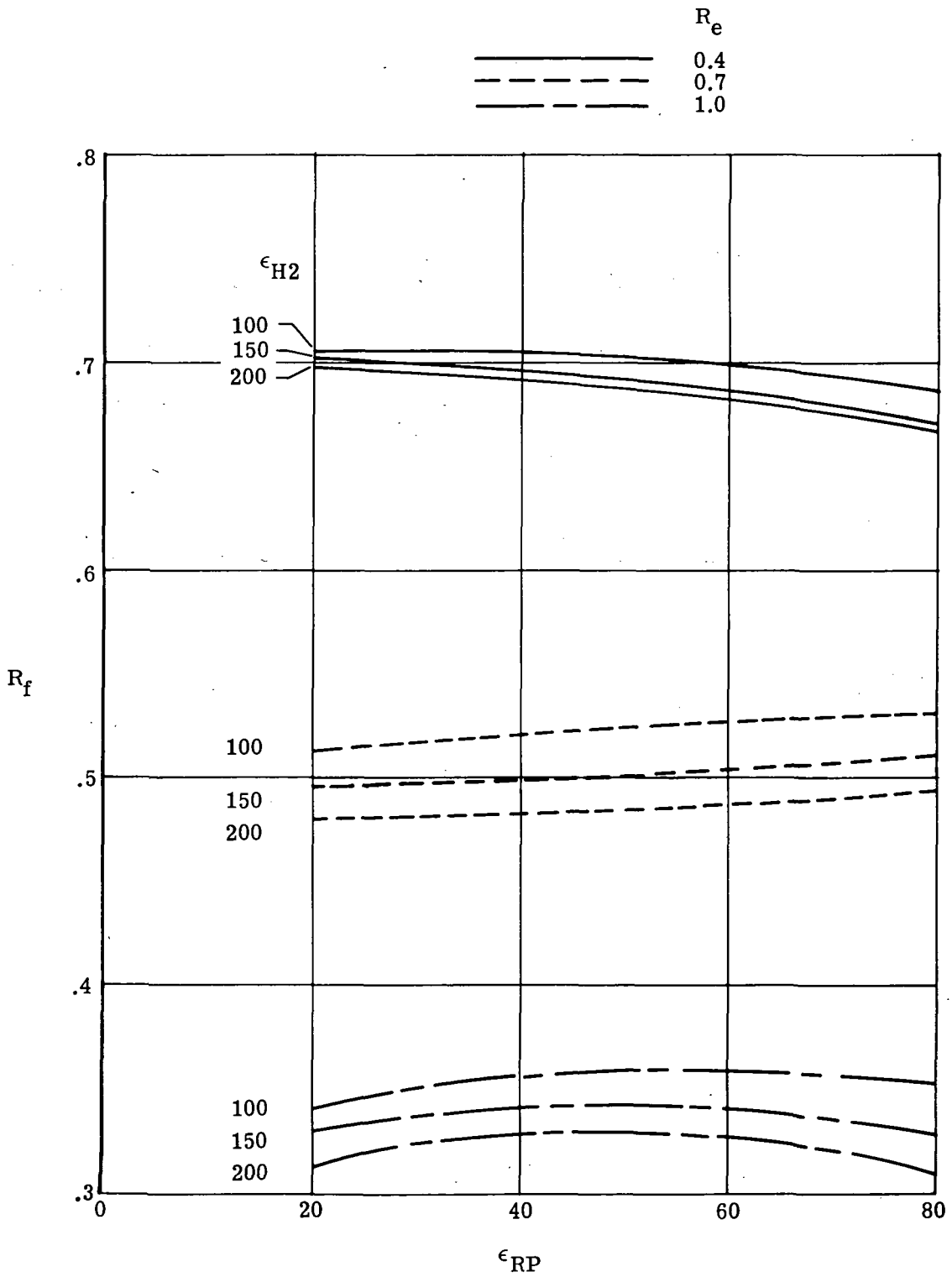

(a) $(T/W)_o = 1.15$.

Figure 10.- Variation of fuel ratio with initial expansion ratio. Series burn.

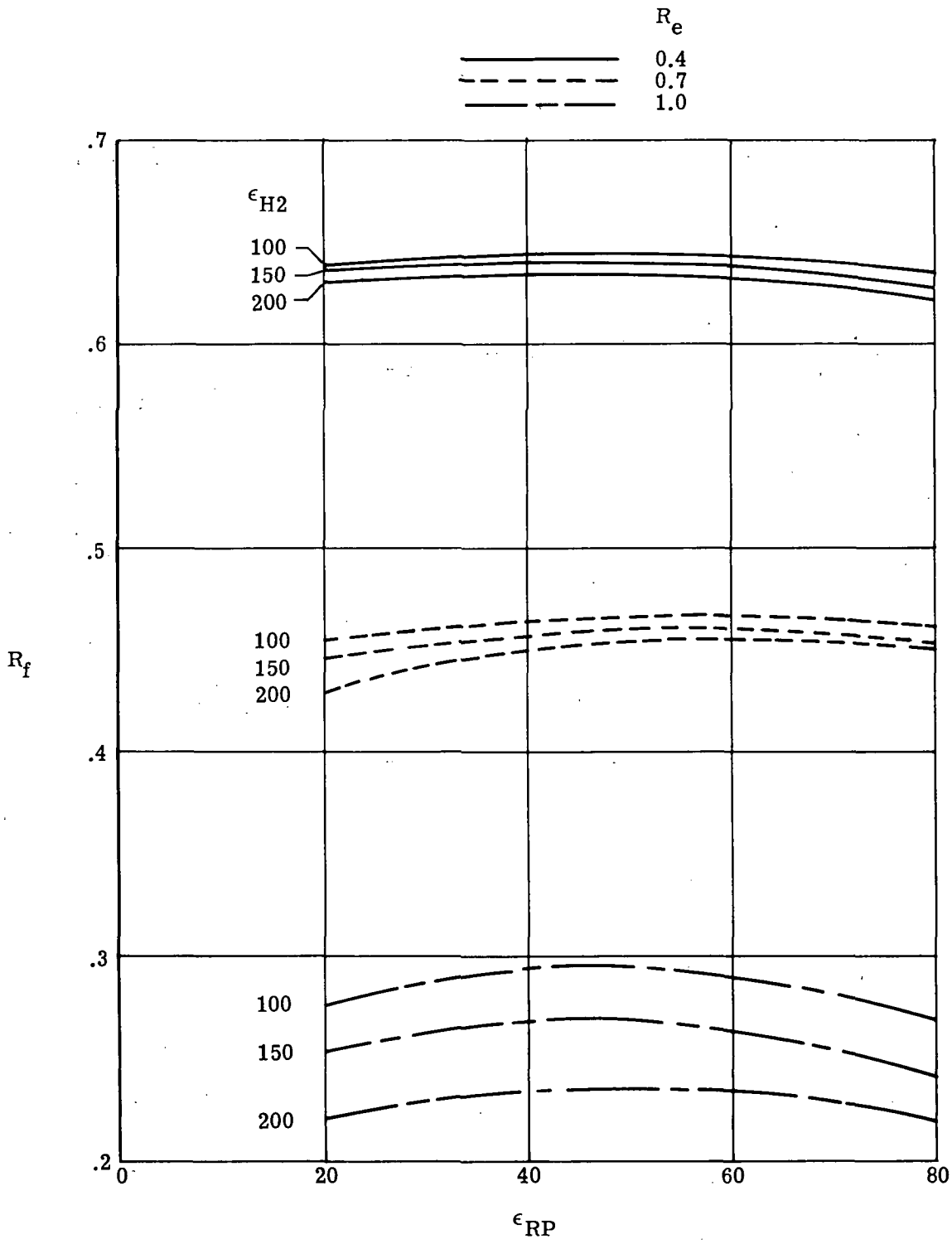

(b) $(T/W)_o$ = 1.30.

Figure 10.- Continued.

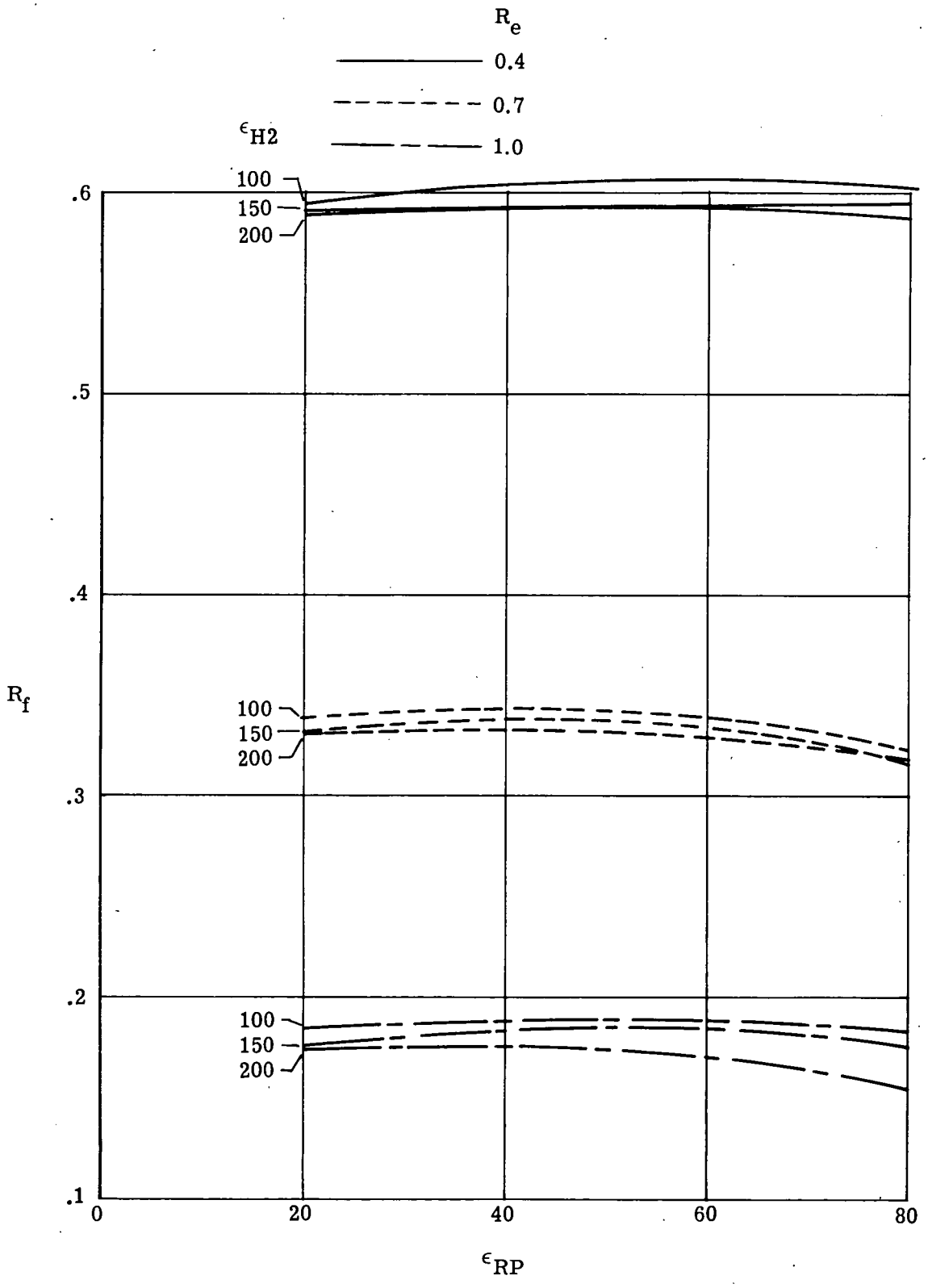

(c) $(T/W)_o = 1.45$.

Figure 10.- Concluded.

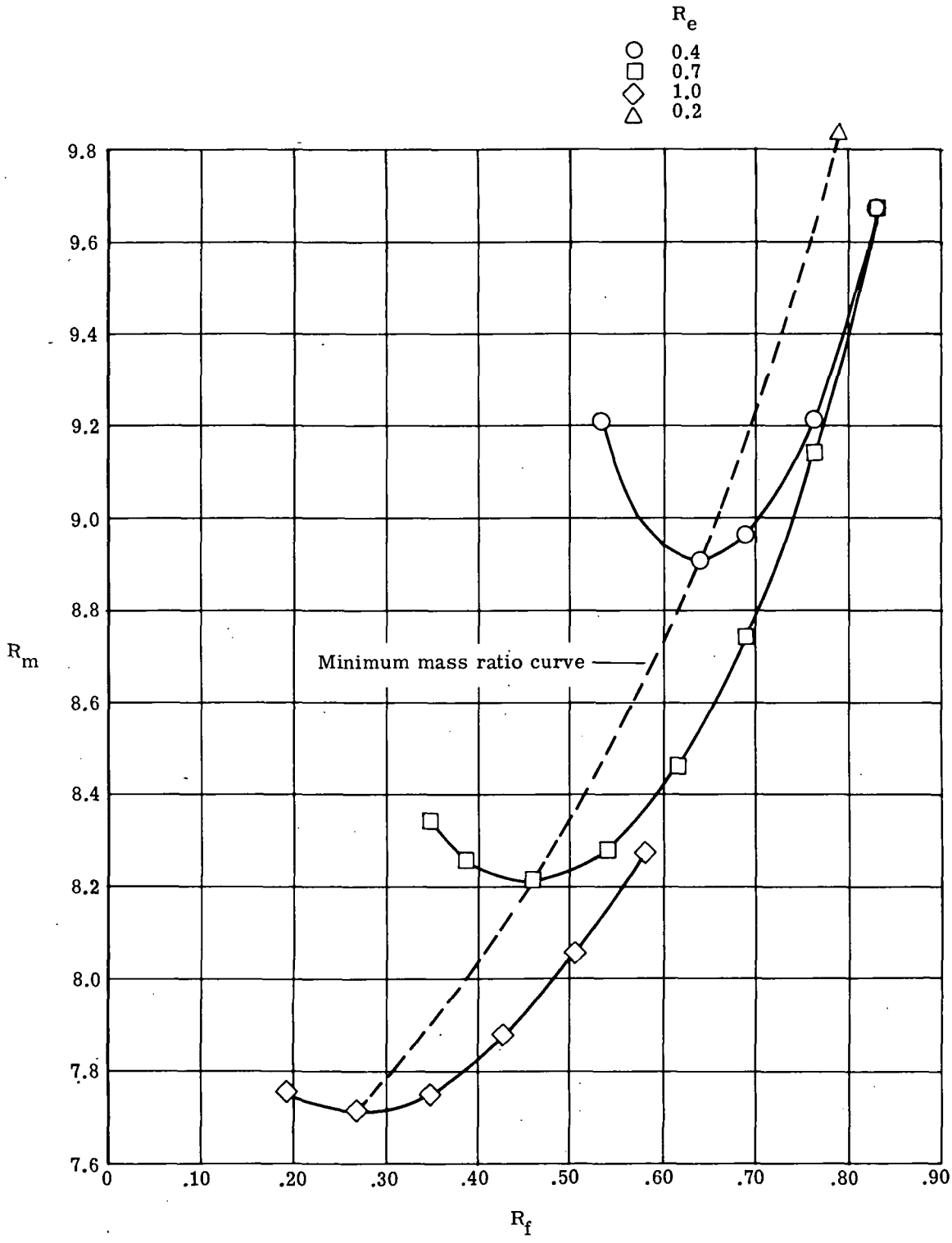

(a) $\epsilon_{RP} = 50$; $\epsilon_{H2} = 150$; $(T/W)_o = 1.30$.

Figure 11.- Variation of mass ratio with fuel ratio. Series burn.

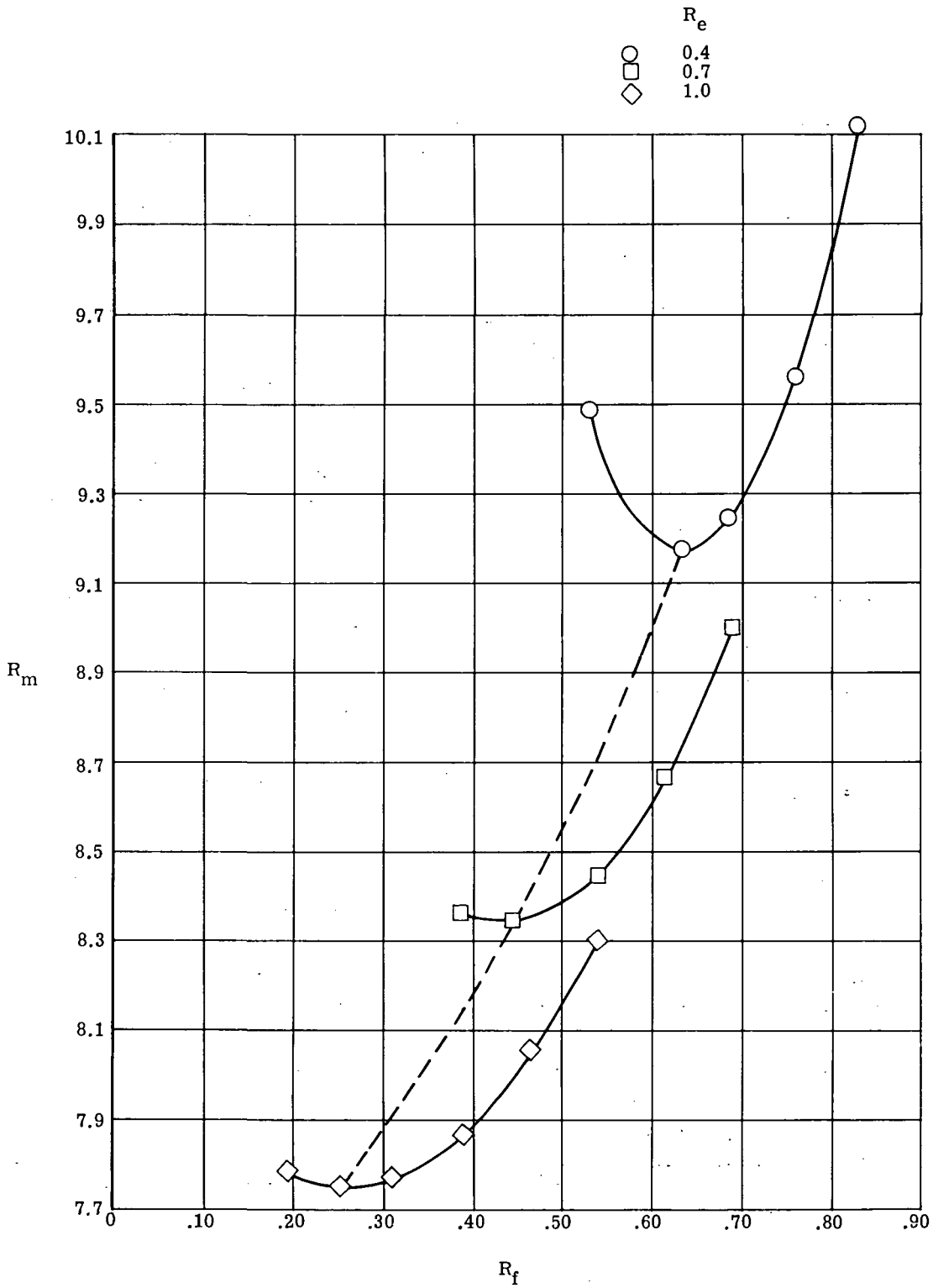

(b) $\varepsilon_{RP} = 20$; $\varepsilon_{H2} = 150$; $(T/W)_o = 1.30$.

Figure 11.- Continued.

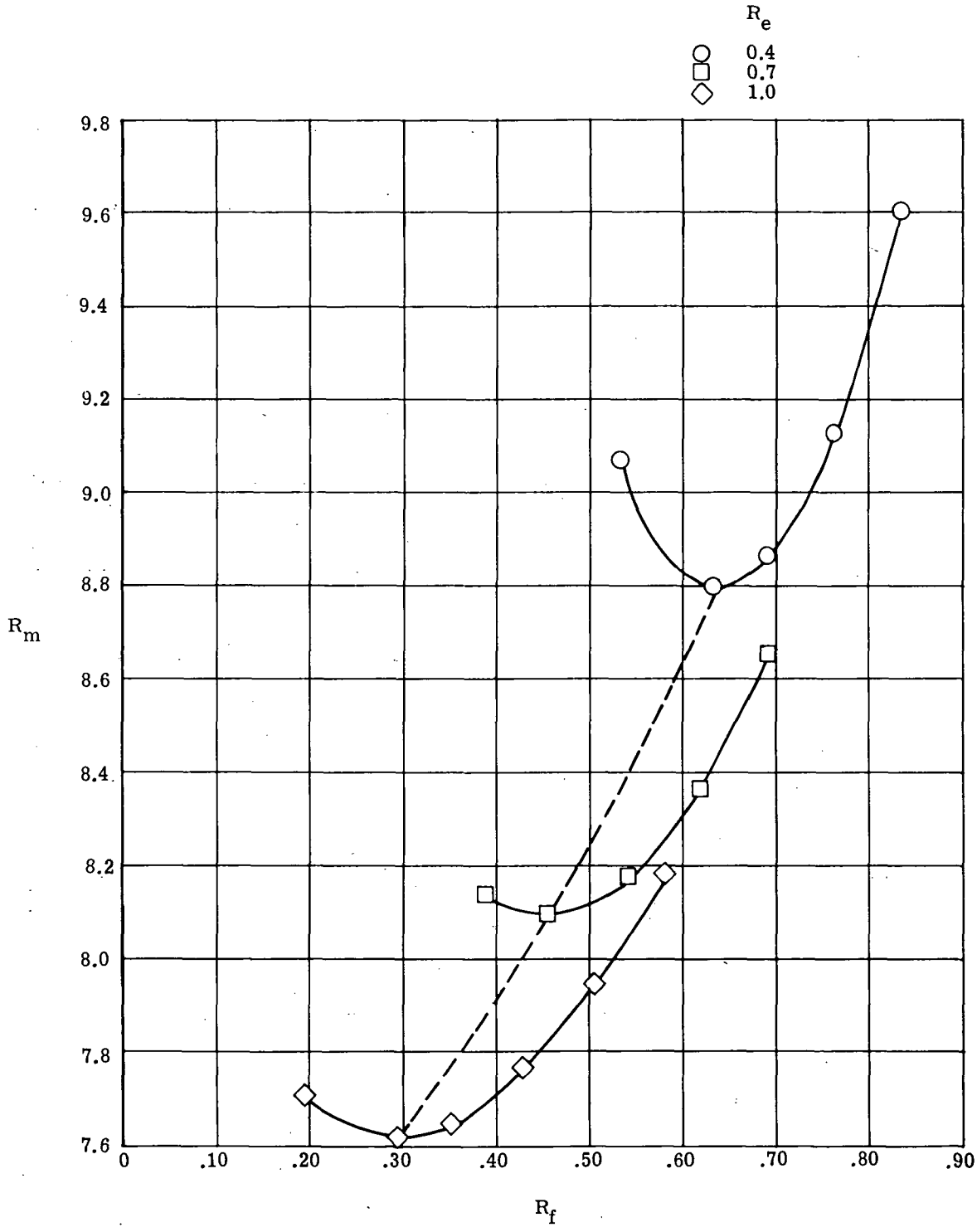

(c) $\varepsilon_{RP} = 50$; $\varepsilon_{H2} = 200$; $(T/W)_o = 1.30$.

Figure 11.- Continued.

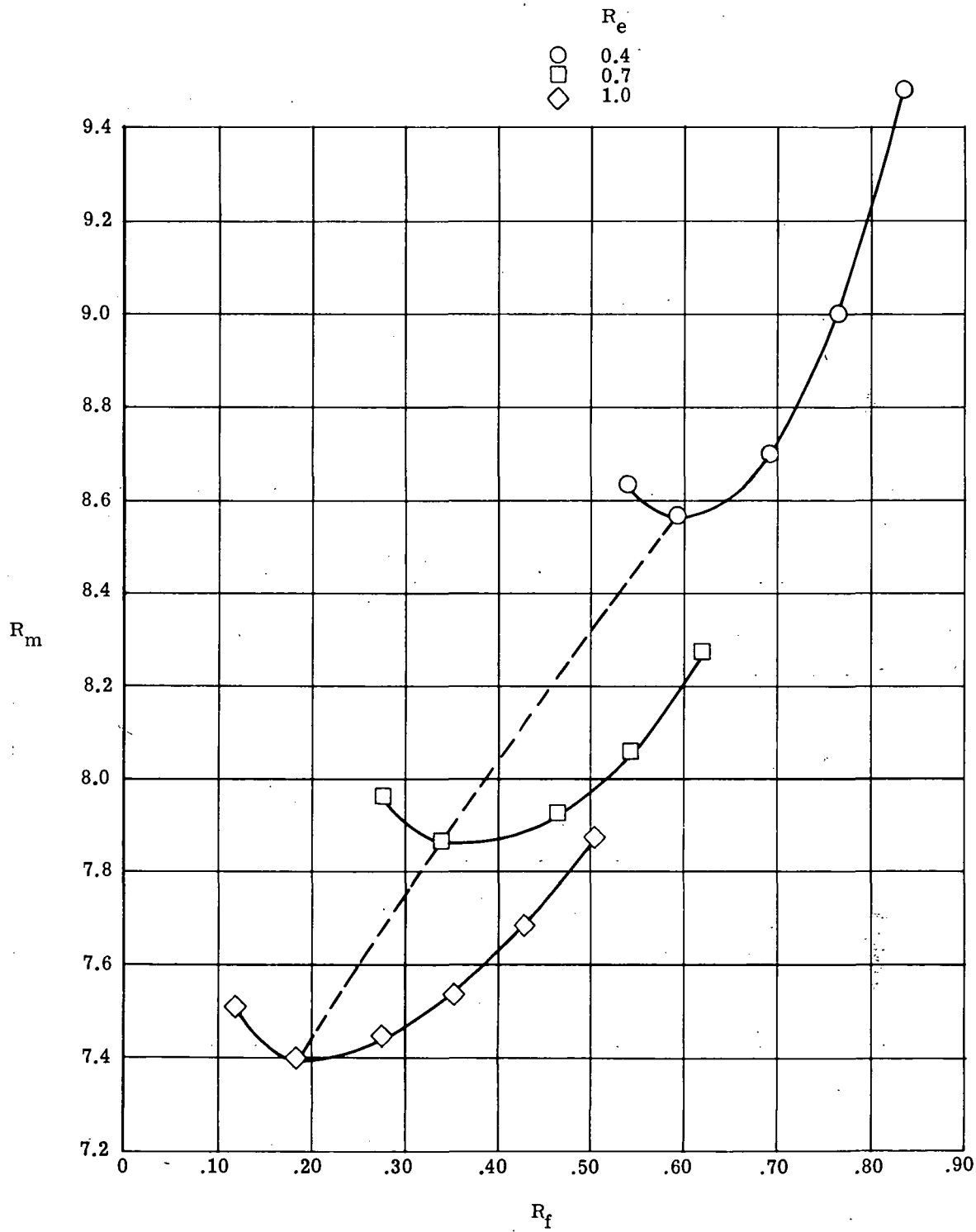

(d) $\varepsilon_{RP} = 50$; $\varepsilon_{H2} = 150$; $(T/W)_o = 1.45$.

Figure 11.- Concluded.

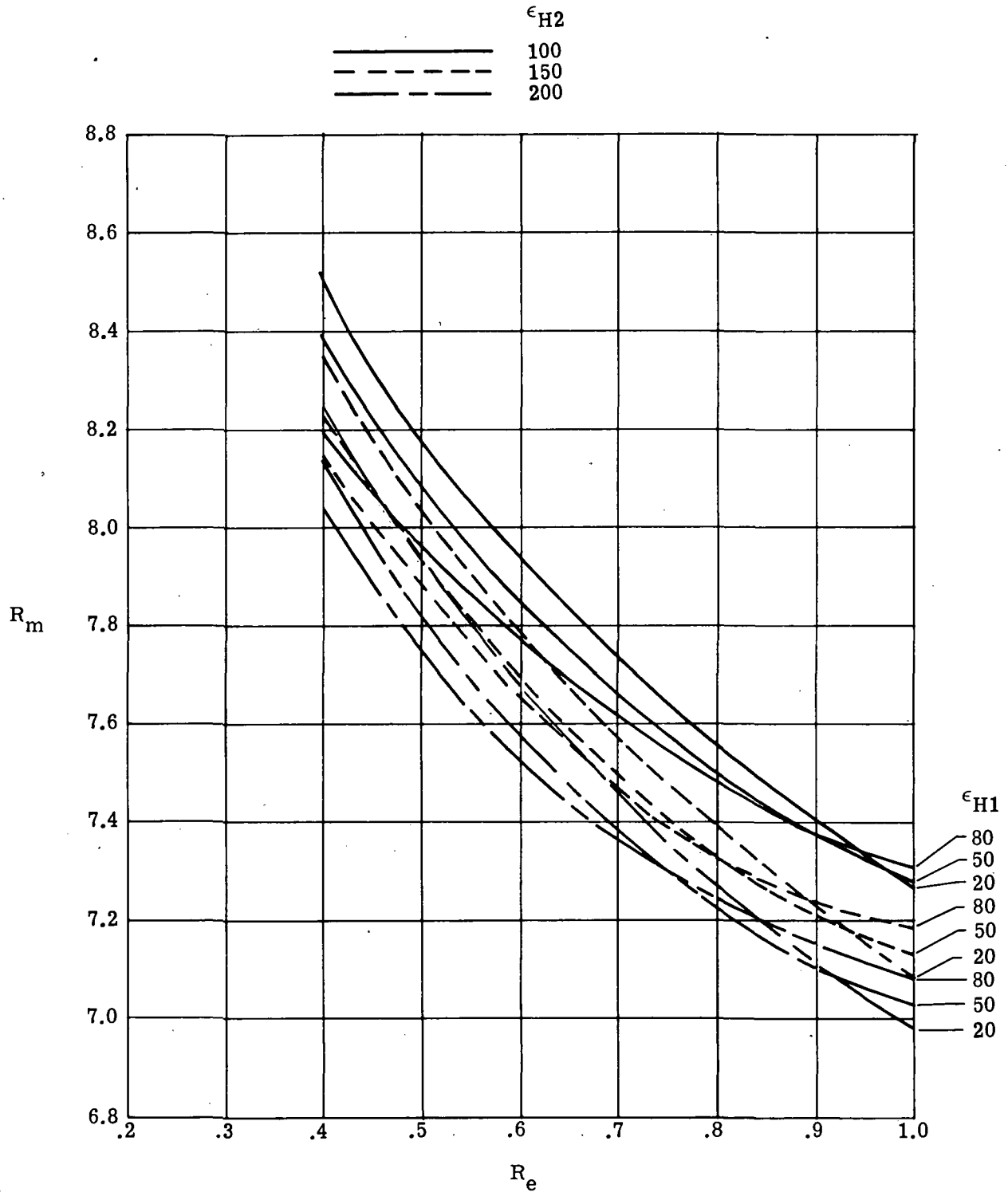

(a) $\epsilon_{RP} = 20.$

Figure 12.- Variation of mass ratio with engine thrust ratio. Parallel burn.

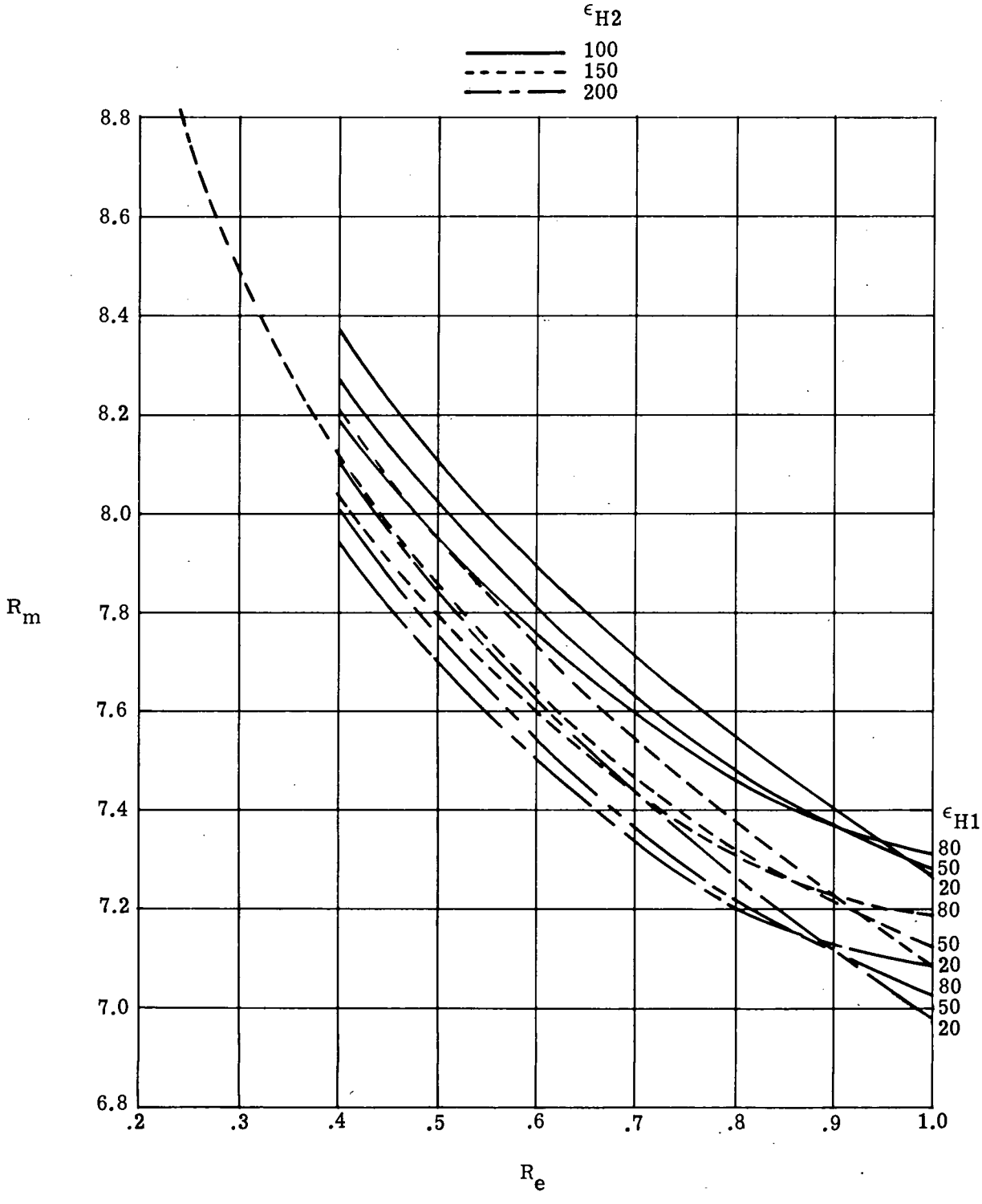

(b) $\varepsilon_{RP} = 50.$

Figure 12.- Continued.

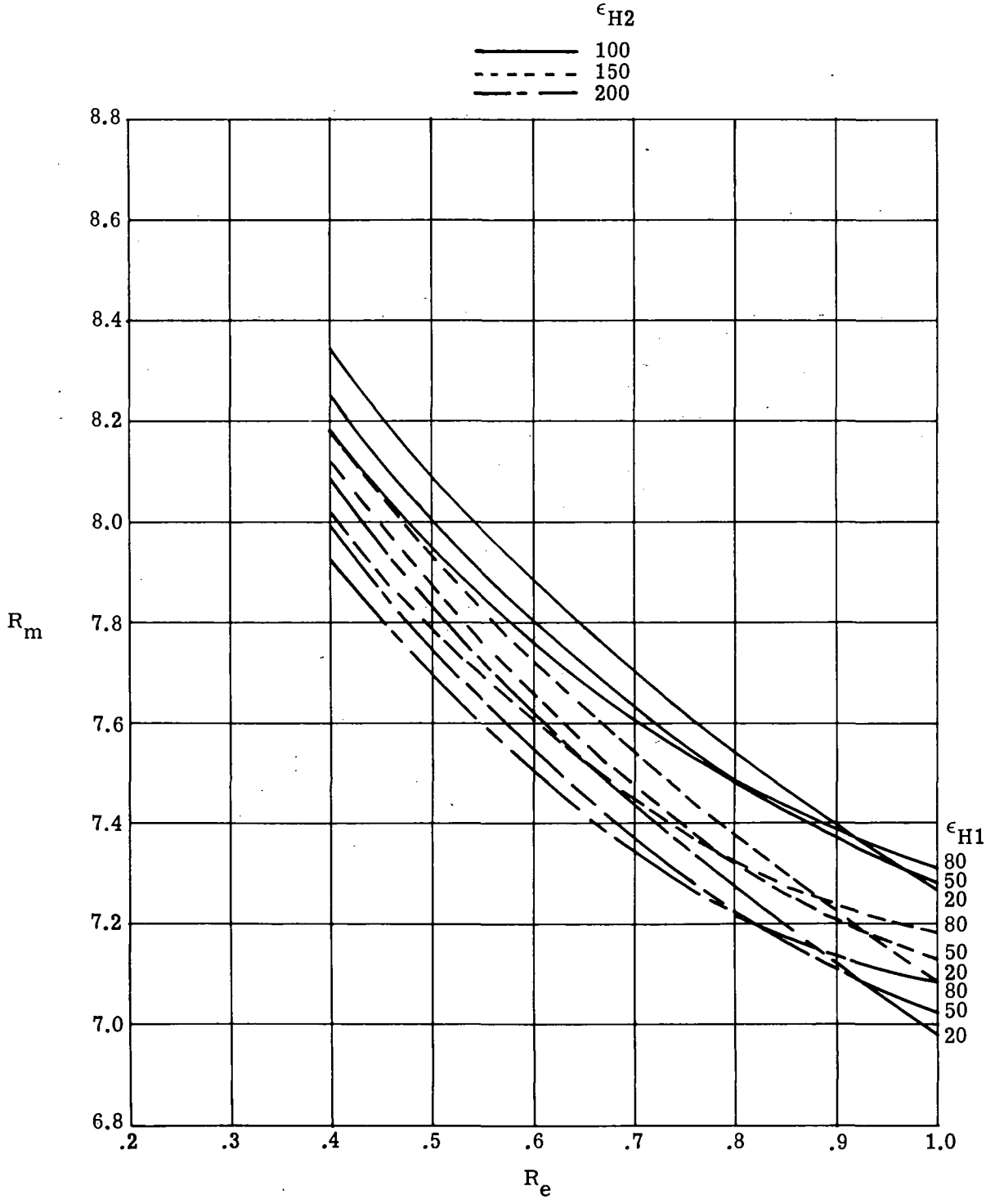

(c) $\varepsilon_{RP} = 80.$

Figure 12.- Concluded.

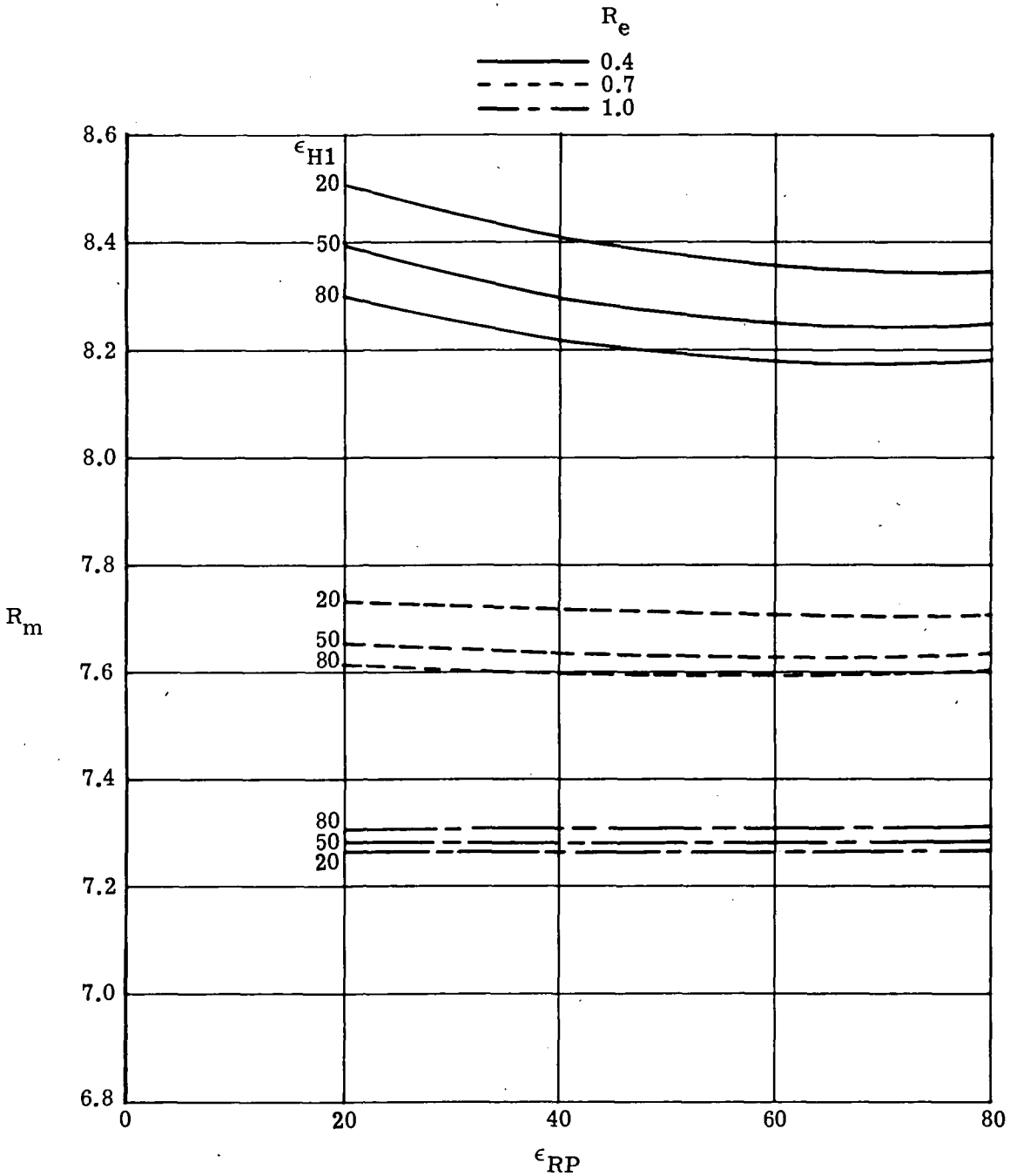

(a) $\varepsilon_{H2} = 100.$

Figure 13.- Variation of mass ratio with RP-1 engine expansion ratio. Parallel burn.

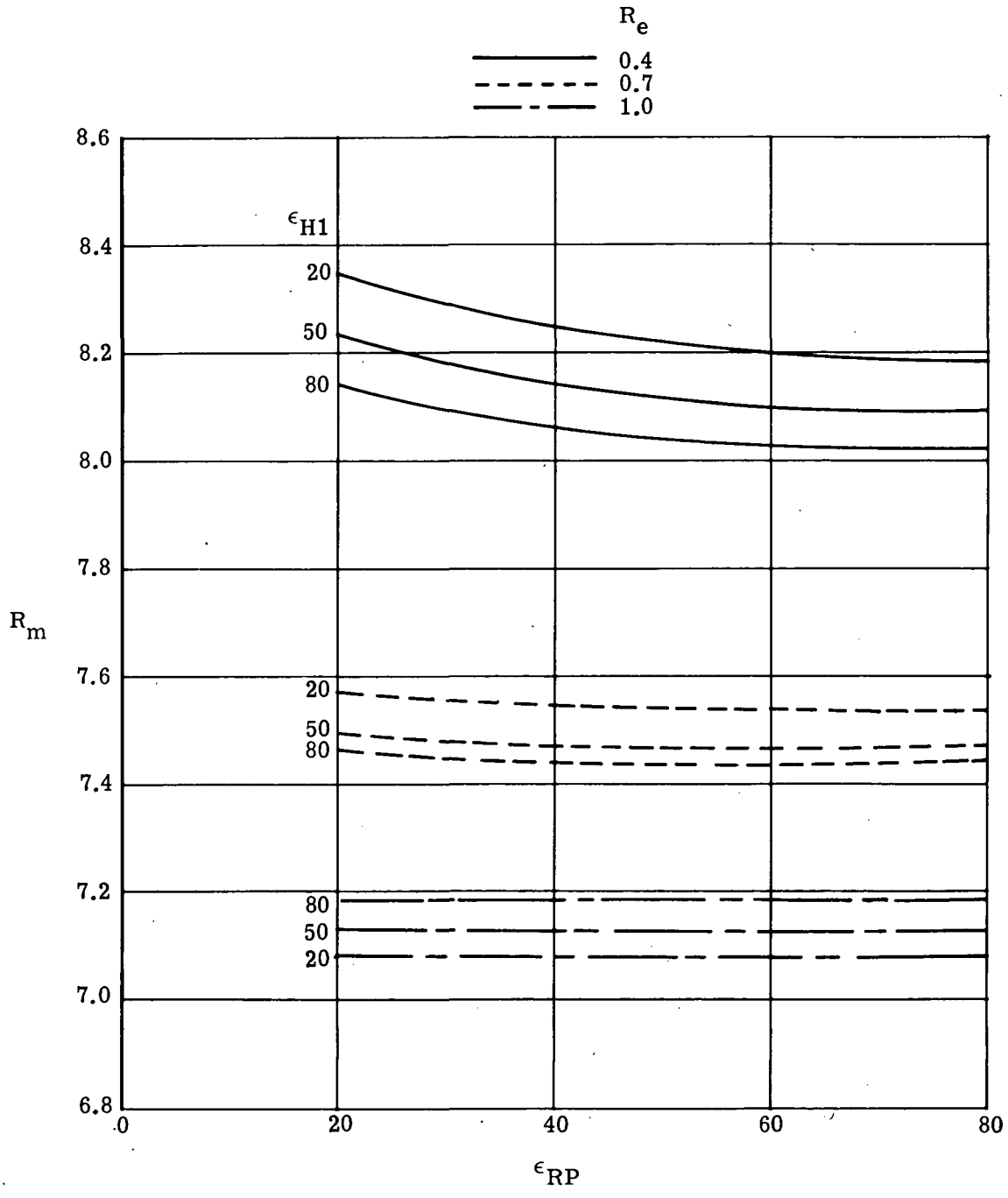

(b) $\epsilon_{RP} = 150.$

Figure 13.- Continued.

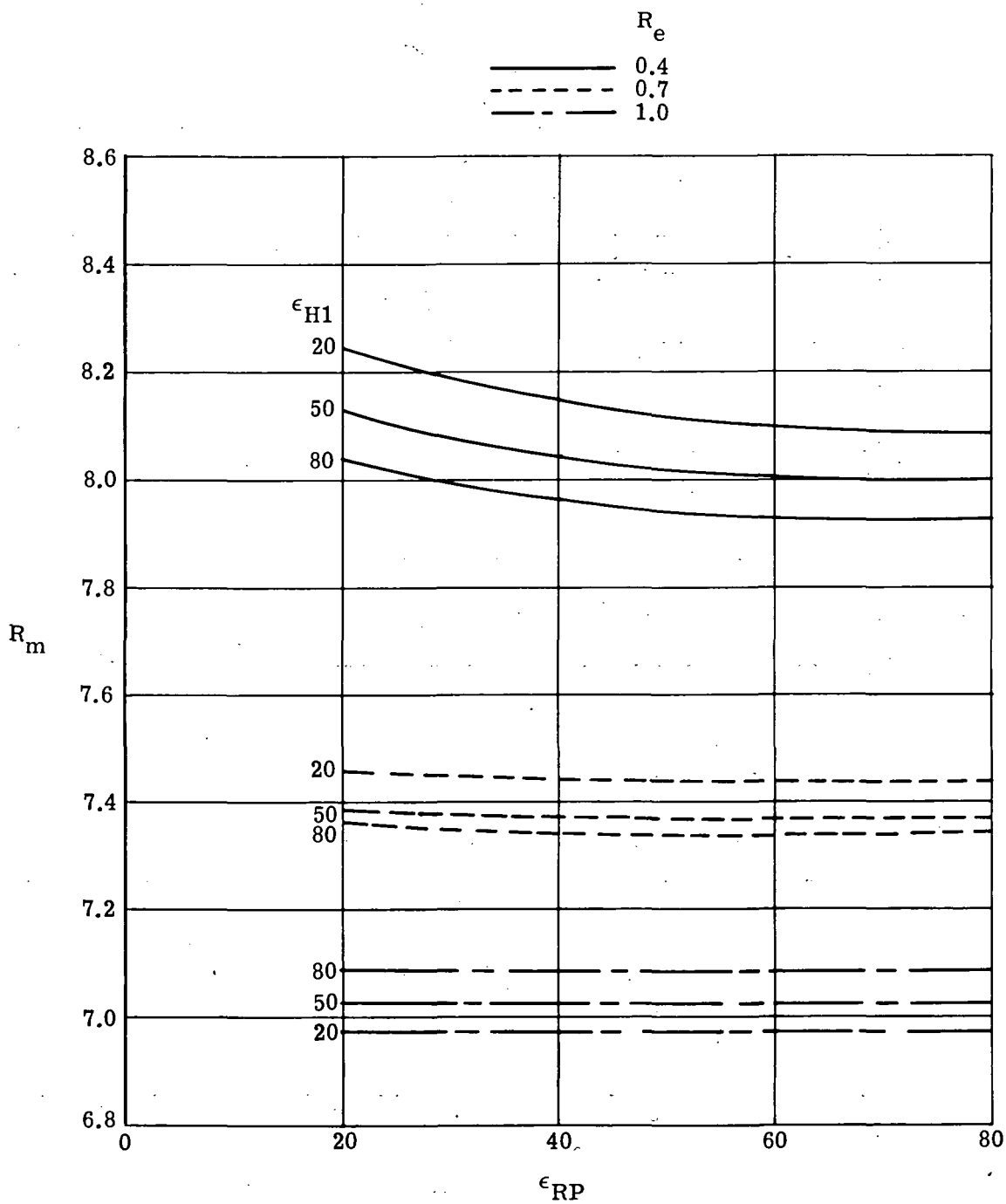

(c) $\epsilon_{H2} = 200.$

Figure 13.- Concluded.

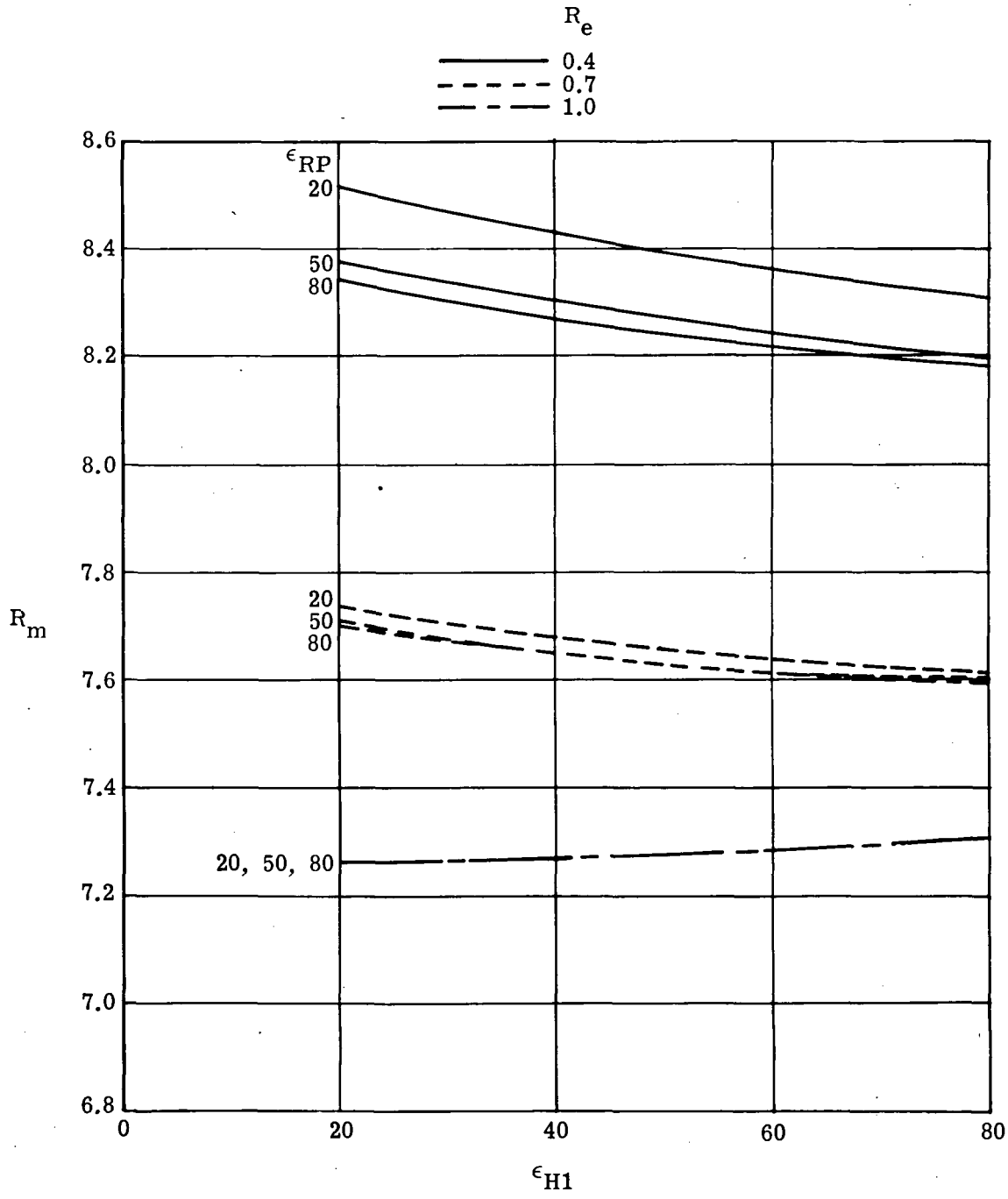

(a) $\epsilon_{H2} = 100.$

Figure 14.- Variation of mass ratio with initial hydrogen engine expansion ratio. Parallel burn.

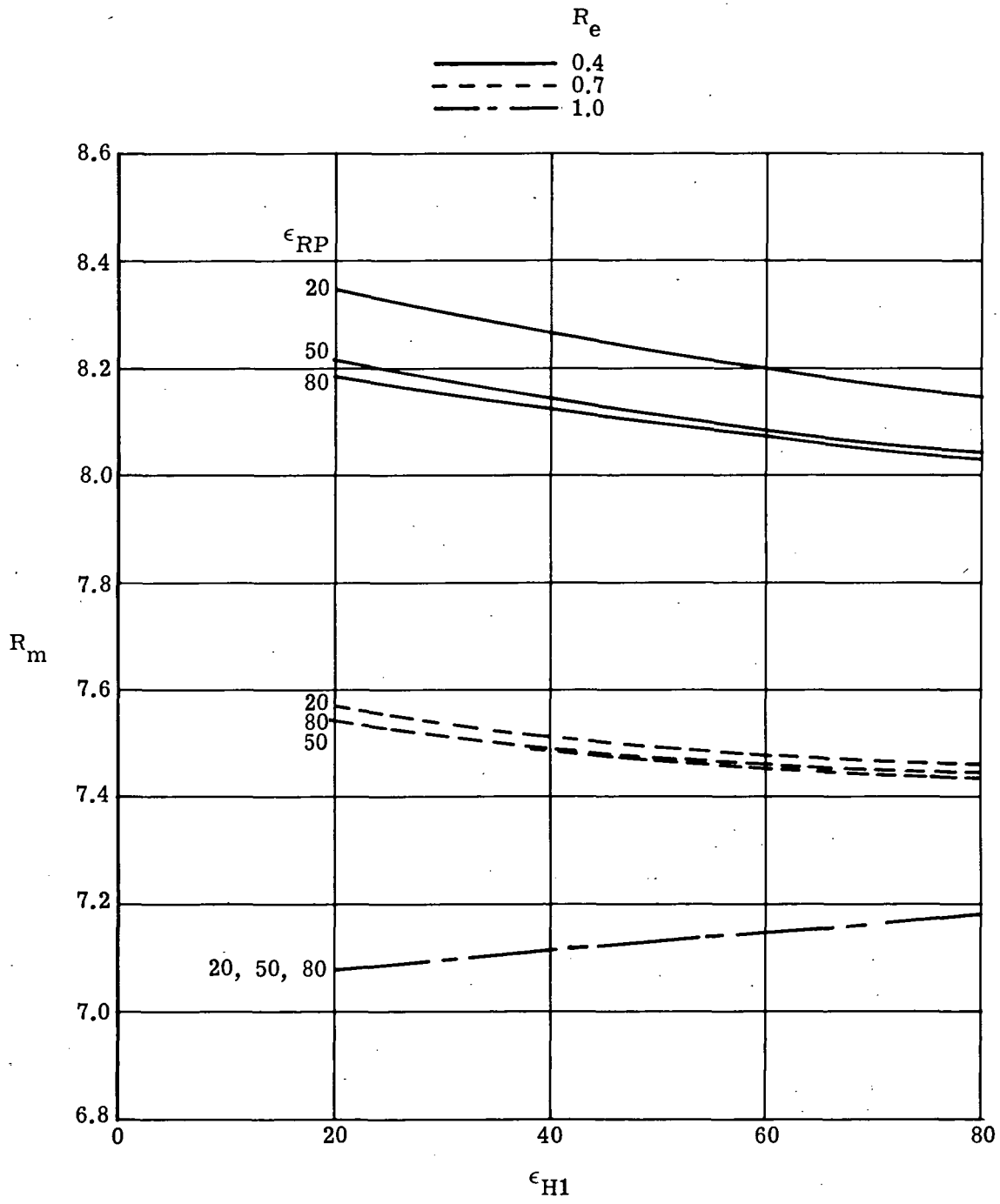

(b) $\epsilon_{H2} = 150.$

Figure 14.- Continued.

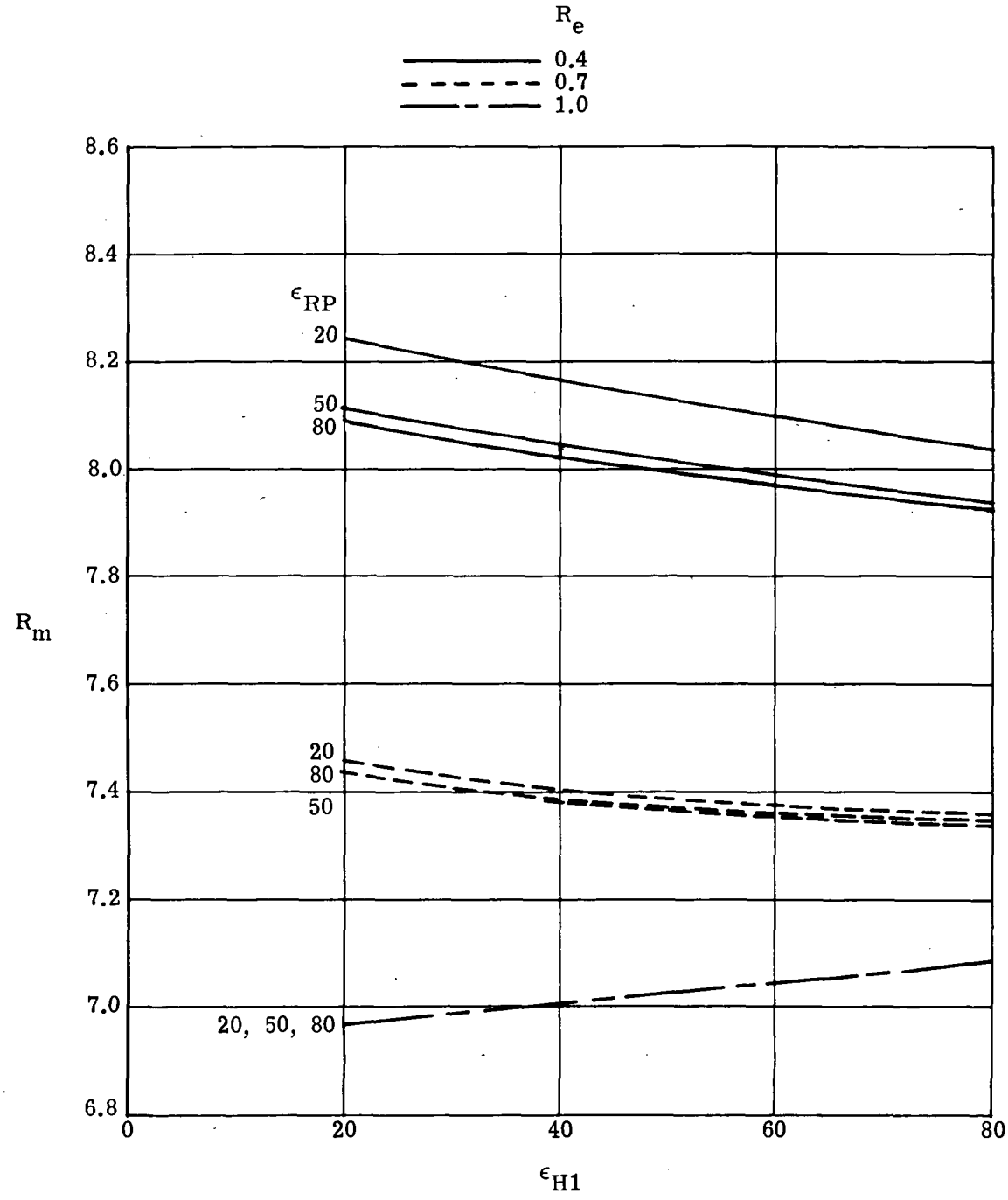

(c) $\epsilon_{H2} = 200.$

Figure 14.- Concluded.

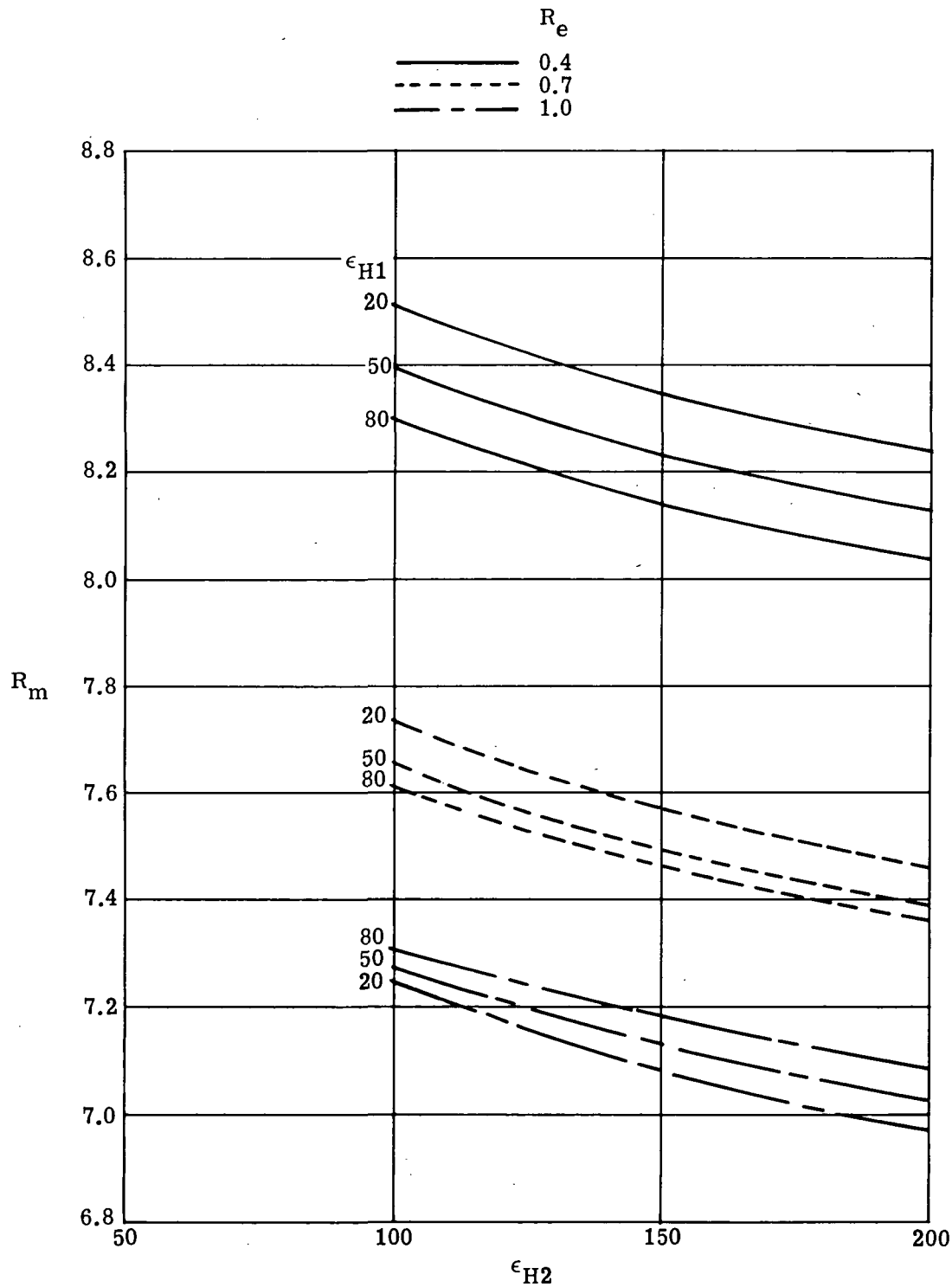

(a) $\epsilon_{RP} = 20.$

Figure 15.- Variation of mass ratio with second hydrogen engine expansion ratio. Parallel burn.

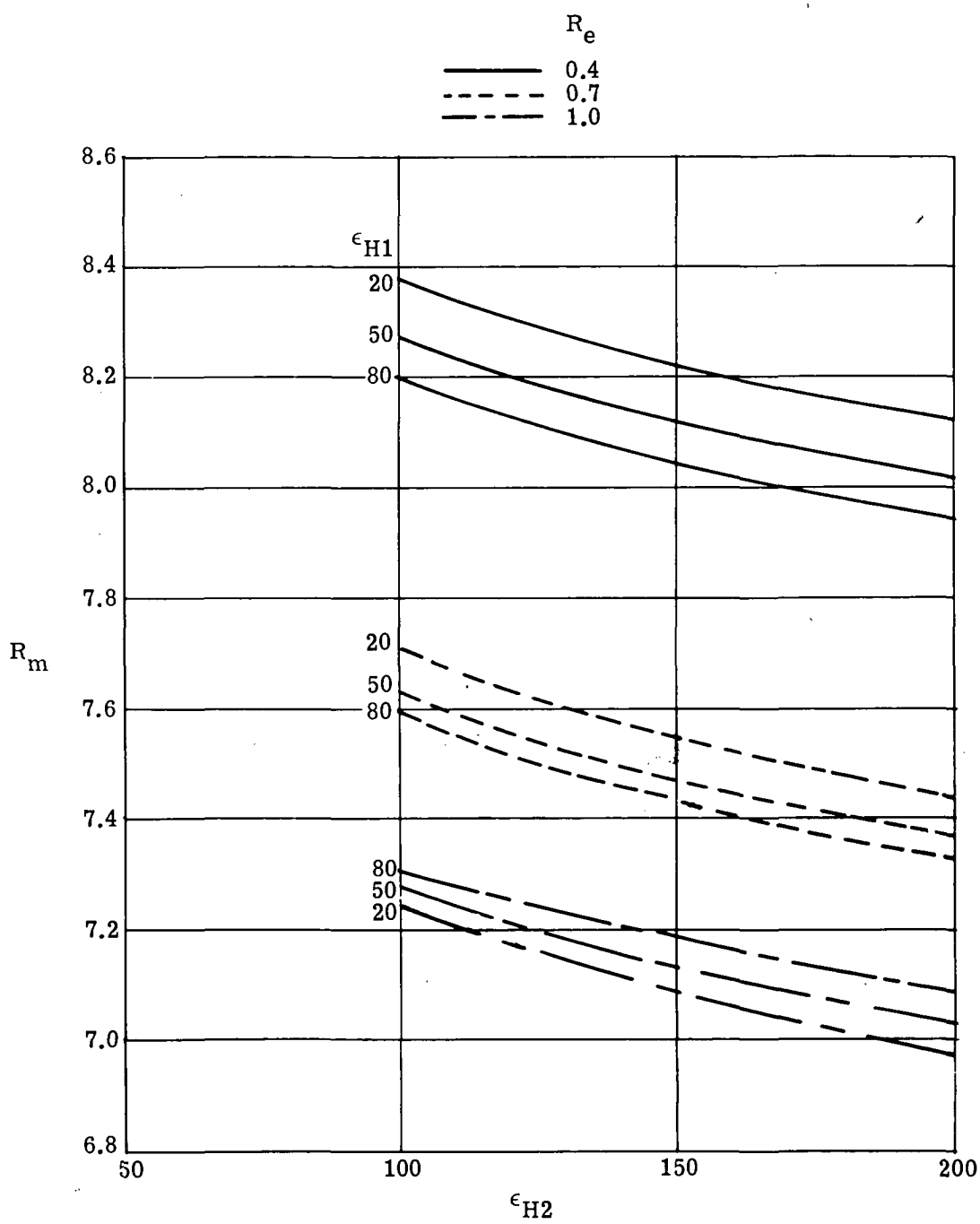

(b) $\varepsilon_{RP} = 50.$

Figure 15.- Continued.

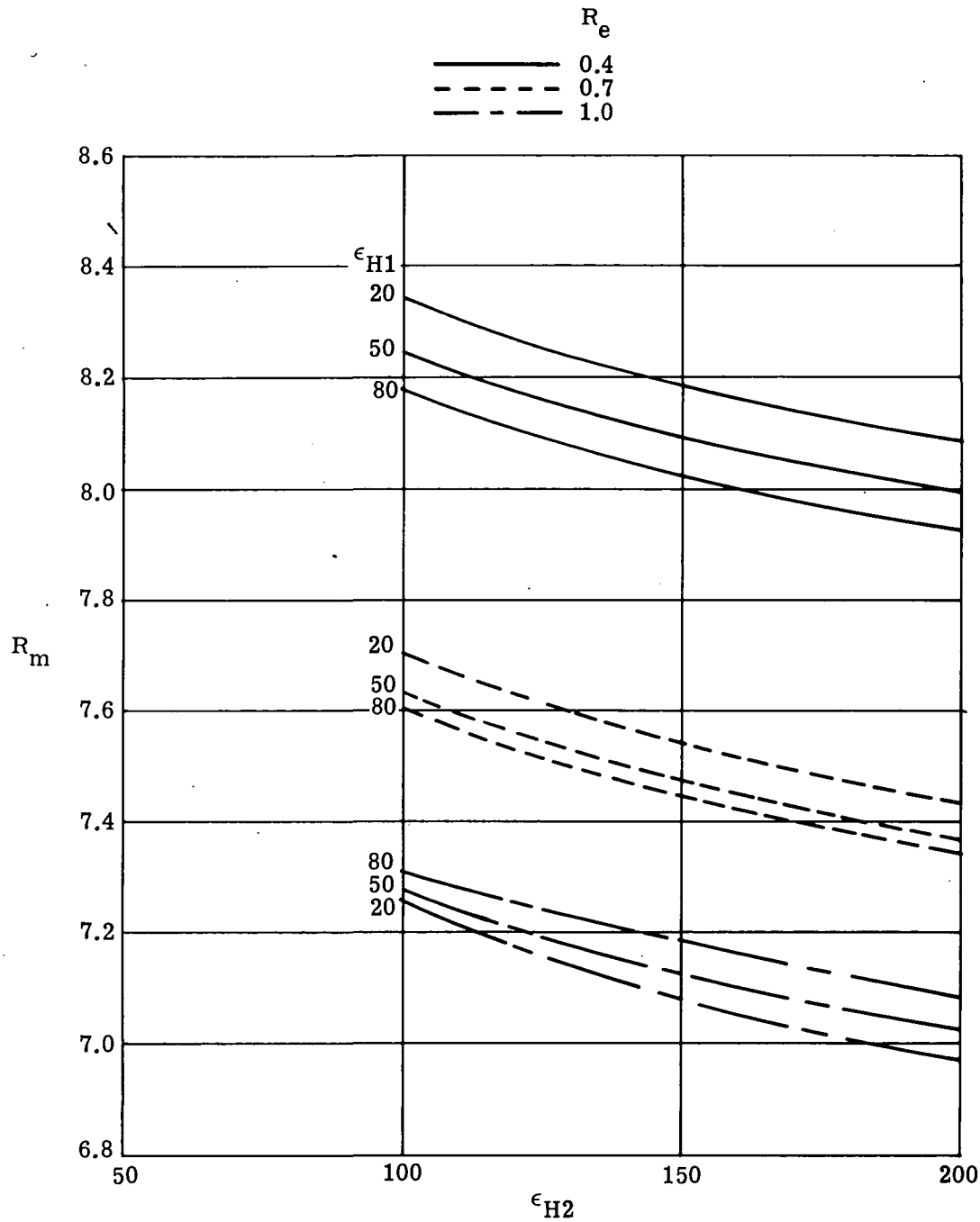

(c) $\varepsilon_{RP} = 80.$

Figure 15.- Concluded.

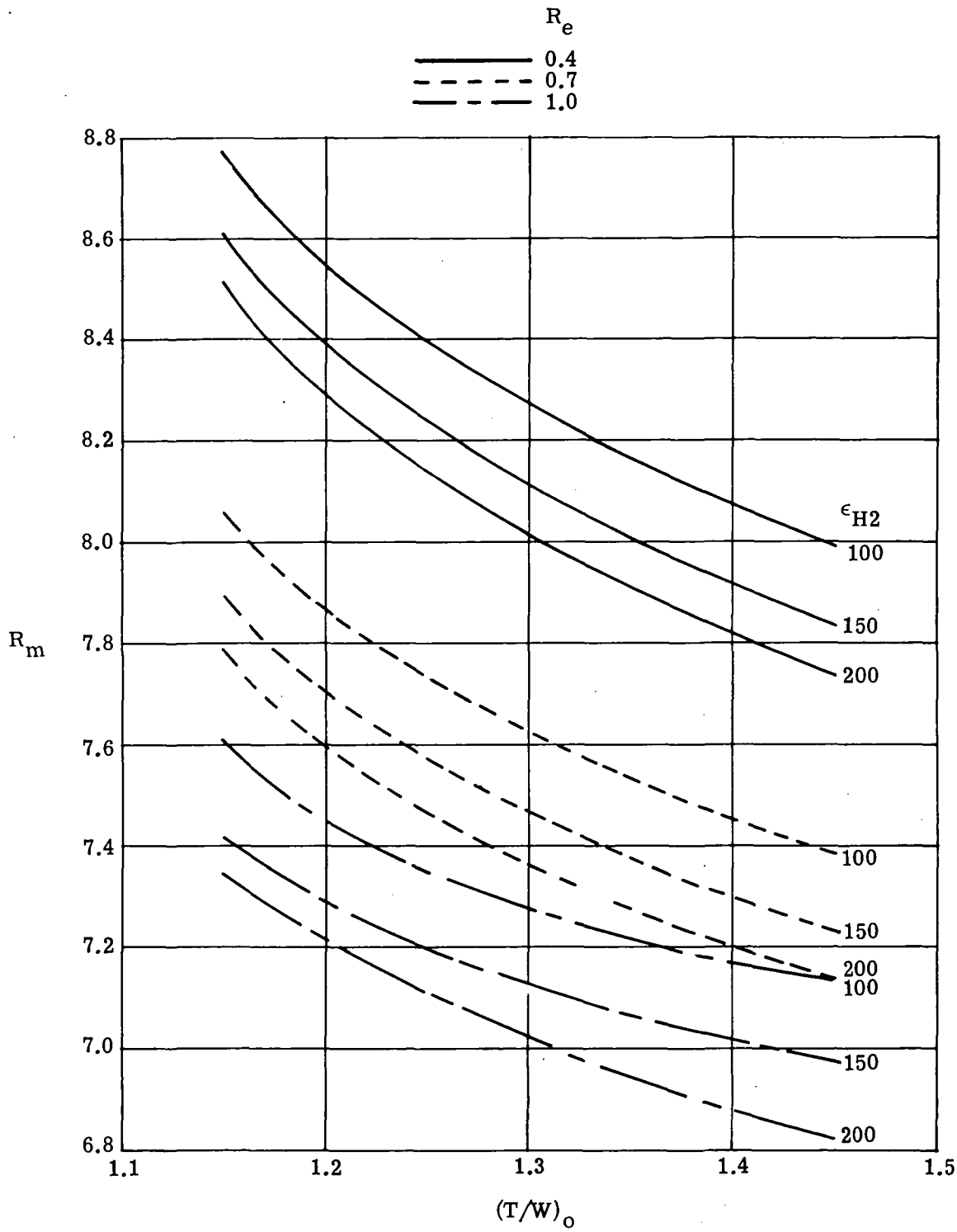

Figure 16.- Variation of mass ratio with initial thrust-weight ratio. Parallel burn; $\epsilon_{RP} = 50$; $\epsilon_{H1} = 50$.

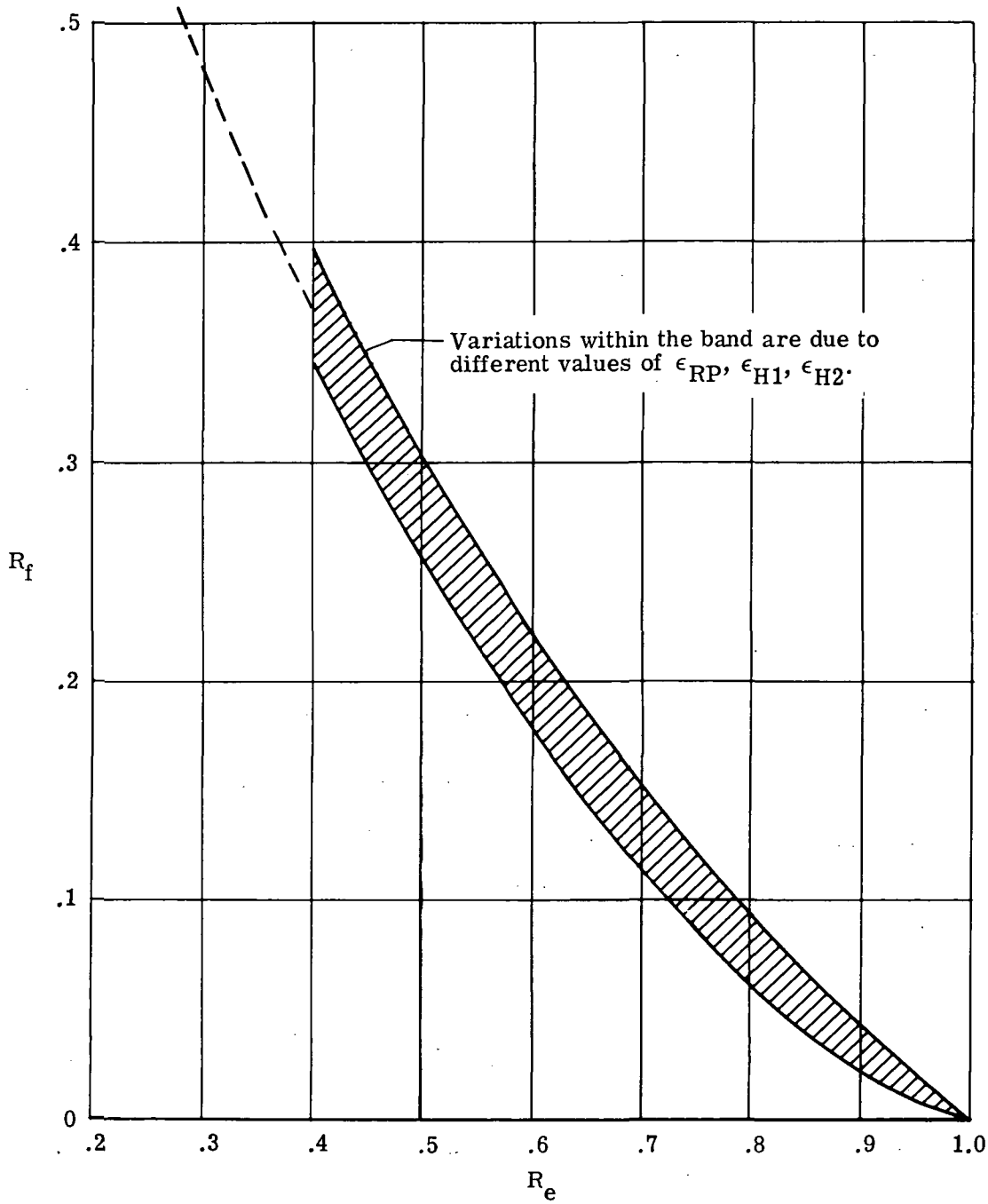

Figure 17.- Variation of fuel ratio with engine thrust ratio. Parallel burn; $(T/W)_o$ = 1.30.

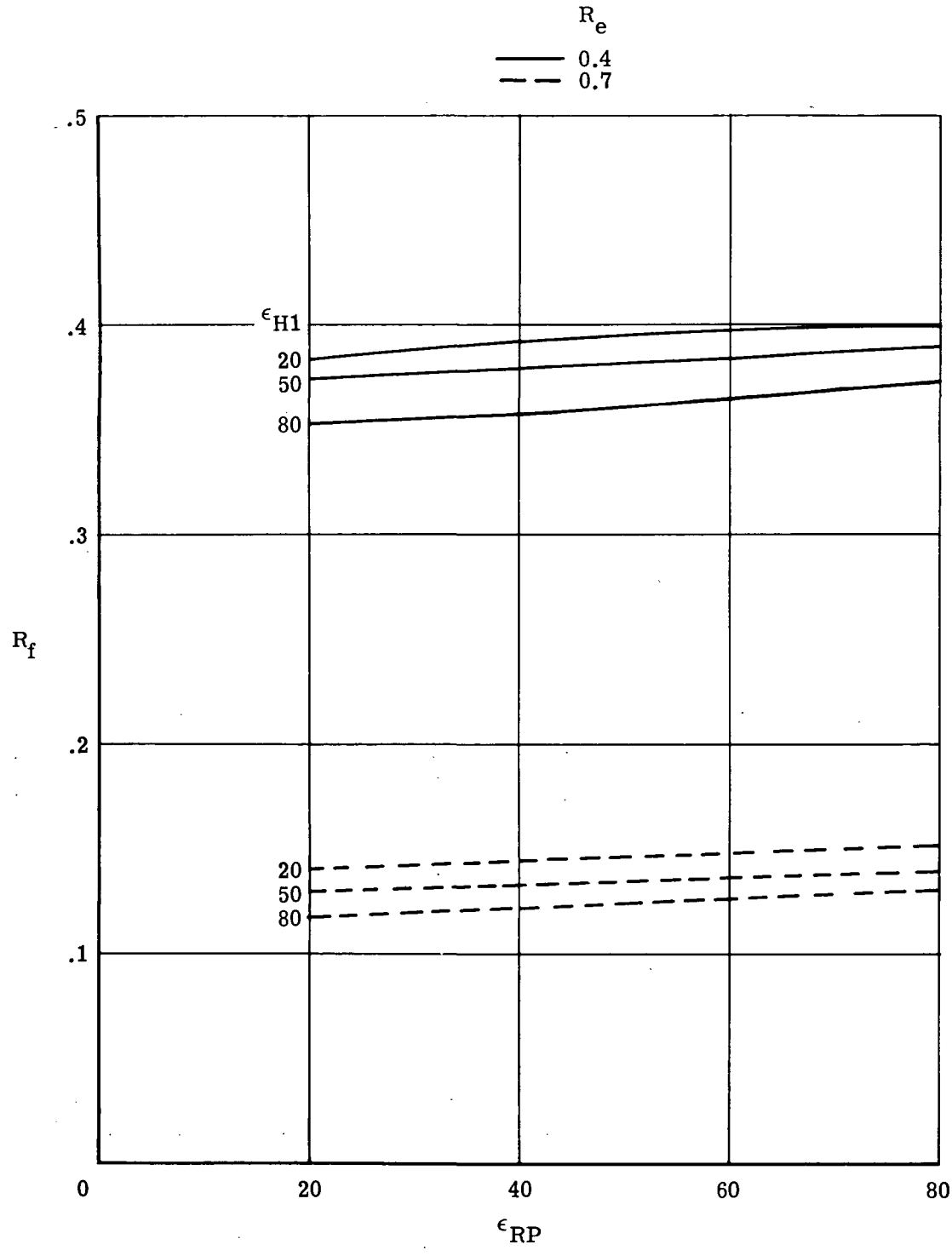

(a) $\epsilon_{H2} = 100.$

Figure 18.- Variation of fuel ratio with RP-1 engine expansion ratio. Parallel burn.

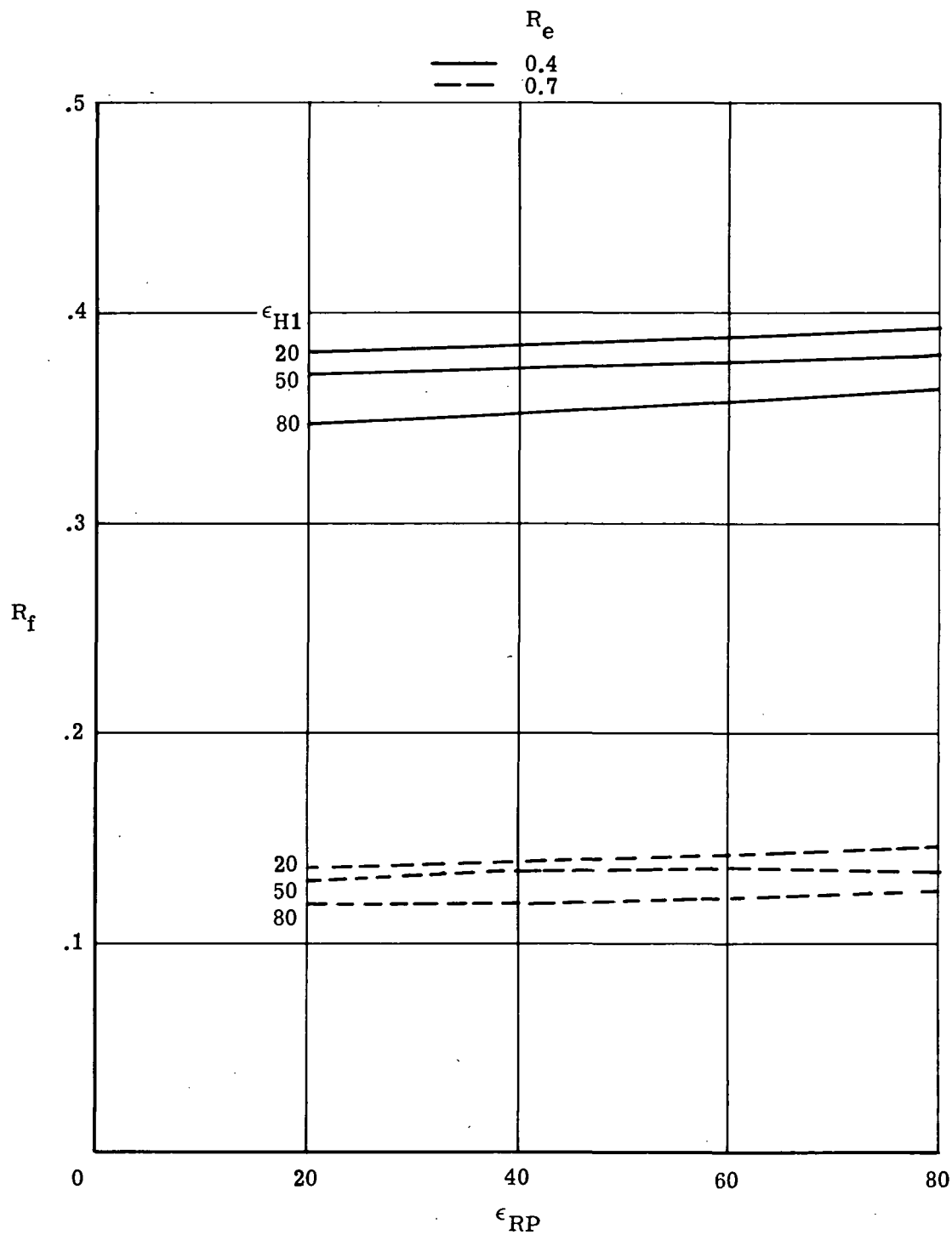

(b) $\epsilon_{H2} = 150.$

Figure 18.- Continued.

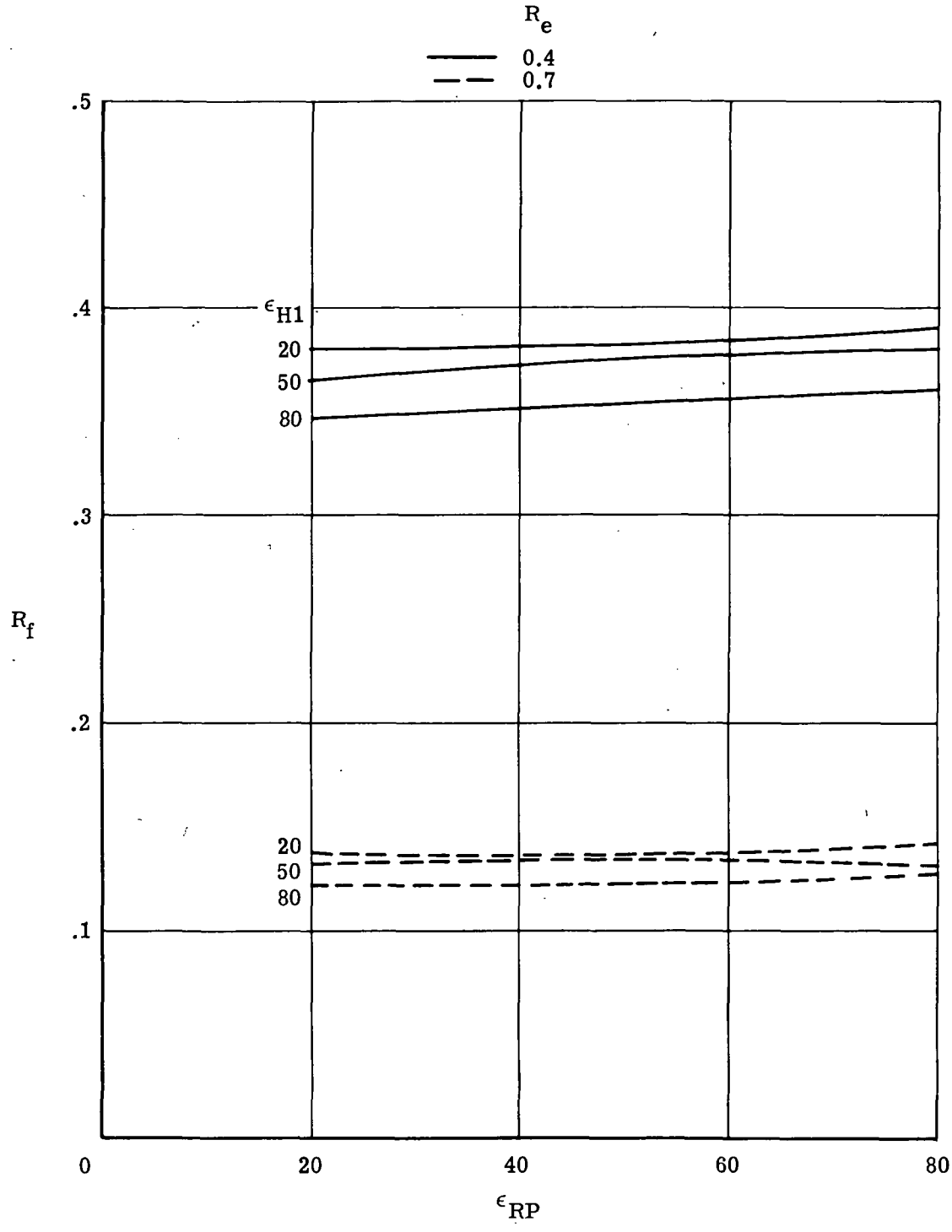

(c) $\epsilon_{H2} = 200.$

Figure 18.- Concluded.

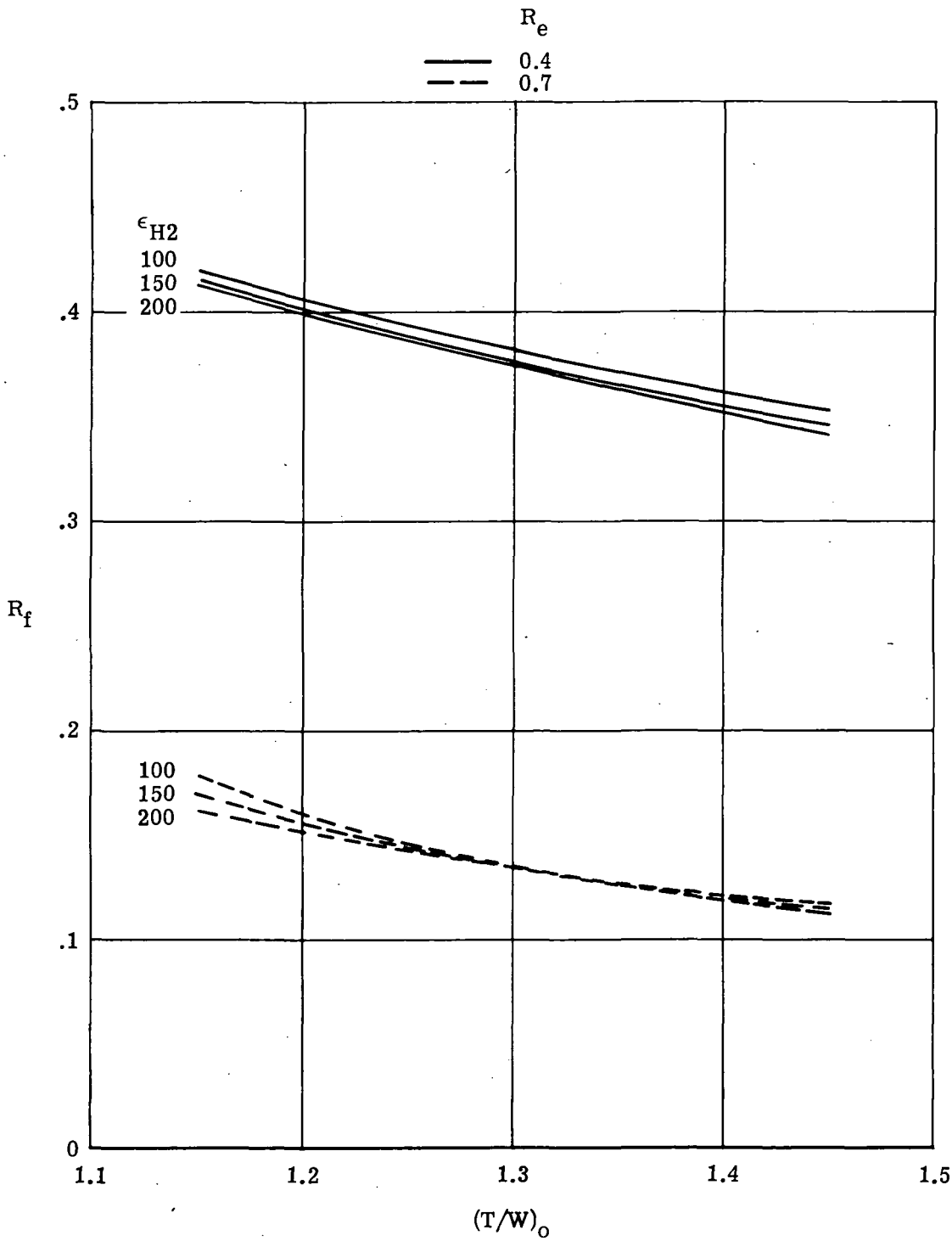

Figure 19.- Variation of fuel ratio with initial thrust-weight ratio. Parallel burn.

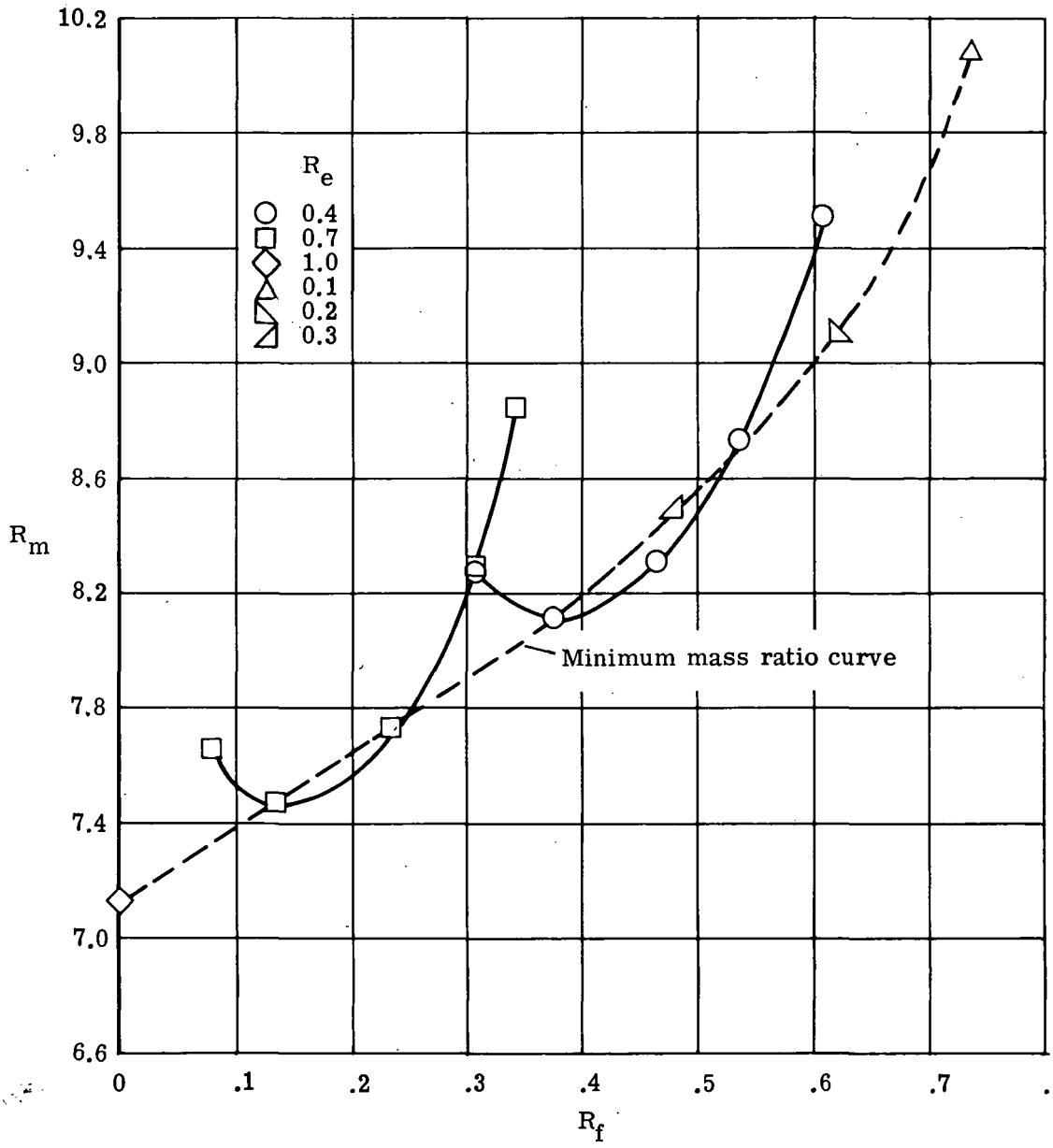

(a) $\varepsilon_{RP} = 50$; $\varepsilon_{H1} = 50$; $\varepsilon_{H2} = 150$; $(T/W)_o = 130$.

Figure 20.- Variation of mass ratio with fuel ratio. Parallel burn.

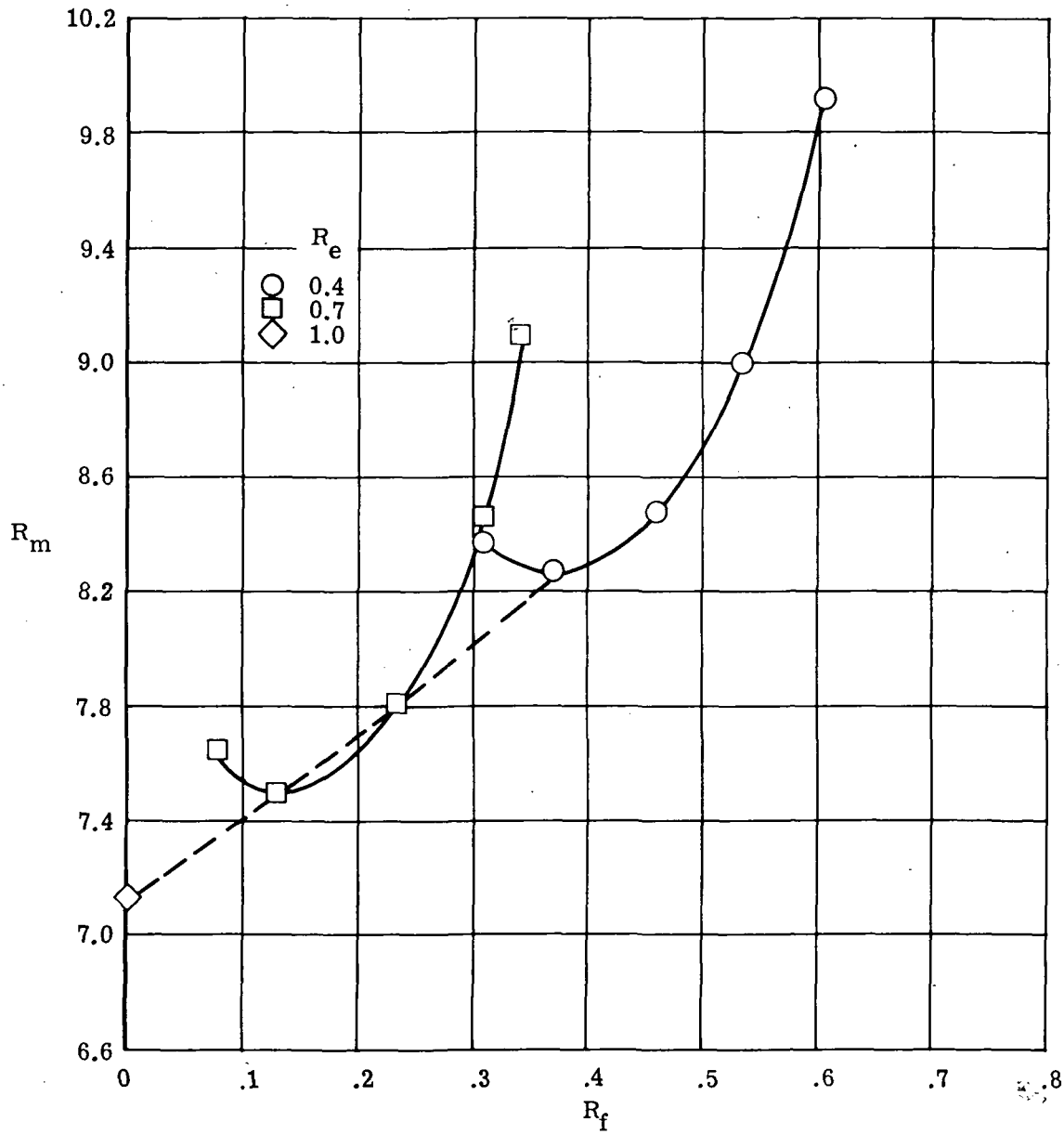

(b) $\varepsilon_{RP} = 20$; $\varepsilon_{H1} = 50$; $\varepsilon_{H2} = 150$; $(T/W)_o = 1.30$.

Figure 20.- Continued.

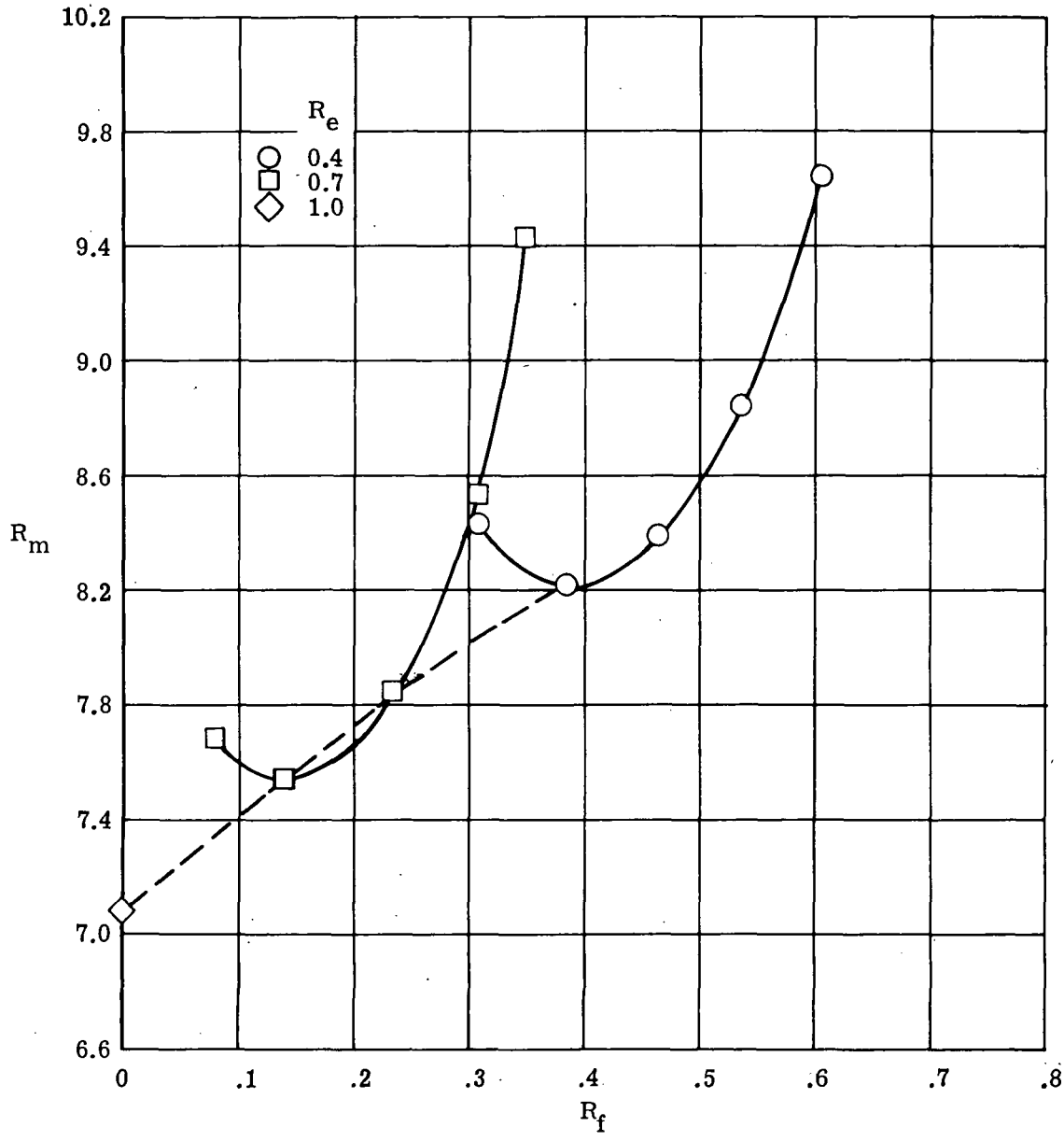

(c) $\varepsilon_{RP} = 50$; $\varepsilon_{H1} = 20$; $\varepsilon_{H2} = 150$; $(T/W)_o = 1.30$.

Figure 20.- Continued.

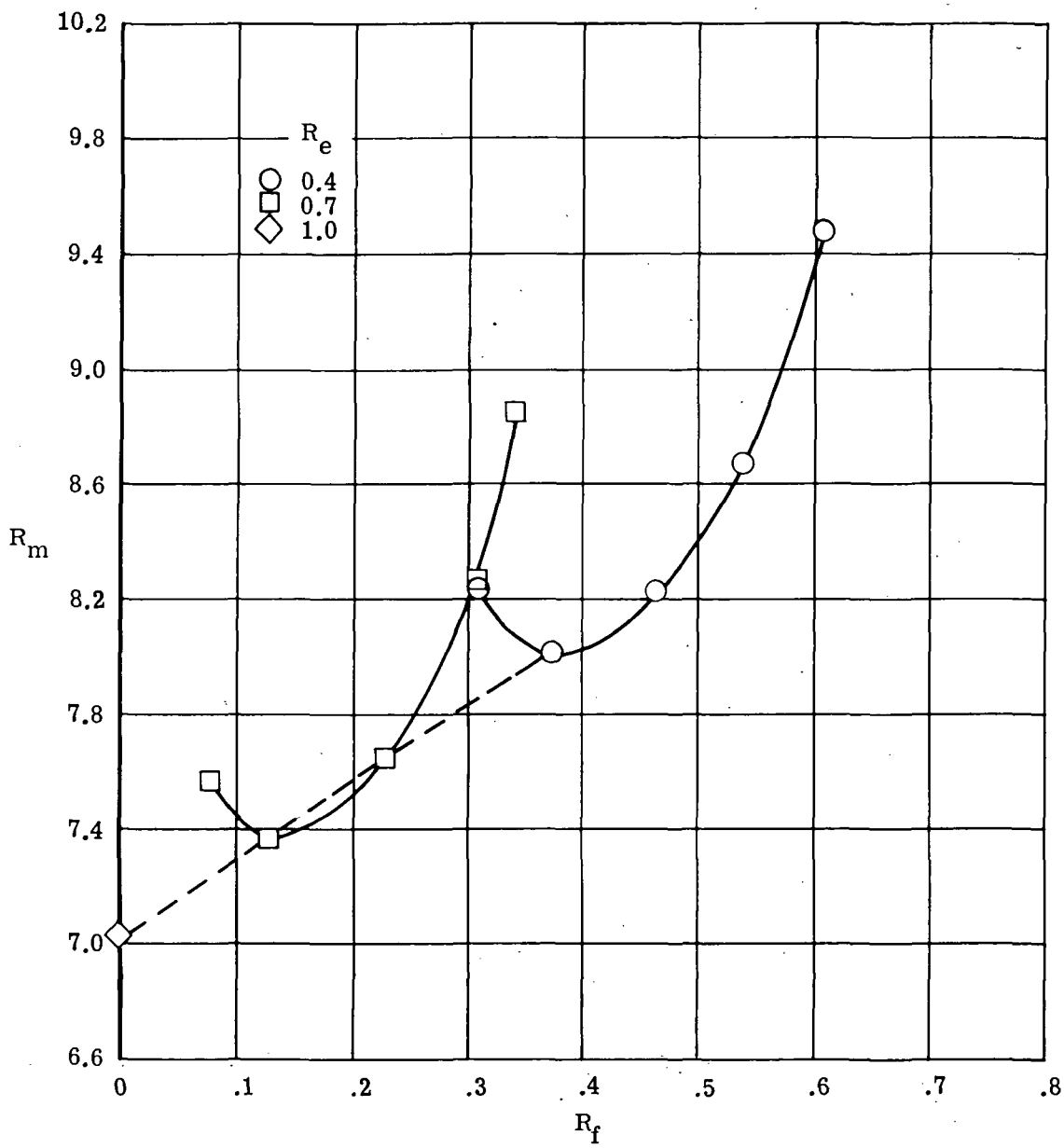

(d) $\varepsilon_{RP} = 50$; $\varepsilon_{H1} = 50$; $\varepsilon_{H2} = 200$; $(T/W)_o = 1.30$.

Figure 20.- Continued.

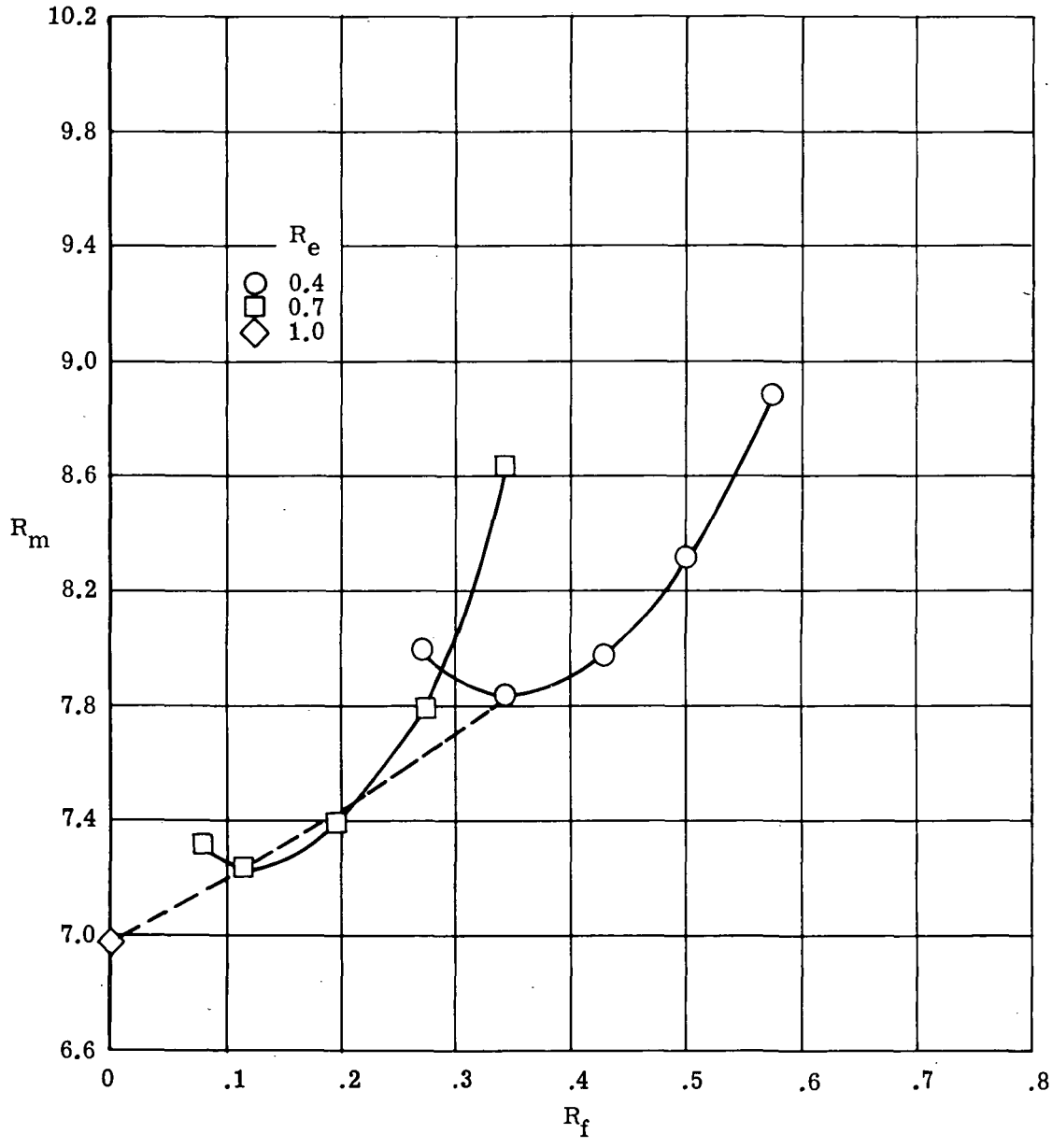

(e) $\varepsilon_{RP} = 50$; $\varepsilon_{H1} = 50$; $\varepsilon_{H2} = 150$; $(T/W)_o = 1.45$.

Figure 20.- Concluded.

1. Report No.	2. Government Accession No.	3. Recipient's Catalog No.
NASA TP-1115		

4. Title and Subtitle	5. Report Date
EFFECT OF PROPULSION SYSTEM CHARACTERISTICS ON ASCENT PERFORMANCE OF DUAL-FUELED SINGLE-STAGE EARTH-TO-ORBIT TRANSPORTS	December 1977
	6. Performing Organization Code

7. Author(s)	8. Performing Organization Report No.
John J. Rehder	L-11933
	10. Work Unit No. 506-26-10-08
9. Performing Organization Name and Address NASA Langley Research Center Hampton, VA 23665	11. Contract or Grant No.
	13. Type of Report and Period Covered Technical Paper
12. Sponsoring Agency Name and Address National Aeronautics and Space Administration Washington, DC 20546	14. Sponsoring Agency Code

15. Supplementary Notes

16. Abstract

The results of a parametric study of ascent performance are presented for a vertical take-off, horizontal landing, single-stage Earth-to-orbit transport vehicle. Two dual-fueled concepts, series burn and parallel burn, were investigated, both of which utilized dual-position rocket nozzles. The analysis was made by systematically varying a set of propulsion similarity parameters, initial thrust-weight ratio, the proportion of the thrust due to dual-position nozzle engines, expansion ratios of the rocket nozzles, and the relative split between the two fuels, hydrogen and hydrocarbon. The data are presented as a series of curves of mass ratio plotted against each of the similarity parameters for various combinations of the other similarity parameters.

17. Key Words (Suggested by Author(s))	18. Distribution Statement
Ascent performance Single-stage-to-orbit vehicle Launch vehicle Rocket propulsion Dual-fuel propulsion	Unclassified - Unlimited Subject Category 15

19. Security Classif. (of this report)	20. Security Classif. (of this page)	21. No. of Pages	22. Price*
Unclassified	Unclassified	63	$5.25

* For sale by the National Technical Information Service, Springfield, Virginia 22161

NASA-Langley, 1977

National Aeronautics and
Space Administration

Washington, D.C.
20546

Official Business
Penalty for Private Use, $300

THIRD-CLASS BULK RATE

Postage and Fees Paid
National Aeronautics and
Space Administration.
NASA-451

NASA

POSTMASTER: If Undeliverable (Section 158 Postal Manual) Do Not Return